DESIGN AND ANALYSIS OF RELIABLE WIRELESS OPTICAL COMMUNICATION SYSTEM FOR THE UNDERWATER CHANNELS

Thesis

Submitted in partial fulfillment of the requirements for the degree of
DOCTOR OF PHILOSOPHY

by

RAMAVATH PRASAD NAIK

DEPARTMENT OF ELECTRONICS AND COMMUNICATION ENGINEERING,
NATIONAL INSTITUTE OF TECHNOLOGY KARNATAKA,
SURATHKAL, MANGALORE -575025

JUNE, 2021

NATIONAL INSTITUTE OF TECHNOLOGY KARNATAKA, SURATHKAL

D E C L A R A T I O N

I hereby *declare* that the Research Thesis entitled **DESIGN AND ANALYSIS OF RELIABLE WIRELESS OPTICAL COMMUNICATION SYSTEM FOR THE UNDERWATER CHANNELS** which is being submitted to the ***National Institute of Technology Karnataka, Surathkal*** in partial fulfillment of the requirement for the award of the Degree of ***Doctor of Philosophy*** in **Department of Electronics and Communication Engineering** is a ***bonafide report of the research work carried out by me***. The material contained in this research thesis has not been submitted to any University or Institution for the award of any degree.

R. Prasad Naik 9/6/2021

155128-EC15FV07, Ramavath Prasad Naik, _____

(Register Number, Name & Signature of the Research Scholar)

Department of Electronics and Communication Engineering.

Place: NITK-Surathkal

Date: 09-June-2021.

NATIONAL INSTITUTE OF TECHNOLOGY KARNATAKA, SURATHKAL

C E R T I F I C A T E

This is to certify that the Research Thesis entitled **DESIGN AND ANALYSIS OF RELIABLE WIRELESS OPTICAL COMMUNICATION SYSTEM FOR THE UNDERWATER CHANNEL** submitted by **RAMAVATH PRASAD NAIK** (Register Number: 155128-EC15FVO7) as the record of the research work carried out by him, is accepted as the *Research Thesis submission* in partial fulfillment of the requirements for the award of degree of **Doctor of Philosophy**.

Research Guide	Chairman - DRPC
(**Prof. U. Shripathi Acharya**)	(**Prof. Ashvini Chaturvedi**)

Acknowledgements

I would like to express my sincere gratitude to my research advisor Prof. U Shripathi Acharya, for guiding me throughout the research work. The valuable suggestions and guidance provided by him kept me on the right track. Discussions with him helped me to understand and analyze the concepts in an intuitive way. I am indebted to him for his support, guidance, and encouragement during my research.

I am grateful to get the right encouragement from Prof. Muralidhar Kulkarni, Dr. Prabu Krishnan and Dr. Shyam Lal. They stood by me during peak and valley times and I have got great encouragement from them. They were supported in technical and non-technical discussions.

I express my gratitude to Prof. M. S. Bhat, Head of the department, Electronics and Communication Engineering during my enrollment for the Ph.D. program and Prof. Lakshminidhi T and Prof. Ashvini Chaturvedi, Head of the Department of E&C Engineering during my research work for their support, help, and encouragement.

I am grateful to my RPAC members, Prof. S M Kulkarni, Department of Mechanical Engineering, and Prof. Lakshminidhi T, Department of E&C Engineering, for giving vital comments and suggestions throughout the research, which helped in improving the quality of research.

I am thankful to my seniors, Goutham Simha G. D (currently Assistant professor in Manipal Institute of Technology), Raghavendra M A N S (currently working in Saankhya Labs) and Shrutkirthi G for their support for technical discussions and the way they motivate me to prepare for various questions and answers for any technical presentation.

I would like to thank the non-teaching staff of Department of E&C: Sanjeev Pujari, Rathish Kumar Thumbay, B Vasudeva Shettigar, Subrahmanya Karanth, Guruthilak Shriyan, and Amitha Amin help me to establish experimental set-up, and also Manohar Shanbhogue K (Senior Technical Assistant, Environmental Laboratory, Civil Department, NITK), M Makesh (Research Scholar, Physics Department, NITK) helping to measure the various parameters of Ocean water and normal water.

I would like to thank all the faculty members and staff of the E&C department, NITK Surathkal, for their assistance.

I would like to express my gratitude to all friends and colleagues at NITK for encouraging me in the good and the bad times, making a memorable stay in NITK. Thanks to Jayaram Reddy M K, J Venkataramaiah, Amardeep Kumar, Neetesh Kumar, and Dipanshu for technical discussions and support during my research work.

I express my gratitude to the Ministry of Electronics & Information Technology (MeitY), Government of India, to provide financial assistance during the research.

I would like to take a moment to my appreciation to Dr. Prashantha Kumar H, Prof. John D'Souza, and Dr. Raghavendra Bobbi to provide technical support, which helped me to learn many technical details.

I would like to thank my parents R Swamy Naik and Jamali Bai, wife Usha Rani, brother R Ramana Naik, sisters Sukanya, Bharathi, brother-in-law V Eswar Naik, and D Lakshmanna, friends Dhanikela Venkata Sreekanth and G Shivaram for their continuous support, love, and encouragement.

I am deeply indebted to all my teachers throughout life, who have guided, encouraged, and inspired me to grow in both technical and personal aspects.

Finally, I would like to thank god for giving me good health, strength, and bliss during my research work.

R Prasad Naik

Place: NITK, Surathkal
Date: 09-June-2021.

Dedicated to
My Dear Parents

Abstract

Internet of Things (IoT) is a technology that deals with devices and protocols employed to interconnect smart devices that are deployed in benign and hazardous environments to collect or exchange information. In recent years, attempts have been made to interconnect devices deployed in underwater environments. These devices have been employed in underwater environments to monitor physical phenomena such as climate and ocean monitoring and enable activities such as underwater surveillance and ocean exploration. This technology is referred to as the Internet of Underwater Things (IoUT). IoUT is a technology, which requires a high degree of information integrity, high data transfer rates and energy efficiency for effective deployment.

Optical signaling gives the flexibility of providing high data-rates than that of acoustic and RF signaling for medium link-ranges. Hence, optical signaling is an excellent candidate to enable high speed IoUT communication link between the underwater devices. The devices that employ optical signaling to enable communication between underwater vehicles and the underwater channel together constitute the Underwater Wireless Optical Communication (UWOC) system. The transmitted optical data experiences beam attenuation, turbulence and pointing errors, all of which can contribute to introduce errors in the received data stream.

We initiated the work in this thesis by conducting experimental work to determine various parameters affecting the propagation of light in an underwater channel and determining the optimum wavelength for UWOC communication. This is followed by a discussion of channel models that are appropriate descriptors of weak and strong turbulence in the underwater medium. Analytic models describing strong and weak turbulence have been derived, and simulation studies (Monte-Carlo simulations) that determine the accuracy of these analytic models have been carried out. The performance of UWOC system is mainly dependent on the underwater turbulence, beam attenuation and pointing errors, to mitigate these effects we have introduced multiple input multiple output (MIMO), forward error control codes and Space-Time Block Codes (STBCs) to the proposed UWOC system. In many instances, the UWOC link operating under the surface of the water has

to be linked with a RF system operating over the water surface. Such a link is referred to as a cooperative RF-UWOC system. Channel models for the combined RF-UWOC system have been drawn up. It has been recognized that in addition to channel induced impediments, a major cause of link outage is the introduction of pointing errors due to the physical displacement of the transmitter-receiver pair, which causes the Line of Sight (LOS) requirement to be disturbed. Loss of LOS has the potential to severely compromise the working of the UWOC/ RF-UWOC system. The performance of the RF-UWOC (co-operative IoT and IoUT) system in the presence of pointing errors has been studied and various outage probabilities have been determined. We have concluded the technical contributions of the thesis by studying underwater image transmission through the turbulent oceanic medium and suggesting various remedial techniques for proper image reception and enhancement.

The thesis has been concluded by drawing conclusions from the research work conducted in the thesis and suggesting avenues for further research.

Keywords: IoT, IoUT, UWOC, Beam Attenuation, Turbulence, Pointing Errors, Co-operative RF-UWOC communication, Transmit/ Receive Diversity, MIMO, STBC and Error Correcting Codes.

Contents

List of Figures

List of Tables

Abbreviations

Short form	Description
5G	Fifth Generation
AF	Amplify and forward
AMF	Adaptive Median Filter
ASCII	American Standard Code for Information Interchange
AWGN	Additive White Gaussian Noise
BCH	Bose Chaudhuri-Hocquenghem
BER	Bit Error Rate
BFSK	Binary Frequency Shift Keying
BPSK	Binary Phase Shift Keying
CDF	Cumulative Distribution Function
CMW	Center Weighted Median
DA	Divergence angle
dB	Decibel
dBm	Decibel milliwatts
DBPSK	Differential Binary Phase Shift Keying
DF	Decode and Forward
EGC	Equal Gain Combining
FEC	Forward Error Correction
FOV	Field Of View
Gbps	Giga bits per second
GF	Galois Field
GFFT	Galois field fourier transform
GG	Gamma-Gamma
GHz	Giga Hertz
HTD	Hyperbolic Tangent Distribution
HTLN	Hyperbolic Tangent Log-Normal
IGFFT	Inverse Galois Field Fourier Transform
IoT	Internet of Things
IoUT	Internet of Underwater Things
Kbps	Kilo bits per second
KHz	Kilo Hertz
KM	Kilo Meter
LASER	Light Amplification by Stimulated Emission of Radiation
LCM	Least Common Multiple
LDPC	Low Density Parity Check
LED	Light Emitting Diode
LN	Log-Normal
LOS	Line of Sight

M-PSK	M-ary Phase Shift Keying
M-QAM	M-ary Quadrature Amplitude Modulation
Mbps	Mega bits per second
MHz	Mega Hertz
MIMO	Multiple-Input-Multiple-Output
MISO	Multiple-Input-Single-Output
MLC	Majority Logic Combining
MLE	Maximum Likelihood Estimation
MSE	Mean Square Error
NOSTBC	Non-orthogonal Space Time Block Codes
NTU	Nephelometric Turbidity Units
OCS	Open Close Sequence
OOK	On-Off Keying
OSTBC	Orthogonal Space Time Block Codes
OWC	Optical Wireless Communication
PD	Photo-Diode
PDF	Probability Density Function
PPM	Pulse Position Modulation
PSNR	Peak Signal to Noise Ratio
PVC	Polymerization of Vinyl Chloride
RF	Radio Frequency
RGB	Red, Green and Blue
RMSE	Root Mean square error
RS	Reed-Solomon
RZ	Return to Zero
SI	Scintillation Index
SC	Selection Combining
SIMO	Single-Input-Multiple-Output
SISO	Single-Input-Single-Output
STBC	Space Time Block Codes
UWOC	Underwater Wireless Optical Communication

List of Symbols

Symbol	Description
B	Bandwidth
c	Channel coded data
C	Attenuation coefficient
$\hat{c}$	De-coded data
D_i	i^{th} detector
I	Irradiance
I_a	Path loss constant
I_d	Dark current
I_t	Irradiance due to turbulence
k	Length of message
K	Wavenumber
K_b	Boltzmann constant
L	Link-range
M	Number of detectors
n	Length of code-word
N	Number of sources
P_t	Transmit power
q	Charge of electron
R_L	Load resistor
s	Data source
$\hat{s}$	Estimated data
t	Number of error correcting capability
T_b	Bit duration
T_e	Absolute receiver temperature
W_i	Weight parameter
Y_i	i^{th} detector's response
α	Primitive element in the field
η	Responsivity
μ_X	Gaussian mean
λ	Wavelength
$\mathbb{E}$	Expectation
$\mathbb{Q}$	Q-function
σ^2	Noise variance
σ^2_{th}	Thermal noise variance
σ^2_{bg}	Background noise variance
σ^2_{th}	Shot noise variance
υ	Binary data
$\lfloor . \rfloor$	Floor operator

Chapter 1

Introduction

It is well known that about 71% of the surface of the earth is covered with water. Exploring, utilizing and monitoring such a vast domain, which is not the natural domain of humankind, requires the use of many sophisticated technologies. An essential enabler of underwater exploration is the availability of robust, high-speed and reliable underwater wireless communication technology, which can enable communication between underwater platforms and over water monitoring stations. These technologies are responsible for enabling safe navigation, disaster monitoring, locating rare oceanic animals, identifying the presence of precious minerals and collections of human-made garbage (to name a few applications). These technologies also help humankind find solutions to many other critical problems such as climate change, location of oil spills, etc. These facts have motivated us to work on the design of high-speed and reliable underwater communication systems.

The infrastructure to be put in place to enable services like ocean monitoring etc. has been referred to the Internet of Underwater Things (IoUT), which is a subclass of the Internet of Things (IoT). IoUT has been defined as the network of connected smart underwater objects. Figure 1.1, shows the possible applications of IoUT.

Three primary signaling schemes have been used to operate IoUT devices. They are Radio-frequency (RF) signals, Acoustic signals and Optical signals. The prevalent RF and acoustic underwater communication systems are limited in terms of data-rate and bandwidth that they can offer. RF signal suffers from high attenuation in the underwater channel. Hence, RF signaling is restricted for use over short link-ranges. The RF system would require large size antennas and very high transmission powers to prolong the higher link range. Experiments have been conducted to determine the distribution of current, driving point impedance, and the magnetic field distribution when an electromagnetic (RF) signal propagates in

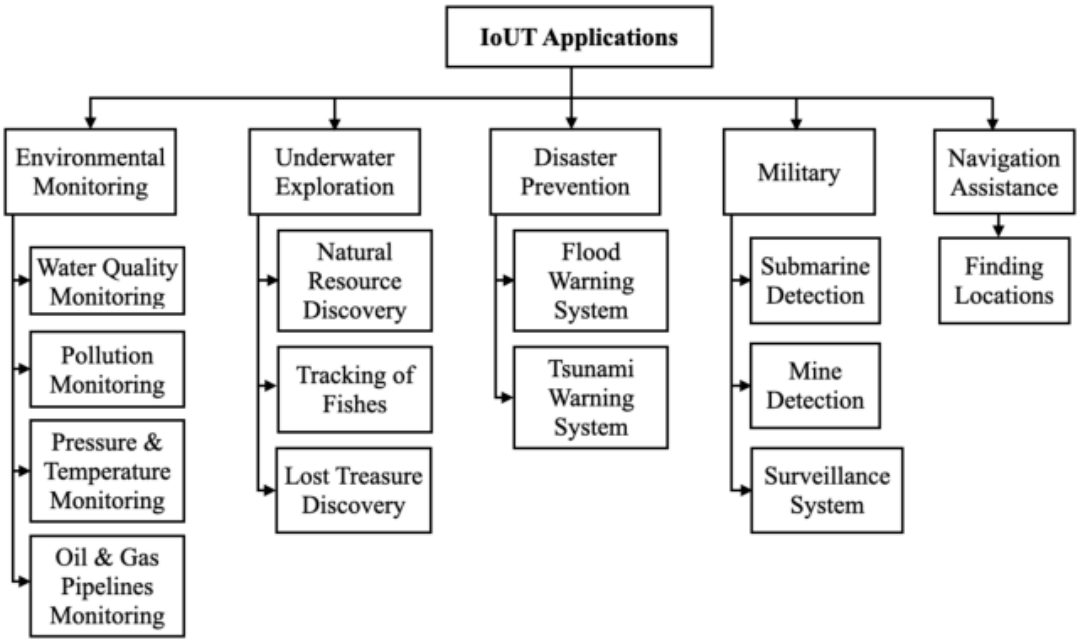

Figure 1.1: Applications of IoUT.

the oceanic water channel. This study is presented in [Siegel and King (1973)]. Currently, acoustic signals are being employed to transmit data for long distances (typically $1 - 10$ km). However, this technology suffers from low data-rates (the maximum data-rates that can be made available by this technology is of the order of 10's of kbps). Further, it also suffers from the impediment of large delay spread, which is due to the nature of acoustic signal while propagating in an underwater medium. In comparison, Optical signaling offers high data-rate (order of 100's of Mbps) over the short-to-medium link-ranges (typically 10's – 100's of meters). The critical difference between RF, acoustic and optical wireless communications links is in bandwidth availability, speed and link range. Table 1.1 shows the benefits and limitations of RF, acoustic and optical communications in terms of speed, bandwidth and range. Optical communication provides a definite advantage when signals possessing large bandwidths have to be conveyed at high-speeds over short-to-medium range links. A study of this table indicates that the performance of Optical transmission is superior to RF and Acoustic transmission in an underwater medium when signals having significant bandwidth have to be communicated over short to medium distances. This is due to favorable propagation characteristics of correctly chosen optical signal wavelengths in an underwater medium. A number of researchers have conducted research directed towards increasing the data-rate and link-range with optical signals in an underwater medium. They have devised techniques to employ optical signaling through the underwater channels

Table 1.1: Comparison of RF, Acoustic and Optical communications

Communication type	BW	Speed of transmission	Link range
RF	MHz	Moderate	Short range (of the order of tens of meters)
Acoustic	KHz	Low	Long range (of the order of 1–10 of KM)
Optical	GHz	High	Short-to-medium range (of the order of 10–100's of meters)

to communicate between underwater entities. This approach has been referred to as Underwater Wireless Optical Communication (UWOC) in literature. This technology offers many advantages such as sizable bandwidth, high transmission speeds, use of unlicensed optical spectrum, ease of set up, low energy consumption and low latencies. Hence, the engineering/ research community has shown considerable interest in harnessing the potential of UWOC in recent years. UWOC technology has the potential to play the role of a strong enabler of high-speed and reliable underwater communication. Our research work has been motivated by the desire to make a positive and definitive contribution to the design of state of the art UWOC links.

1.1 Underwater wireless optical communication link

Unlike wireless communication, Free-Space or Underwater Optical communication can provide high data transfer rates, without requiring the procurement of expensive electromagnetic spectrum. These advantages of optical communication have motivated researchers to devote time and other resources to develop high-speed and reliable optical communication links. A lot of work has gone into investigating the use of UWOC for developing high-speed short-to-medium distance communication links for strategic and commercial applications.

Optical wireless communication (OWC) requires the presence of line of sight. Information is usually modulated on an optical carrier wave at a suitable wavelength chosen to minimize losses due to absorption and scattering. The most commonly employed modulation scheme is On-Off Keying (OOK), where the binary electrical signal directly drives the optical source. The block diagram in Figure 1.2 describes the blocks and the interconnections in an UWOC link. As shown

in the figure, the UWOC link consists of the transmitter, the receiver, and the underwater optical channel. A brief description of these blocks is presented in the next subsections.

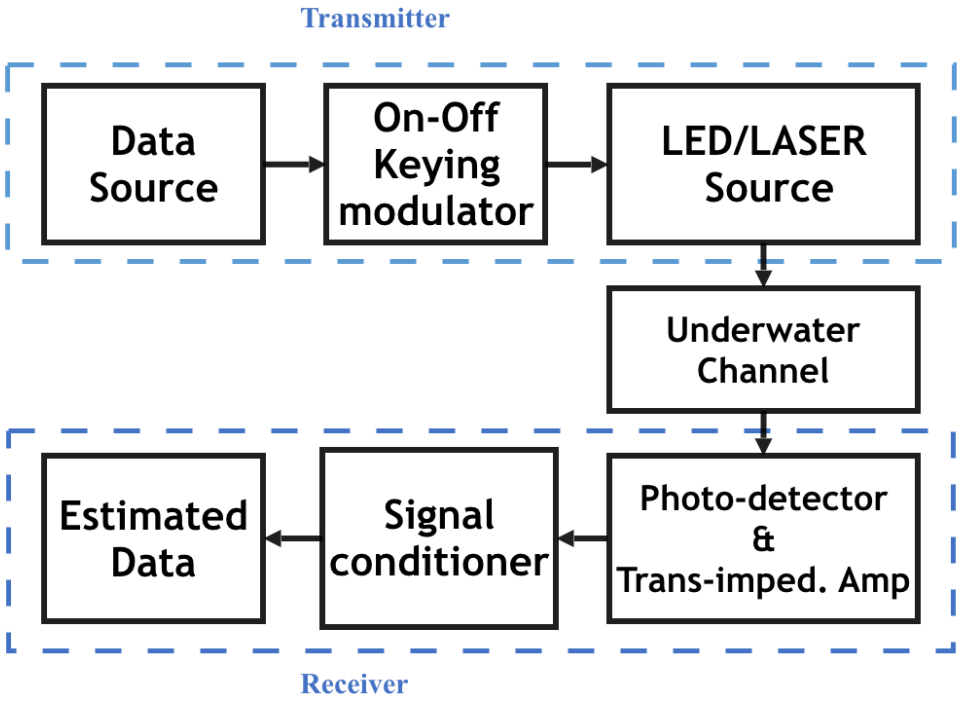

Figure 1.2: Block diagram of a typical UWOC link.

1.1.1 Transmitter

The data source consists of a text/ photo/ video message converted into ASCII symbols and then into binary digits. A random number generator generating sequences of suitable length can also be employed. These binary digits are used to modulate the optical source using OOK modulation. The transmitter section consists of a driver circuit, the LED/ LASER source and a collimated lens arrangement to focus the light beam into the water column.

1.1.2 Receiver

A collimated lens arrangement followed by photo-detector (PD) is employed at the receiver to detect the transmitted optical data. The PD delivers a current proportional to the incident light intensity to the load (information sink). A Transimpedance amplifier is usually employed in this arrangement to convert the current into an equivalent voltage. This is further processed by a two-level comparator, which is used to regenerate the stream of 0's and 1's.

1.1.3 Underwater optical channel

The aquatic medium is a harsh and dynamically changing communication medium. The transmitted optical data experiences beam attenuation, underwater turbulence and transceiver pointing errors all of which can contribute to introduce errors in the transmitted bit stream. A brief account of these phenomena is presented in the following subsections.

1.1.3.1 Beam attenuation

In an UWOC system, the optical signal undergoes beam attenuation through the mechanisms of absorption and scattering. Absorption reduces the photon count, which leads to a reduction in the intensity of the received light wave. Beam scattering deviates the path of incident light from a straight trajectory and causes propagation through one or more additional paths due to localized non-uniformities in the medium. Some of these deviant paths may not reach the receiver location and hence, the energy contained in these paths is lost. Figure 1.3, shows the absorption and scattering of the transmitted irradiance.

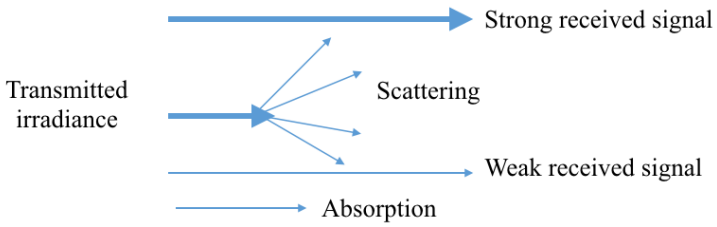

Figure 1.3: Absorption and scattering of optical beam.

The experimental results of the absorption of light for different wavelength light sources is shown Figure 1.4. It is evident that the absorption is minimum at 470 to 530 nm (blue, green) and 620 to 700 nm (red) wavelengths. This result has been obtained with the help of an experiment conducted with the AU 2701 model UV-VIS double beam spectrophotometer. After considering the effects of beam scattering, it was observed that wavelengths in the range of $450 - 530$ nm exhibit minimum attenuation in underwater environment. Hence, we have employed a suitable LED/LASER source operating at a wavelength 470 nm in our experimental, analytic and simulation studies.

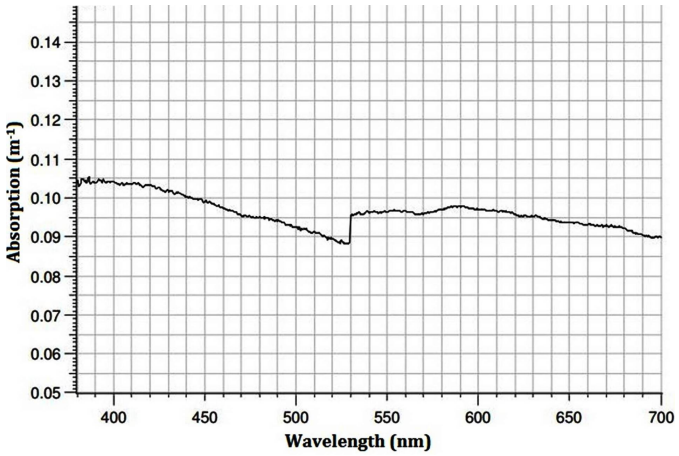

Figure 1.4: Experimental results of absorption with respect to source wavelength.

1.1.3.2 Underwater turbulence

Underwater turbulence is due to the movement of the water medium. This causes the received irradiance to fluctuate from higher to lower intensities. Figure 1.5 shows the variation of light in the presence of turbulence. It illustrates the light intensity reduction due to turbulence. The strength of the turbulence is characterized by Scintillation Index (SI). For weak turbulence, the value of SI lies between 0 and 1. Medium turbulence is characterized by values of SI approximately equal to 1. Strong turbulence is characterized by values of SI greater-than 1.

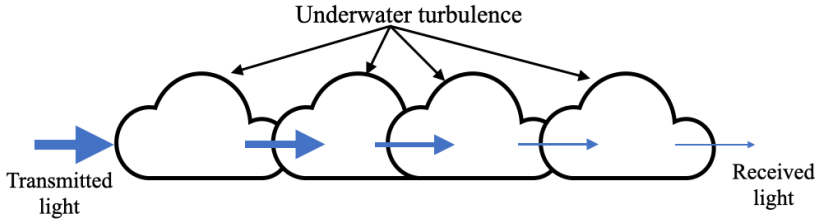

Figure 1.5: Effect of turbulence on light.

1.1.3.3 Pointing errors

The mechanical misalignment between the optical transceivers due to vibration can cause pointing errors. Such errors are a common cause of deterioration of the link quality in practical UWOC systems. Figure 1.6 shows the occurrence of pointing errors between the underwater vehicles like torpedo and ship. In UWOC links pointing errors are created due to movement of sea creatures/ ships or other

marine equipment which have the effect of causing temporary dislocation in the positions of transmitter/ receiver.

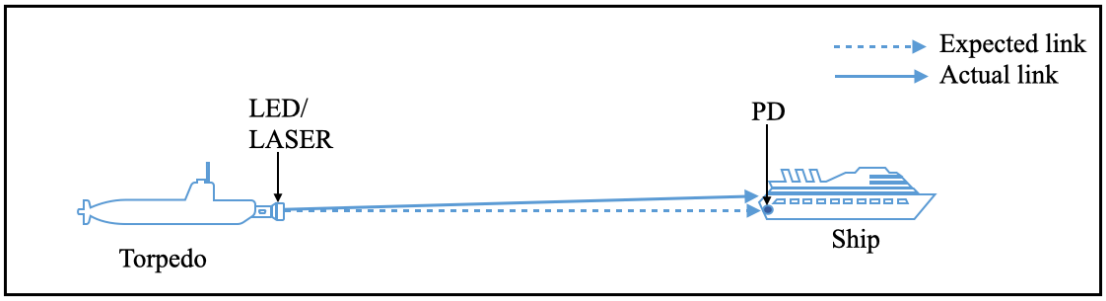

Figure 1.6: Optical signal pointing errors between underwater vehicles.

1.2 Prior work

Underwater communication was initiated with the use of acoustic signals [Miller (1959), Zielinski and Barbour (1978), Baggeroer *et al.* (1981), Quazi and Konrad (1982), Jackson and Kliman (1992), Essebbar *et al.* (1994)]. Underwater acoustic communication can provide a relatively long-range. However, it has several disadvantages as well, which limits its application. The throughput of the system is limited to a maximum of a few Kilobits per second (kbps). In addition to lower throughput, acoustic signals also experience high attenuation while propagating in an underwater medium. This requires the use of larger transmit powers to establish reliable communication. Hence, the performance of UWOC systems is superior to acoustic communication systems in applications where high-speed communication over short-to-medium links (typically 100's of meters)is required to be established [Schill *et al.* (2004), Farr *et al.* (2010)]. A review on practical considerations and solutions in UWOC has been demonstrated in [Sun *et al.* (2020)] and optimum wavelengths for use in UWOC lie in the range of 450-510 nm (blue or green LED) [Morel (1974)]. Our experimental results conducted with the AU 2701 model UV-VIS double beam spectrophotometer have corroborated result is shown in Figure 1.4, which shows the attenuation of the optical beam with respect to varying optical source wavelength. These wavelengths are characterized by minimum absorption and dispersion. In [Schill *et al.* (2004)], the authors used cyan, blue and green Luxeon LEDs (LUMILEDS) as light sources and SLD-70 BG2A photo-diode. These LEDs and detectors have a good trade-off between speed and sensitivity. In [Doniec *et al.* (2010)], authors have reported underwater optical communication

under short, medium and long ranges. They have presented successful symbol detection and packet rate versus distance plots for the three different ranges using 470 nm blue LEDs in a pool. Underwater turbulence of different strengths has been modeled statistically. The experimental setup of turbulent flow induced scintillation on deep ocean wireless optical communication is presented in [Weng *et al.* (2019)]. These models are based on Kolmogorovs atmospheric turbulence model presented in [Ata and Baykal (2014)]. Oceanic turbulence is the result of refractive index change caused by temperature and salinity fluctuations. The variation of the refractive index affects the performance of the UWOC system [Korotkova *et al.* (2012)]. The study of the effect of pointing errors on the free-space optical transceivers has been presented in [Sandalidis *et al.* (2008)]. They have derived a mathematical model which is well suited to represent the effects of pointing errors. The effect of beam attenuation depends upon the nature of the medium. This is calculated using Beer-Lambert's law. The PDF representing the combined effect of beam attenuation, turbulence and pointing errors is described in [Krishnan and Kumar (2014)] for a free-space optical channel exhibiting strong turbulence. In UWOC systems, these effects impose a significant power penalty on the performance of a communication system, which can be combated by the use of Forward Error Correcting (FEC) codes, transmit/receive diversity techniques, and MIMO schemes. FEC codes for the UWOC link to mitigate the effects of underwater turbulence are presented in [Kaushal and Kaddoum (2016)]. An UWOC system using Reed-Solomon (RS) code was investigated in [Cox *et al.* (2008)]. Simpson et al implemented a real-time RS code for interfacing with an underwater vehicle at 5 Mbps [Simpson *et al.* (2010)].

It is well known that the effect of turbulence can be mitigated by the use of spatial diversity, optical amplification and channel coding techniques. Single-Input to Multiple-Output (SIMO) schemes such as maximum receiver combining (MRC), equal gain combining (EGC) and selection combining (SC) have been employed to mitigate the effect of turbulence in UWOC systems [Liu *et al.* (2015*a*)]. It has been demonstrated that the performance of the EGC scheme is superior to all other schemes in the turbulent underwater medium [Liu *et al.* (2015*a*)].

The performance improvement obtained by the use of the EGC scheme along with the optical amplifier is proposed in [Boucouvalas *et al.* (2016)]. The performance of the UWOC system can be further improved by employing multiple transmit sources along with the multiple detectors at the receiver. This issue has been discussed in detail in discussed in [Jamali *et al.* (2016)].

1.3 Problem statement and Thesis contribution

Detailed problem statement and thesis contributions discussed in this section.

1.3.1 Problem statement

This thesis's primary focus is to carry out experimental studies and mathematical analysis of different constructive communication schemes that can be used to enable reliable Underwater Wireless Optical Communication (UWOC). Various approaches, such as FECs, Diversity, and MIMO techniques, have been analyzed and validated using simulation. The concept of relaying with the use of RF links has also been explored to increase the link range. The thesis has made the following contributions:

An experimental UWOC system has been designed and set up to gain a first-hand understanding of the challenges and opportunities presented by UWOC. A thorough study of channel models has followed this, channel induced impairments and noise on the performance of underwater optical channels. We have synthesized mathematical models to simulate the effects of various impairments experienced by the propagating signal in seawater, such as turbulence and turbidity. As the transmission capacity of UWOC is limited to the short-to-medium range, we have studied and proposed relaying schemes involving RF technology to increase the transmission range. This has led to the design and performance analysis of co-operative RF–UWOC communication link using Amplify-and-Forward (AF) as well as Decode-and-Forward (DF) relays.

Transmit/ receive diversity, and MIMO schemes have been designed to exploit the fact that many channels provide a multi-path environment. Multiple paths between the transmitters and receivers can be viewed as individual data-carrying pipes. The UWOC channel also provides a multi-path environment due to the inherent scattering of light during propagation. We have proposed MIMO and diversity schemes to combat the effects of signal fading. In addition to MIMO schemes, FEC schemes have also been proposed. These schemes enhance the reliability of information transfer by adding additional redundant bits that allow the errors introduced by the channel to be detected and corrected. The main aim of conducting this research is to identify the key factors that limit the reliability of information transfer in UWOC channels and to propose effective techniques to minimize the effect of these impediments on the process of information transfer. Our aim in conducting this research work is to address these requirements and propose constructive solutions to meet these challenges.

1.3.2 Thesis contribution

A detailed account of the research work carried and described in various chapters is listed below.

- We have started the description of research work by designing and prototyping an experimental UWOC set up operating in the presence of weak underwater turbulence and air bubbles. The benefits of various forms of diversity combining have been quantified. A simple Bose-Chaudhuri-Hocquenghem (BCH) code has also been employed to improve the integrity of information transfer. The BER performance of the system has been determined as a function of transmit power.

- We have attempted to seek a deeper understanding of underwater turbulence by proposing a new probability density function (PDF) to characterize weak turbulence.

- We have derived closed-form analytic equations to determine the BER for UWOC systems employing MIMO and forwarding error correcting codes. Monte-Carlo simulations have validated the accuracy of the predictions made by these equations.

- A co-operative RF–UWOC communication system has been proposed. The performance of this co-operative scheme has been validated by determining closed-form solutions for the BER. Monte-Carlo simulations have further validated these results.

- We have also investigated the challenges involved in underwater image transmission. We have attempted to mitigate the impediments introduced by the UWOC channel by the use of suitable filters.

- We have concluded the thesis by suggesting various research problems that can be tackled by the interested researcher.

- A block diagram describing the various challenges, mitigation techniques, and the contribution made by this thesis to overcome the UWOC channel impediments is described in Figure 1.7

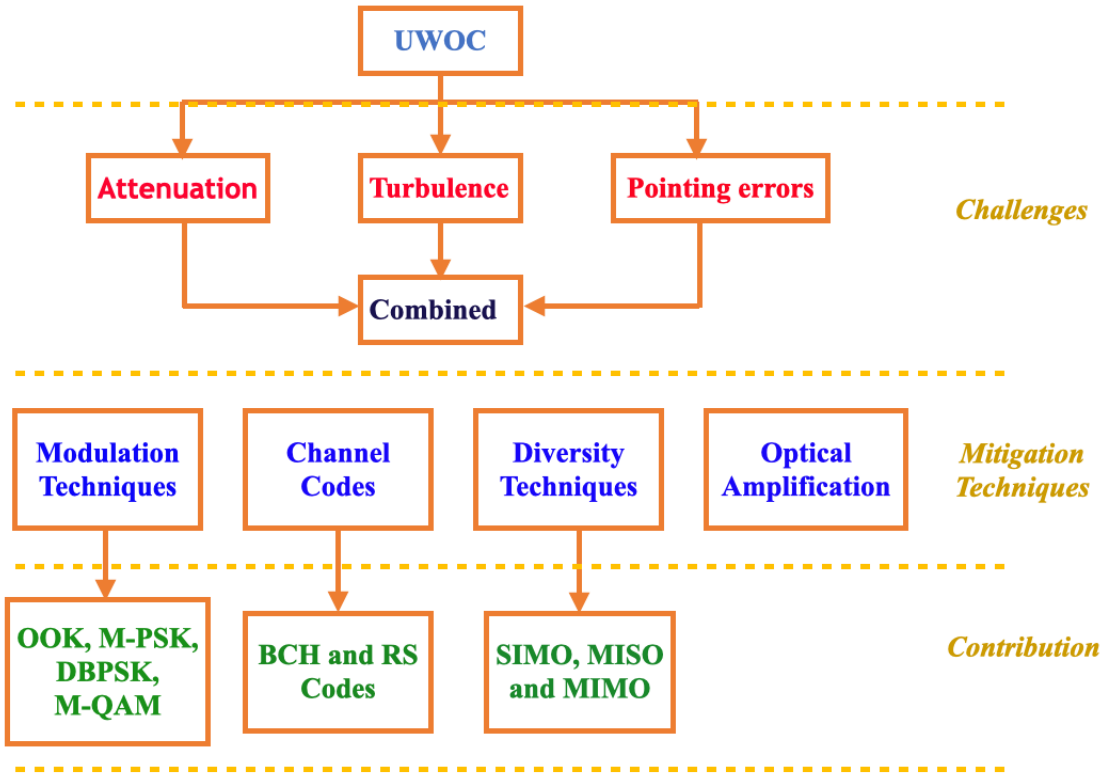

Figure 1.7: Diagram illustrating various contribution made in the thesis.

1.4 Thesis Organization

There are eight chapters in this Thesis dissertation.

Chapter 1: This chapter provides a brief introduction to UWOC system. A brief exposition of the UWOC system challenges to error-free data transfer and various approaches to mitigate the effects of channel induced impairments have been presented.

Chapter 2: This chapter presents an UWOC system performance in the presence of weak and strong turbulence regimes. The Monte-Carlo simulation BER performance compared with the results obtained by using closed-form analytic equations.

Chapter 3: In this chapter, we have presented an experimental demonstration of UWOC system in the presence of air bubbles and weak turbulence for varying turbidity levels. The improvement obtained in the BER at the receiver by the use of a BCH code and receiver diversity schemes to mitigate the effects of underwater turbulence and air bubbles is demonstrated and quantified by plots.

Chapter 4: This chapter presents analytic results supported by Monte-Carlo simulations of the performance of a RS-coded MIMO UWOC system. The MIMO configuration and the channel code are used to mitigate the effects of beam attenuation and weak turbulence exhibited by the channel. A novel contribution of this chapter is the modeling of weak oceanic turbulence by the hyperbolic tangent distribution function. This has not been done by any prior researcher to the best of our knowledge.

Chapter 5: In order to provide improved throughput and enhanced reliability we have employed an orthogonal STBC (OSTBC) and a non-orthogonal STNC (NOSTBC) along with OOK modulation to improve the reliability of UWOC.

Chapter 6: In this chapter, we have developed an analytic model which describes the performance of a co-operative RF–UWOC link. We have determined the performance of both amplify-forward (AF) and decode-forward (DF) relaying schemes. A new probability density function (PDF) has been proposed to model the perturbations introduced by weak oceanic turbulence on an UWOC link.

Chapter 7: In this chapter, we have undertaken simulation studies of underwater image transmission using optical signaling. Adaptive median filtering techniques have been employed to eliminate errors and enhance the quality of the received image.

Chapter 8: This last chapter summarizes the major contributions of the thesis and presents discussions on future research that can be undertaken.

Chapter 2

UWOC System in the Presence of Weak and Strong Turbulence Scenarios

2.1 Introduction

The strength of the turbulence phenomenon is represented with the help of Scintillation Index (SI) values. If the value of SI lies between 0 to 1, turbulence is classified as being weak. If the value of SI exceeds 1, turbulence is classified as being strong. The oceanic parameters that influence SI are link-range, dissipation rate of mean square temperature, kinetic energy and strength of temperature-salinity parameters. In this chapter, we have investigated the Bit Error Rate (BER) performance of On-Off Keying (OOK) modulated UWOC system under weak and strong turbulence regimes for varying link-ranges using analytic and simulation techniques. The BER performance has been determined and plotted using analytic and simulation means. It is observed that under conditions of weak as well as strong turbulence, there is a close correspondence between results obtained by analytic means and Monte-Carlo simulation.

The remaining part of this chapter is organized as follows. In Section 2.2, channel models for weak and strong underwater turbulence are presented. Monte-Carlo simulations, which have been extensively employed in the thesis, have been discussed in Section 2.3. Analytical equations describing the probability of error for both weak and strong turbulence conditions have been derived in Section 2.4. The results obtained by analysis and simulation have been discussed in Section 2.5. The chapter has been concluded in Section 2.6.

2.2 Channel Model

The variation in SI with link-range (L) for a plane wave is given as [Korotkova *et al.* (2012)],

$$\sigma_I^2 = 8\pi^2 k^2 L \int_0^1 \int_0^\infty \mathcal{K}\Phi_n(\mathcal{K}) \left(1 - \cos\left(\frac{L\xi\mathcal{K}^2}{k}\right)\right) d\mathcal{K}d\xi \tag{2.1}$$

where $k = 2\pi/\lambda$ is wave number and $\Phi_n(\mathcal{K})$ represents the the power spectrum of oceanic turbulent water. This parameter is described by equation (2.2)

$$\Phi_n(\mathcal{K}) = \frac{0.388 \times 10^{-8} \epsilon^{-1/3} \mathcal{K}^{-11/3} \chi_T}{\omega^2} \left[1 + 2.35\,(\mathcal{K}\xi)^{2/3}\right] \left(\omega^2 e^{-A_T\delta} + e^{-A_S\delta} - 2\omega e^{-A_{TS}\delta}\right) \tag{2.2}$$

In this equation, $\Phi_n(\mathcal{K})$ depends on the turbulence kinetic energy dissipation rate ϵ, dissipation rate temperature and salinity χ_t, length of Kolmogorov micro-cell ξ, and relative varying temperature-salinity parameter variation with respect to depth of the ocean ω. The parameters $A_T = 1.863 \times 10^{-2}$, $A_S = 1.9 \times 10^{-4}$, $A_{TS} = 9.41 \times 10^{-3}$ and $\delta = 8.284\,(\mathcal{K}\upsilon)^{4/3} + 1.2978\,(\mathcal{K}\upsilon)^2$ are from [Korotkova *et al.* (2012)].

The scintillation Index (SI) for varying link range is shown in Figure 2.1. The SI values for link-range 250 and 400 m links are 0.85 (weak) and 3.50 (strong) respectively. Underwater weak and strong turbulence are model with Log-Normal (LN) and Gamma-Gamma (GG) density functions respectively [Jamali *et al.* (2018)].

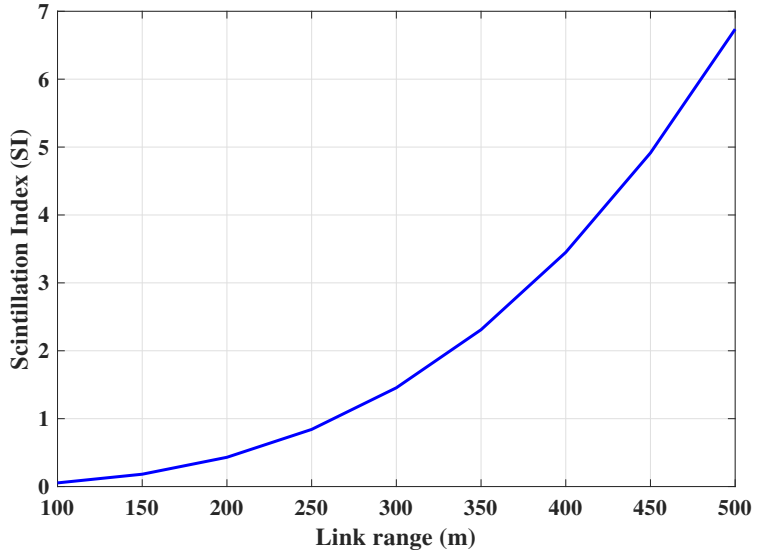

Figure 2.1: SI variation with respect to Link range.

2.2.1 Gamma-Gamma density function

The PDF characterized by strong turbulence are represented with the GG density function is given as,

$$f_I(I) = \frac{2(ab)^{(a+b)/2}}{\Gamma(a)\Gamma(b)} I^{\frac{a+b}{2}-1} K_{a-b}\left(2\sqrt{abI}\right), \quad I \geq 0 \tag{2.3}$$

where a and b are effective numbers of large and small scale turbulence eddies respectively, $\Gamma(\cdot)$ represents Gamma function, $K_{a-b}(\cdot)$ is modified Bessel function of the second kind of order $(a-b)$ and its representation in power series [Bayaki *et al.* (2009)] as follows,

$$K_{a-b}(2\sqrt{abI}) = \frac{\pi}{2\sin(\pi(a-b))} \sum_{j=0}^{\infty} \left(C_{j,I}^{(a,b)} - C_{j,I}^{(b,a)} \right) \tag{2.4}$$

where $C_{j,I}^{(a,b)} = \frac{(abI)^{\frac{(2j-a+b)}{2}}}{\Gamma(j-a+b+1)j!}$. Substituting equation (2.4) in (2.3) yields as,

$$f_I(I) = C \sum_{j=0}^{\infty} \left(C_j^{(a,b)} I^{j+b-1} - C_j^{(b,a)} I^{j+a-1} \right) \tag{2.5}$$

where $C = \frac{(ab)^{(a+b)/2}}{\Gamma(a)\Gamma(b)} \frac{\pi}{\sin(\pi(a-b))}$. The Cumulative Distribution Function (CDF) of GG is obtained using $F_I(I) = \int_0^I f_I(I)dI$ is given as,

$$F_I(I) = C \sum_{j=0}^{\infty} \left(\frac{C_j^{(a,b)} I^{j+b}}{j+b} - \frac{C_j^{(b,a)} I^{j+a}}{j+a} \right) \tag{2.6}$$

The n^{th} moment is $\mathbb{E}(I^n) = \frac{\Gamma(a+n)\Gamma(b+n)}{\Gamma(a)\Gamma(b)}(ab)^{-n}$. The SI is associated with the parameters a and b is given by, $\sigma_I^2 = \frac{1}{a} + \frac{1}{b} + \frac{1}{ab}$.

2.2.2 Log-Normal density function

The Probability Density Function (PDF) associated with the underwater weak turbulence is represented with Log-Normal density function and is given as,

$$f_I(I) = \frac{1}{2I\sqrt{2\pi\sigma_X^2}} \exp\left(-\frac{(\ln(I) - 2\mu_X)^2}{8\sigma_X^2} \right), \quad I \geq 0 \tag{2.7}$$

where I is received irradiance, μ_X and σ_X^2 are mean and variance of Gaussian distributed random variable $X = 0.5 \ln I$ respectively. CDF is given as,

$$F_I(I) = \frac{1}{2} + \frac{1}{2} erf\left(\frac{\ln(I) - 2\mu_X}{\sqrt{8\sigma_X^2}}\right) \tag{2.8}$$

where, $erf(\cdot)$ is error function and is given as, $erf(x) = 2/\sqrt{\pi} \int_0^x \exp(-t^2)dt$. The n^{th} moment is $\mathbb{E}(I^n) = \exp(2n\mu_X + 2\sigma_X^2 n^2)$. In order to normalize the PDF, we set $\mathbb{E}(I) = 1$, which leads $\mu_X = -\sigma_X^2$. The SI depends on the Log-Normal Gaussian variance σ_X^2 and is given as, $\sigma_I^2 = \exp(4\sigma_X^2) - 1$.

2.3 Optimised Simulations of UWOC system

In this section, we present the process of simulation carried for the UWOC system.

An OOK modulated UWOC system equipped with LASER source at transmitter and Photo-Detector (PD) at the receiver is assumed to constitute the transmitter and receiver. A data stream $s \in (0,\ 1)$ of $l = 10^6$ samples is modulated with LASER source with transmit power P_t. This sequence of light pulses is transmitted through a turbulent underwater channel (modeled with the appropriate channel coefficient) that depends on the turbulence level. The PD at the receiver converts the optical signal into equivalent voltages. The data obtained at the PD is given as,

$$Y = \eta\sqrt{P_t T_b} sI + n \tag{2.9}$$

where, η represents detector's responsivity in terms of A/W units, P_t represents transmit power in dB, T_b is bit duration in seconds, s is a transimitted symbol, I is received irradiance and n is an Additive White Gaussian Noise (AWGN) of zero mean and σ^2 variance. Data is estimated by use of maximum likelihood estimation is,

$$\hat{s} = \underset{\tilde{s} \in \{0,1\}}{argmin} \left|\left| Y - \eta\sqrt{P_t T_b}\tilde{s}I \right|\right|^2 \tag{2.10}$$

The BER is computed by using the expression, $BER = \sum_{i=1}^{l}(s_i \oplus \hat{s}_i)/l$ for varying transmit power, where $\oplus$ is Exclusive-OR operator.

2.4 Analytical BER evaluation

In this Section, we have derived BER equations by employing suitable analysis for OOK modulated UWOC system.

The distribution of received data $\hat{s}$ when transmitted binary data is represented by $s = 0$ and 1 is shown in Figure 2.2. In this diagram, $P_1 = P(\hat{s}/s = 1)$ shows the distribution of the received signal when $s = 1$ is transmitted and $P_0 = P(\hat{s}/s = 0)$ denotes the distribution of the received signal when $s = 0$ is transmitted.The threshold is set at the midway point $T = \left(\mathbb{E}(Y)\Big|_{s=0} + \mathbb{E}(Y)\Big|_{s=1}\right)\Big/2 = \eta I\sqrt{P_t T_b}/2$ and $m_1 = \mathbb{E}(Y)\Big|_{s=1} = \eta I\sqrt{P_t T_b}$. Probability of error (BER) associated with OOK modulated UWOC system for equiprobable bits (equal number of 0's and 1's are transmitted) is,

$$P_e = \frac{1}{2}\int_0^\infty \left(\sum_{i=0}^{1} P\left(\frac{\hat{s} = 1 - i}{s = i, I}\right)\right) f_I(I)dI \tag{2.11}$$

where $P(\hat{s} = 1/s = 0)$ Gaussian PDF with mean 0 and variance σ^2 and $P(\hat{s} = 0/s = 1)$ also Gaussian PDF with mean $\eta I\sqrt{P_t T_b}$ and variance σ^2 respectively. Integrating Equation (2.11) with the threshold $T = \left(\mathbb{E}(Y)\Big|_{s=0} + \mathbb{E}(Y)\Big|_{s=1}\right)\Big/2 = \eta I\sqrt{P_t T_b}/2$, leads the BER as,

$$P_e = \int_0^\infty \mathbb{Q}(\zeta I)\, f_I(I)dI \tag{2.12}$$

where $f_I(I)$ is LN/GG PDF for weak/strong turbulence conditions respectively and $\mathbb{Q}(x) \triangleq (1/\sqrt{2\pi})\int_x^\infty \exp(-y^2/2)dy$ and $\zeta = \eta\sqrt{\frac{P_t T_b}{4\sigma^2}}$.

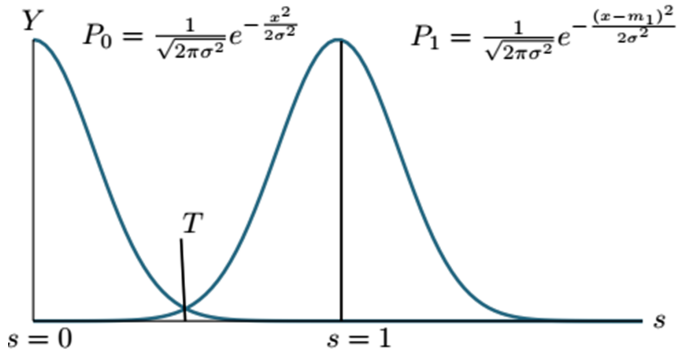

Figure 2.2: Received density function

2.4.1 Weak turbulence

The BER associated with weak turbulence UWOC system can be determined by the equation,

$$P_e = \frac{1}{2\sqrt{2\pi\sigma_X^2}} \int_0^\infty \exp\left(-\frac{\left(\ln I - 2\mu_X\right)^2}{8\sigma_X^2}\right) \mathbb{Q}\left(\zeta I\right) \frac{dI}{I} \tag{2.13}$$

Substituting I with $\exp(2x)$ in equation (2.13), the resultant equation is given as,

$$P_e = \frac{1}{\sqrt{2\pi\sigma_X^2}} \int_0^\infty \exp\left(-\frac{\left(x - \mu_X\right)^2}{2\sigma_X^2}\right) \mathbb{Q}\left(\zeta \exp\left(2x\right)\right) dx \tag{2.14}$$

An exact solution to equation (2.14) does not exist [Peppas *et al.* (2017)]. A closed-form solution for equation (2.14) can be obtained by using substitution and Gauss-Hermite quadrature polynomials (described in Appendix B). This procedure results in the probability of error, P_e being described as,

$$P_e \approx \frac{1}{\sqrt{\pi}} \sum_{i=1}^{l} W_i \mathbb{Q}\left(\zeta \exp\left(2\sqrt{2}\sigma_X x_i + 2\mu_X\right)\right) \tag{2.15}$$

where, W_i is weight of i^{th} order approximation.

2.4.2 Strong turbulence

The BER associated with a UWOC system experiencing strong turbulence can be determined by substituting equation (2.5) in equation (2.12),

$$P_e = C \sum_{j=0}^{\infty} \int_0^\infty \mathbb{Q}\left(\zeta I\right) \left(C_j^{(a,b)} I^{j+b-1} - C_j^{(b,a)} I^{j+a-1}\right) dI \tag{2.16}$$

Invoking Q-function approximation [i.e., $\mathbb{Q}(x) \approx 1/12 \exp\left(-x^2/2\right) + 1/4 \exp\left(-2x^2/3\right)$ from Chiani *et al.* (2003*a*)] in equaton (2.16) yields,

$$P_e \approx C \sum_{j=0}^{\infty} \int_0^\infty \left(\frac{1}{12} \exp\left(-\frac{\zeta^2 I^2}{2}\right) + \frac{1}{4} \exp\left(-\frac{2\zeta^2 I^2}{3}\right)\right) \left(C_j^{(a,b)} I^{j+b-1} - C_j^{(b,a)} I^{j+a-1}\right) dI \tag{2.17}$$

Equation (2.17) can be simplified using $\int_0^\infty I^{\alpha-1} \exp(-\beta I^2) dI = \frac{1}{2}\left(\frac{1}{\beta}\right)^{\alpha/2} \Gamma\left(\frac{\alpha}{2}\right)$. The resulting closed-form solution for the probability of error (BER) is,

$$P_e = C \sum_{j=0}^{\infty} \left[\mathscr{M}_1^j C_j^{(a,b)} \Gamma\left(\frac{j+b}{2}\right) - \mathscr{M}_2^j C_j^{(b,a)} \Gamma\left(\frac{j+a}{2}\right)\right] \tag{2.18}$$

where $\mathscr{M}_1^j = \frac{1}{24}\left(\frac{2}{\zeta^2}\right)^{(j+b)/2} + \frac{1}{8}\left(\frac{3}{2\zeta^2}\right)^{(j+b)/2}$ and $\mathscr{M}_2^j = \frac{1}{24}\left(\frac{2}{\zeta^2}\right)^{(j+a)/2} + \frac{1}{8}\left(\frac{3}{2\zeta^2}\right)^{(j+a)/2}$.

2.5 Simulation and Analytical Results

In this section, we present the BER results obtained by analytic means and corroborated by Monte-Carlo simulation. These results are obtained under conditions of both weak and strong turbulence. The BER values are determined as a function of transmit power (dB). The system parameters considered in the evaluation of performance are: $\eta = 0.15\ A/W,\ R_b = 500\ Mbps,\ \alpha = 0.75,\ \beta = 1.08$. In Figure 2.3, solid lines shows the simulation results and dash-dotted lines shows the results obtained from closed-form analytic equations (2.18), (2.15).

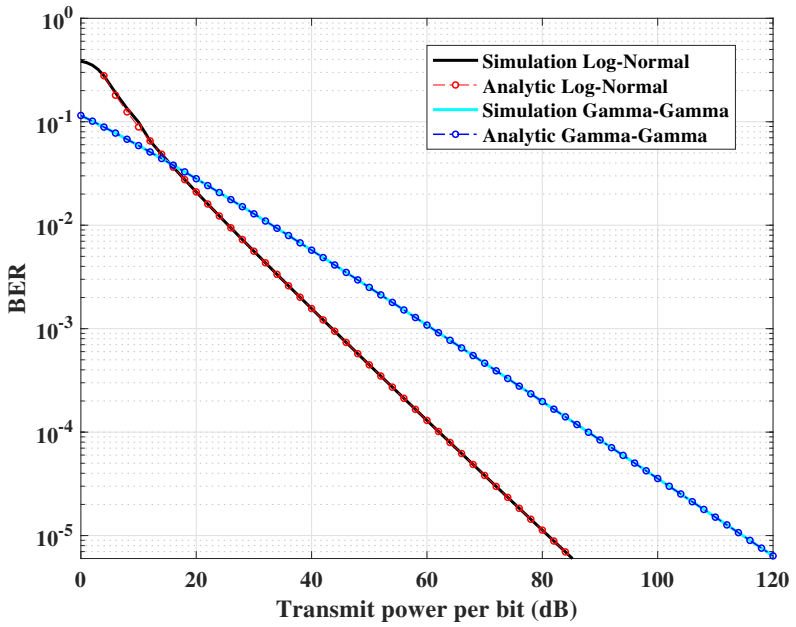

Figure 2.3: BER of UWOC under weak and strong turbulence regime.

It can be inferred from the figure that strong turbulence characterized by GG channel model requires more than 30 dB transmit power when compared with the weak turbulence characterized by LN channel to obtain a BER of 10^{-5}.

2.6 Conclusion

The BER performance of the UWOC system obtained using analytical equations corresponds very closely to the values obtained using Monte-Carlo simulations. It

is observed that an increase in link-range can increase the turbulence strength from weak to strong. This affects the power budget of the system. In this chapter, we have observed that the UWOC system in the presence of strong turbulence will require about 30 dB additional transmit power as compared to a system experiencing weak turbulence to deliver a BER of 10^{-5}.

From Figure 2.1, it can be seen that the value of SI exceeds 1 only when the link range is greater than or equal to 300 m. In our study, we have considered medium distance links having a range of up to 300 m. The turbulence experienced over these links is predominantly weak turbulence. Hence, in the remaining part of the Thesis, we have focused our attention on proposing channel models, determining BER expressions, postulating constructive solutions to reducing transmit power for a given BER (Channel coding, Diversity combining and MIMO) and studying the challenges involved in image transmission over an UWOC medium perturbed by weak turbulence.

Chapter 3

BCH Coded Receiver Diversity based UWOC Link: Design and Implementation over the Turbid and Turbulent Seawater Channel Medium

In this chapter, we have designed and carried out performance analysis of an experimental UWOC system in the presence of air bubbles and weak turbulence for varying turbidity levels of the aquatic optical medium. The major factors that limit the performance of the UWOC system are: absorption, scattering and beam fluctuations. The effect of these impediments can be mitigated by employing transmitter/ receiver diversity schemes and channel codes. We have employed receiver diversity (selection combining (SC), majority logic combining (MLC) and equal gain combining (EGC)) techniques augmented with Bose-Chaudhuri-Hocquenghem (BCH) codes in the system designed and prototyped by us, to enhance the performance of on-off keying modulated UWOC system. The Bit Error Rate (BER) expressions are derived for the proposed system and results are validated using both analytic and experimental means. Three receiver configurations namely SC, MLC and EGC augmented with a BCH code have been set up and their performance has been quantified. The results show that SC, MLC and EGC receiver combining techniques augmented with the chosen BCH code provide a power gain (measured in terms of reduced transmit power) of 4 dB, 6 dB and 8 dB from un-coded single-input single-output system respectively at a BER of 10^{-5}.

3.1 Introduction

Optical communication provides high data transfer rates, with the associated advantage of not requiring the procurement of the expensive bandwidth spectrum as would be required for equivalent wireless communication systems. These advantages of optical communication have motivated researchers to develop high-speed and reliable optical communication links. Considerable amount of effort has been expended by many researchers to investigate the use of UWOC for developing high-speed short-distance communication links for strategic and commercial applications. The underwater channel is different from the free-space channel in that it presents higher attenuation to the propagating wave when compared with the free-space atmospheric channel. This is brought about by scattering and absorption of the optical signal in the water medium. Scattering deviates the path of the transmitted optical signal and absorption in the medium reduces the photon count, which in turn leads to a reduction in the intensity of received light at the receiver. In addition to absorption and scattering, beam fluctuation is one of the major limiting factors of the UWOC system. Beam fluctuations arise due to the turbulence and air bubbles present in the underwater medium [Oubei *et al.* (2017), Zhao *et al.* (2017)]. In [Jamali *et al.* (2016), Liu *et al.* (2015*b*)], the authors have studied the analytical BER performance of OOK modulated multiple-input multiple-output UWOC systems. In [Mattoussi *et al.* (2018)], the authors have attempted to mitigate the effect of underwater turbulence in order to improve the performance of UWOC systems by empoying Reed-Solomon (RS) and Low-Density Parity-Check (LDPC) codes.

3.1.1 Major contributions

This chapter describes the performance of optical communication operating through a seawater with different turbidity levels. The channel is composed of a transperent water tank having dimensions of $5 \times 0.5 \times 0.5\ m^3$. The transmission speed is set at 1 $Mbps$. Channel impediemnts such as turbulence and air bubbles have been created by rotating paddles and aerators. To the best of our knowledge, the effects of underwater turbulence have been studied using analytic and simulation means only. While many methods have been proposed to mitigate the effects underwater turbulence, the efficacy of these methods have been evaluated using simulation and analytic means only. In this chapter, we have made an attempt, possibly for the first time to experimentally mitigate the effects of underwater turbulence, air bubbles, and beam attenuation for varying turbidity levels using receiver di-

versity techniques and error-correcting codes. It can be observed from the data presented in this cahpter that the proposed BCH code augmented with diversity reception combining techniques enhances the performance of the UWOC system in the presence of turbulence and beam attenuation.

The remaining part of this chapter is organized as follows, Section 3.2 describes the system model, Section 3.3 is devoted to description of the experimental set-up and statistical distribution of received irradiance, Section 3.4 gives a brief exposition of BCH encoding and decoding, Section 3.5 provides information about the analytic models used to describe lightwave propagation in seawater, Section 3.6 is devoted to a discussion of experimental and analytical results. This is followed by last section summarizing all the research contributions made in this chapter Section 3.7.

3.2 System model

The information bits of the data source are modulated using On-Off Keying (OOK) by employing a LED source operating at 470 nm wavelength. Turbulence is generated in the water medium by the use of an aerator blowing air bubbles. At the receiver, a photo-diode (PD) followed by a suitable trans-impedance circuit, converts the variations in light intensity into electrical voltages.

Figure 3.1 is a block diagram of a UWOC system employing receiver diversity combined with a BCH encoder/ decoder. In this set up, L denotes the length of the underwater channel, s represents the transmitted binary data, and c denotes the BCH encoded bit sequence respectively. This data is input to the LED driver circuit which drives the source LED using OOK. $D_1,\ D_2, \ldots,\ D_M$ are M independent and identical PDs. A distance of 5 cm is maintained between any two PDs in the receiver which employs diversity combining. $Y_1,\ Y_2, \ldots,\ Y_M$ are the responses of $D_1,\ D_2, \ldots,\ D_M$ respectively and Y represents the response after suitable diversity combining of the outputs of the M PDs. $\hat{c}$ and $\hat{s}$ represent the recovered decoded data and the estimated information sequence respectively.

At the transmitter side, binary '1' and binary '0' are transmitted with power P_t and absence of power respectively for T_b sec duration. The output of the i^{th} PD is modeled by,

$$Y_i = \eta_i \sqrt{P_t T_b}\, \Upsilon I_i + n_i, \quad 1 \leq i \leq M \tag{3.1}$$

where $\Upsilon \in \{0, 1\}$ should be replaced by s for un-coded and by c for BCH coded UWOC system, P_t represents the transmit power of LED source, T_b represents the

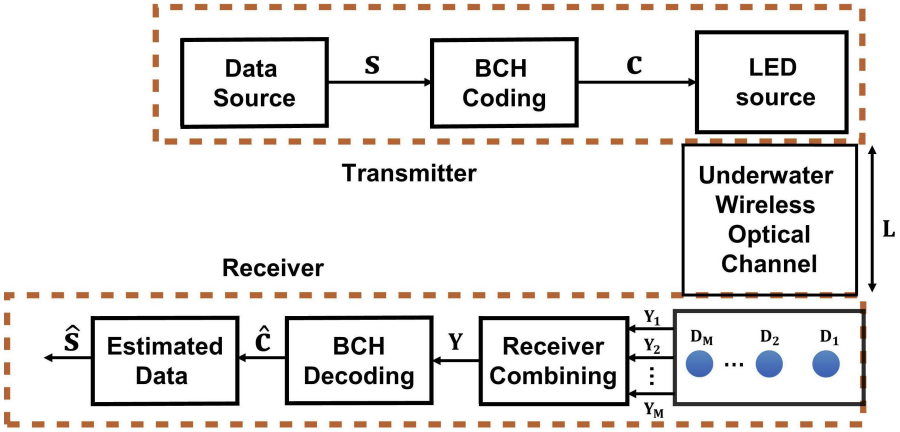

Figure 3.1: Block diagram of BCH coded receiver diversity combining UWOC

bit duration, I_i, η_i and n_i respectively denote the i^{th} channel received irradiance, responsivity of the i^{th} PD and additive Gaussian noise added on the i^{th} channel. Channel noise is assumed to possess zero mean and variance σ^2. The Sources of noise are thermal noise, shot noise and background noise. The resulting noise variance can be calculated by adding the individual variances [Jamali and Salehi (2015), Jaruwatanadilok (2008)]. Hence, $\sigma^2 = \sigma_{th}^2 + \sigma_{ss}^2 + \sigma_{bg}^2$, where variance due to thermal noise, shot noise and background noise can be computed as, $\sigma_{th}^2 = 4K_bT_eB/R_L$, $\sigma_{ss}^2 = 2q\eta I_dB$ and $\sigma_{bg}^2 = 2q\eta P_{BG}B$ respectively, where $K_b = 1.38 \times 10^{-23}\ J/K$ is the Boltzmann constant, $T_e = 256$ is absolute receiver temperature in Kelvin, $B = 2/T_b$ is electronic bandwidth, bit duration $T_b = 1\ \mu s$, $q = 1.6\times10^{-19}\ C$ is the charge of an electron, $\eta = 0.15\ A/W$ is the PD responsivity, $I_d = 1\ nA$ is dark current of the PD, and $P_{BG} = 0.1\ nW$ is the received background noise power. These data are specified from the data sheet [ThorLab's (2017)]. The noise variances due to thermal, shot and background noise are calculated by substituting these values in corresponding noise variance equations. From the obtained values, it is clear that the variance of thermal noise ($\sigma_{th}^2 = 5.6\times10^{-16}$) is approximately six orders of magnitude higher than the variance of shot noise ($\sigma_{ss}^2 = 6.4 \times 10^{-22}$) and approximately seven orders of magnitude greater than background noise variance ($\sigma_{bg}^2 = 9.6\times10^{-24} \approx 1\times10^{-23}$). The noise source in the UWOC link is dominated by thermal noise when compared with noise source due to shot noise and background noise. So the dominant noise mevhanism is Thermal noise which can be modeled by the Gaussian distribution.

3.3 Experimental Set-up

In this section, the major components (LED, PD and underwater channel) involved in the UWOC system and the details of experimental set-ups for receiver diversity techniques are presented.

3.3.1 LED

A blue LED of 470 nm central wavelength $LXML-PB01-0040$ is employed to transmit optical data through the underwater medium. The maximum optical power that can be delivered by this LED source is 500 mW [LumiLED's (2017)].

3.3.2 Photo-diode

Silicon PD FDS 100 is employed at the receiver to detect the transmitted optical data. Figure 3.2 shows the receiver circuit diagram. The power supply voltage undergoes low pass filtering prior to being applied to the PD [ThorLab's (2017)]. This low pass filter is constructed using the resistor-capacitor pair, R_1, C_1. It is used to protect the PD from the sudden changes in the bias voltage. The response of PD (current that depends on incident optical energy) is passed through the load resistance (R_L), which converts incident optical energy into equivalent voltage levels (data reconstruction). We have chosen R_1 equal to 1 $K\Omega$, C_1 equal to 0.1 μF, which yields a low pass filter cut-off frequency of 1.6 kHz, the bias voltage is chosen to be 15 V and load resistance $R_L = 50\ \Omega$.

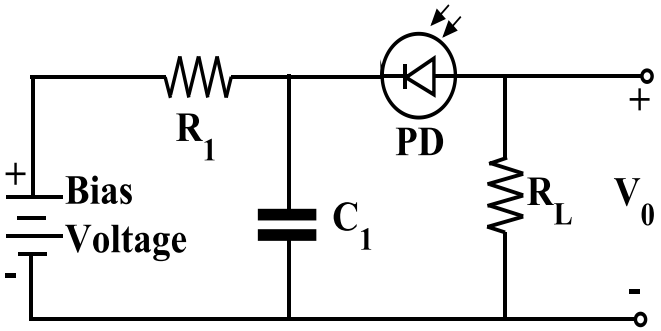

Figure 3.2: Receiver circuit diagram

3.3.3 Underwater channel

Seawater is a mixture of water with various chemical elements and materials, which can induce refractive index variation in the channel. This can cause attenuation

(absorption and scattering) of the propagating optical beam, which affects the performance of the UWOC system. The substances commonly found in seawater are chlorophyll, dissolved organic and inorganic materials and sediment. As a result of the presence of these materials, the medium exhibits turbidity. The measured values of conductivity, salinity, turbidity, absorption, and scattering for a seawater sample collected from the Arabian sea (near NITK Surathkal) have been tabulated in Table 3.1.

Table 3.1: Experimental measurements of seawater

Parameter	Turbidity	Conductivity	Salinity	Absorption	Scattering
Measured Value	8 NTU	22.5 mS/cm	14.28 ppt	0.095 m^{-1}	0.3095 m^{-1}

In addition to attenuation brought about by absorption and scattering, underwater turbulence has the potential to degrade the performance of the UWOC system further. In our set up, we have made arrangements to create an environment to study the effects of these phenomena. To induce turbulence in a turbid environment, four aerating jets (each having an airflow rate of 3 l/m) are used to generate different sized bubbles. Two wavemakers (an airflow rate of 3.5 l/m) are used to generate waves and weak turbulence. In general, river and seawater possess turbidity values equal to approximately 5 and 10 Nephelometric Turbidity Unit (NTU), respectively. So in this chapter, we have realized UWOC system characterized by 5 and 10 NTU turbidity levels. Different values of turbidity are created by the addition of calculated amounts of insoluble particles (Kaolin powder) to the water medium. Figure 3.3 shows the set-up of the seawater channel. The effect of background noise can be minimized using an optical bandpass filter with a central wavelength of 470 nm and a band of 35 nm, which passes the information-bearing signal lying between (470 ± 35) nm and eliminates other wavelength signals. We have employed the BP 470/35 optical bandpass filter in our experimental work.

3.3.3.1 Text data transmission and reception

In Figure 3.4, we have provided samples of the transmitted text and the text material recovered at the receiver in the presence of turbulence at a transmit power of 25 dBm. The figure shows that the turbulence can cause changing higher intensities into lower, resulting in random errors in the received data, which leads to either data corruption or misplaced binary data that can be interpreted with some other alphabet in the received texterror data highlighted with the yellow color in the received data sample.

(a)

(b)

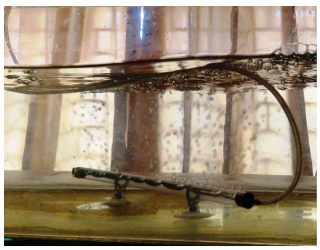

(c)

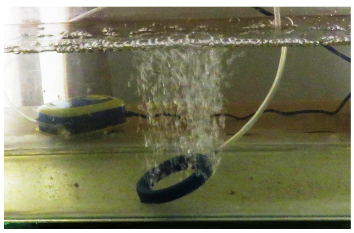

(d)

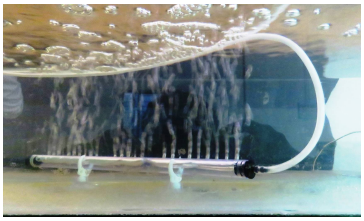

(e)

Figure 3.3: Experimental set-up for the proposed UWOC system (a) Front view, (b) Top view of 5 m link, and (c) Waves and weak turbulence generation using wave maker (d) and (e) Air bubble bubble generation using aerating jets

"Indian Space Research Organisation [ISRO]/Department of Space Centres/Units are engaged in Research and Development activities in development of Space Application, Space Science and Technology for the benefit of society at large and for serving the nation by achieving self-reliance and developing capacity to design and build launch Vehicles and Communication/Remote Sensing Satellites and thereafter launch them. ISRO strives to serve the nation in the areas of television broadcast, Location based services, telecommunication, meteorological application and in management of our natural resources. The Indian Space Programme continues to pursue successful goals on all fronts in meeting the objective of achieving self-reliance in space technology and its applications for national development"

(a)

"Indian plce Researc' Organisati/j [ASRO]/Department of Space Centres/Units are engaged hn Recearah and DepElopment activities in developme,t of SOace Applicataon, Spaca Science and Technology for the bodnefht of society ' t large and fgr seRvine the nation by achieving self-redia.cE an' developing capa#iliy to design and buidd Laench Vahicles al Coemtrication-Remote ensing Satellies and thereafter launch them. ISRO strives to serve the notion in the Argas of television broadcast, Location based serVices teleco0mum.cation, mereorological application and in managhyment of our nat'ral resources. jhe Indian Srace Programmd continues to purrue succeszful g#als on all frjkts in meeting the obolctive of achimving self-reliajce in space technoloty and ids applicattois for national develnpient"

(b)

Figure 3.4: (a) Transmitted data (b) Received data

3.3.4 Channel Estimation

In order to understand the behavior of the channel, a sequence of pilot bits were transmitted through the channel of length 5 m, width 0.5 m and height 0.5 m at turbidity level of 10 NTU. The distribution of received optical power at the receiver is shown in Figure 3.5. It is observed that there is a good fit with the Log-Normal density function.

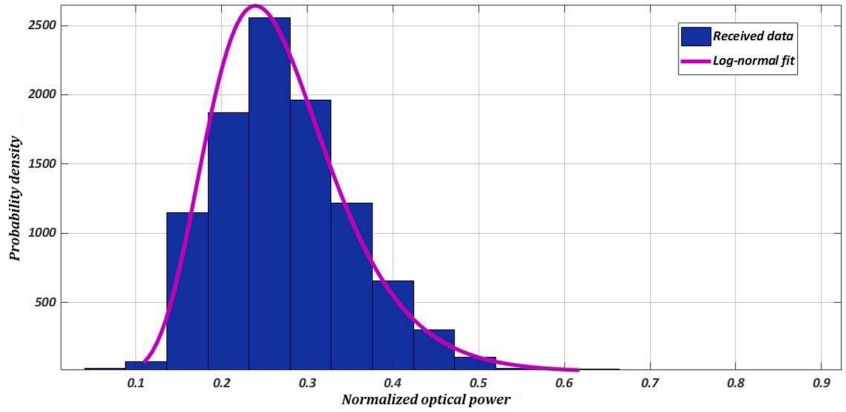

Figure 3.5: Histogram of received data with log-normal fit

3.3.5 Receiver diversity

In this system, a single LED source has been deployed at the transmitter and M identical PDs have been deployed at the receiver. The responses of the M PDs are combined using three different strategies to enhance the performance of the UWOC system. A comparison of their relative efficacies is also determined. The three diversity techniques employed in this chapter are Selection Combining (SC), Majority Logic Combining (MLC) and Equal Gain Combining (EGC). These strategies are outlined in the next section.

3.3.5.1 Selection Combining

SC selects maximum received irradiance among all the PD's response. Figure 3.6 shows the receiver of $1 \times M$ SC scheme, where $Y_1,\ Y_2, \ldots,\ Y_M$ are PD responses. The most superior response Y is (maximum) among $Y_1,\ Y_2, \ldots,\ Y_M$ is determined and estimated data $\hat{s}$ obtained by passing the combined response Y through a two level comparator. The block diagram of the system is illustrated in Figure 3.6.

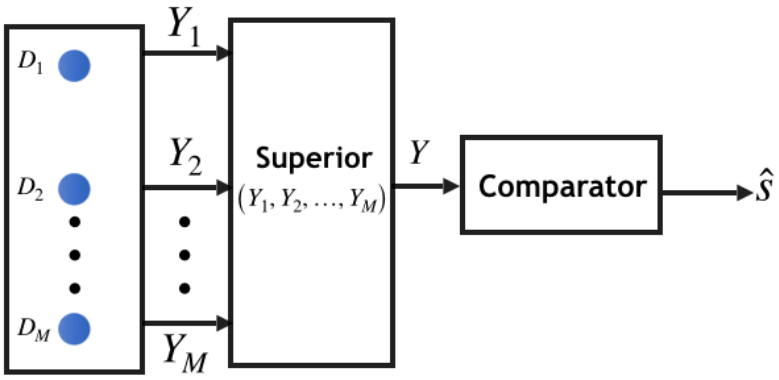

Figure 3.6: $1 \times M$ selection combining

3.3.5.2 Majority Logic Combining

MLC scheme recovers the data transmitted over the channel by determining the majority of the logical responses of all PDs employed at the receiver. Figure 3.7 shows the receiver of $1 \times M$ MLC scheme, where *mode* represents majority of incoming responses. $Y_1,\ Y_2, \ldots,\ Y_M$ represent the responses of the PDs, $\hat{s}_1,\ \hat{s}_2, \ldots,\ \hat{s}_M$ represent the comparator responses and $\hat{s}$ is majority of $\hat{s}_1, \hat{s}_2, \ldots, \hat{s}_M$.

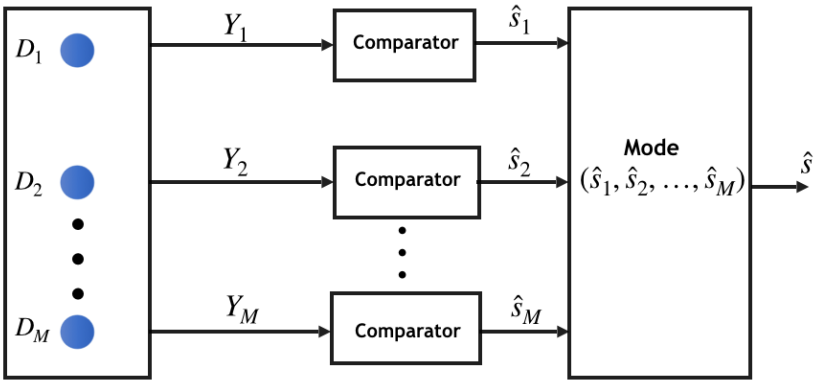

Figure 3.7: $1 \times M$ majority logic combining

3.3.5.3 Equal Gain Combining

In EGC scheme, the combined response is average of response obtained by M PDs i.e, $Y = \sum_{i=1}^{M} \frac{Y_i}{M}$. Estimated data can be obtained by passing the EGC combined data to a comparator of a suitable threshold. Figure 3.8 is the receiver of $1 \times M$ EGC scheme.

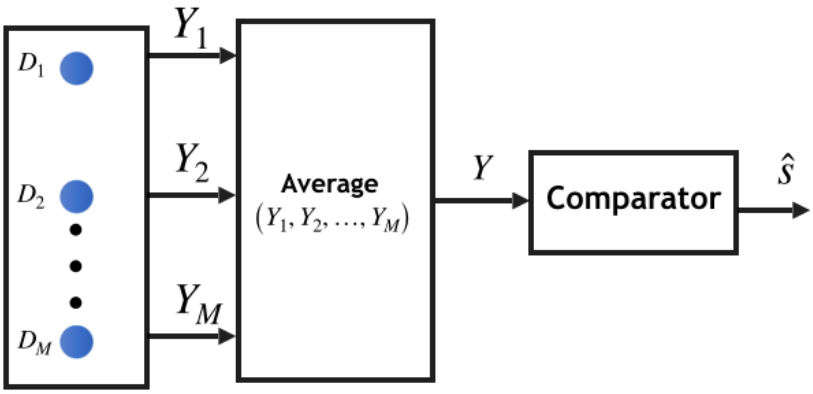

Figure 3.8: $1 \times M$ equal gain combining

3.4 Bose-Chaudhuri-Hocquenghem codes

In underwater channels, optical data can be attenuated (absorption and scattering) due to the presence of turbidity in the medium [Davies-Colley and Smith (2001)]. Hence, there is a finite probability that the transmitted data can be distorted and corrupted. This corruption introduces errornous bits in the data stream. In order to detect and correct errors introduced by the medium, a suitable channel code has to be employed. Based on the experimental observation, the turbid underwater channel set up by us was adding 30% errors on an average in the transmitted data stream (three out of ten bits on an average were observed to be in error). So we have chosen to employ the ($n = 31,\ k = 11$) BCH code to detect and correct errors introduced by the channel in this study. BCH codes constitute a family of powerful error correcting codes. They are designed to correct t bits in error over a span of $n = 2^m - 1$ bits. They are defined over the Galois Field $GF(2^m)$, where m is any real positive integer ($m \geq 3$). The field elements are represented by $\{0,\ 1,\ \alpha,\ \alpha^2, \ldots,\ \alpha^{2^m-2}\}$ (where α is a primitive element in the field $GF(2^m)$) [Lin and Costello (2001), MacWilliams and Sloane (1977)]. These elements are partitioned into conjugacy classes. Each conjugacy class has an associated minimal polynomial. The generator polynomial of a BCH code is obtained by determining the least common multiple of the minimal polynomials associated with the elements $\alpha^b,\ \alpha^{b+1}, \ldots,\ \alpha^{b+\delta-2}$, where b is an integer ≥ 1 and δ is the design distance, which equals to $2t + 1$. The generator polynomial is computed as,

$$g(x) = LCM\{M_b(x),\ M_{b+1}(x), \ldots,\ M_{b+\delta-2}(x)\} \tag{3.2}$$

where, $M_i(x)$ represents the minimal polynomial of i^{th} conjugacy class. Elements in the same conjugacy class have same minimal polynomial. The generator polynomial for the BCH code employed in our set up is specified by parameters, $m = 5$, $t = 4$ and $b = 1$ is $g(x) = LCM\{M_1(x),\ M_2(x),\ M_3(x),\ M_4(x),\ M_5(x),\ M_6(x),\ M_7(x),\ M_8(x)\} = M_1(x) \times M_3(x) \times M_5(x) \times M_7(x)$. Minimal polynomials of various conjugacy classes contained in the field $GF(2^5)$ are specified in Table 3.2. The generator polynomial obtained by computing the product of minimal polynomials is,

$$g(x) = 1 + x^2 + x^4 + x^6 + x^7 + x^9 + x^{10} + x^{13} + x^{17} + x^{18} + x^{20} \tag{3.3}$$

Table 3.2: Minimal polynomials of $GF(2^5)$ for $t = 4$

Congugacy Class	**Minimal Polynomial**
$\{\alpha,\ \alpha^2,\ \alpha^4,\ \alpha^8,\ \alpha^{16}\}$	$M_1(x) = 1 + x^2 + x^5$
$\{\alpha^3,\ \alpha^6,\ \alpha^{12},\ \alpha^{24},\ \alpha^{17}\}$	$M_3(x) = 1 + x^2 + x^3 + x^4 + x^5$
$\{\alpha^5,\ \alpha^{10},\ \alpha^{20},\ \alpha^9,\ \alpha^{18}\}$	$M_5(x) = 1 + x + x^2 + x^4 + x^5$
$\{\alpha^7,\ \alpha^{14},\ \alpha^{28},\ \alpha^{25},\ \alpha^{19}\}$	$M_7(x) = 1 + x + x^2 + x^3 + x^5$

A generator matrix representation for the BCH code is also possible. For our code, the generator matrix ($\mathbf{G}_{11\times31}$) is obtained by carrying out certain algebraic manipulations on the generator polynomial $g(x)$[Lin and Costello (2001)] . Encoded data is obtained by carrying out the operation, $\mathbf{c}_{1\times31} = \mathbf{s}_{1\times11}\mathbf{G}_{11\times31}$. This BCH encoded data is transmitted over the water medium (channel) using the LED as the modulating device. At the receiver, the data is passed through a two-level comparator with suitably designed thresholds, which are used to regenerate the data stream. This data may contain errors introduced by the channel. The Berlekamp-Massey decoding algorithm is employed to detect and correct errors in the received bitstream [Blahut (2003), Moon (2005)].

3.5 Analytical evaluation of UWOC system

In this section, we present the distribution of UWOC channel and closed-form analytical BER expressions for SISO link and $1 \times M$ receiver diversity combining schemes with and without BCH code.

3.5.1 Channel Model

Based on the experimental results obtained in Section 3.3.4, the received irradiance behavior is observed to fit the log-normal density function with fair accuracy.

Hence, the log-normal density function is considered as a turbulence channel model for further analysis. The amount of attenuation depends on the level of turbidity in the medium. The received irradiance in the presence of attenuation and weak turbulence can be characterized as [Yang *et al.* (2014)],

$$I = I_a I_t \tag{3.4}$$

where, I_a is deterministic path loss constant due to the beam attenuation and is given as $I_a = \exp(-\left(C(\lambda)\right) L)$ from Beer-Lambert's law, $C(\lambda)$ is an attenuation coefficient [Farid and Hranilovic (2007)], L is link-range and I_t represents the received irradiance due to turbulence only. The received irradiance due to weak underwater turbulence is modeled with log-normal density function [Jamali *et al.* (2018)], which is given as,

$$f_{I_t}(I_t) = \frac{1}{2I_t} \frac{1}{\sqrt{2\pi\sigma_X^2}} \exp\left(-\frac{\left(\ln(I_t) - 2\mu_X\right)^2}{8\sigma_X^2}\right) \tag{3.5}$$

where, μ_X and σ_X^2 are mean and variance of Gaussian random variable $X = \frac{1}{2}\ln(I_t)$. The density function of combined turbulence and attenuation effect can be obtained as,

$$\begin{aligned} f_I(I) &= \left|\frac{d}{dI}\left(\frac{I}{I_a}\right)\right| f_{I_t}\left(\frac{I}{I_a}\right) \\ &= \frac{1}{I_a} \frac{1}{2\left(\frac{I}{I_a}\right)} \frac{1}{\sqrt{2\pi\sigma_X^2}} \exp\left(-\frac{\left(\ln\left(\frac{I}{I_a}\right) - 2\mu_X\right)^2}{8\sigma_X^2}\right) \\ &= \frac{1}{2I} \frac{1}{\sqrt{2\pi\sigma_X^2}} \exp\left(-\frac{\left(\ln\left(\frac{I}{I_a}\right) - 2\mu_X\right)^2}{8\sigma_X^2}\right) \end{aligned} \tag{3.6}$$

From the received pilot data, the mean and variance are to be $\mathbb{E}(I) = 0.989$ and $\sigma_I^2 = 4.8 \times 10^{-3}$ respectively. The mean and variance are respectively described by $\mathbb{E}(I) = \exp(2\mu_X + 2\sigma_X^2)$ and $\sigma_I^2 = \exp(4\sigma_X^2 - 1) \times \exp(4\sigma_X^2 + 4\mu_X)$. Populating appropriate values yields, $\mu_X = -6.7 \times 10^{-3}$ and $\sigma_X^2 = 1.2 \times 10^{-3}$. Table 3.3, shows the received data for 10^6 pilot data transmission.

Table 3.3: Received data set.

0.98825536439977	1.0228888404955	0.96681139274698	0.89970893515784
0.96894098088205	0.98532122890725	0.93039499853506	0.83960987332535
0.87401453771718	0.98431529500565	0.91301336043288	0.89243963231010
0.96735428548950	0.93360828293968	1.1753975471035	1.0097536729997
0.93146345734679	1.0588477135665	1.1066041116613	1.0138823818039
0.92191098113213	0.97724550626770	1.0073800102366	1.0105431171245
0.91021754647693	0.99033520912399	0.90488987909327	0.97823216464380
⋮	⋮	⋮	⋮
⋮	⋮	⋮	⋮
1.05485548236646	0.947233992320477	1.04230115005729	1.04741226122348

3.5.2 BER evaluation

In this subsection, the closed-form analytic BER expressions for SISO, $1 \times M$ SC, MLC and EGC combining schemes with and without BCH code have been determined.

3.5.2.1 Single Input Single Output

The received OOK modulated data in the presence of turbulent underwater channel is modeled as,

$$Y = \eta I \sqrt{P_t T_b} s + n \tag{3.7}$$

The BER reduces to the form,

$$P_{siso} = \int_0^\infty \mathbb{Q}\left(r\eta I \sqrt{\frac{P_t T_b}{4\sigma^2}}\right) f_I(I)\, dI \tag{3.8}$$

where, r is code-rate, '1' for un-coded system and equal to k/n for $(n,\ k)$ coded system and $\mathbb{Q}(z) \triangleq \frac{1}{\sqrt{2\pi}} \int_z^\infty \exp\left(-\frac{y^2}{2}\right) dy$. Substituting I by $\exp(2x)$ and then evaluating Equation (3.8) using Gauss-Hermite quadrature polynomial (given in Appendix B) yields,

$$P_{siso} \approx \frac{1}{\sqrt{\pi}} \sum_{i=1}^{l} W_i \mathbb{Q}\left(\zeta I_a \exp\left(x_i \sqrt{8\sigma_X^2} + 2\mu_X\right)\right) \tag{3.9}$$

where, W_i is the weight of i^{th} order approximation and $\zeta = r\eta\sqrt{\frac{P_t T_b}{4\sigma^2}}$. P_{siso} is calculated for instantaneous values of x.

3.5.2.2 Selection Combining

Selection combining technique is based on selecting the output of that PD which provides the maximum irradiance among all receivers. The received signal using selection combining is expressed as,

$$Y = \max\{Y_1,\ Y_2,\ \ldots,\ Y_M\} = \eta\sqrt{P_t T_b} s I_{sc} + n \tag{3.10}$$

where $I_{sc} = \max\left(I_1 I_a,\ I_2 I_a, \ldots,\ I_M I_a\right)$. The received signal is completely dependent on maximum irradiance. The BER when the ouputs of M number of PDs are aggregated using selection combining with single-source OOK modulated channel input is expressed as,

$$P_{sc} = \int_0^\infty f_{I_{sc}}(I_{sc}) \mathbb{Q}\left(\zeta I_{sc}\right) dI_{sc} \tag{3.11}$$

The Probability Density Function (PDF) of SC scheme $f_{I_{sc}}(I_{sc})$ is expressed as (refer Appendix C),

$$f_{I_{sc}}\left(I_{sc}\right) = \frac{M}{2I_{sc}\sqrt{2\pi\sigma_X^2}} \exp\left(-\frac{\left(\ln(I_{sc}/I_a) - 2\mu_X\right)^2}{8\sigma_X^2}\right)\left(\frac{1}{2} + \frac{1}{2} erf\left(\frac{\ln(I_{sc}/I_a) - 2\mu_X}{\sqrt{8\sigma_X^2}}\right)\right)^{M-1} \tag{3.12}$$

where, $erf(x) \triangleq \frac{2}{\sqrt{\pi}} \int_0^x \exp\left(-t^2\right) dt$. Substituting equation (3.12) in equation (3.11) which yields,

$$P_{sc} = \frac{M}{\sqrt{\pi}} \int_0^\infty \exp\left(-h^2\right) Q\left(\zeta I_a \exp\left(h\sqrt{8\sigma_X^2} + 2\mu_X\right)\right) \times \left(\frac{1}{2} + \frac{1}{2} erf\left(h\right)\right)^{M-1} dh \tag{3.13}$$

where, $h = \left(\ln(I_{sc}/I_a) - 2\mu_X\right)/\sqrt{8\sigma_X^2}$. equation (3.13) is computed using Gauss-Hermite quadrature polynomial (given in Appendix B) as,

$$P_{sc} \approx \frac{M}{\sqrt{\pi}} \sum_{i=1}^{l} W_i Q\left(\zeta I_a \exp\left(h_i\sqrt{8\sigma_X^2} + 2\mu_X\right)\right)\left(\frac{1}{2} + \frac{1}{2} erf\left(h_i\right)\right)^{M-1} \tag{3.14}$$

where W_i and h_i are calculated for various values of I_{sc}.

3.5.2.3 Majority Logic Combining

MLC scheme recovers the transmitted data over the channel based on the majority of the logical responses. In this scheme, the link between the source LED to individual PD is modeled like a SISO link, so the final MLC response is dependent

on M individual SISO links. The probability of error is evolved as,

$$P_{mlc} = \sum_{i=\lfloor \frac{M+1}{2} \rfloor}^{M} \binom{M}{i} P_{siso}^{i} \left(1 - P_{siso}\right)^{M-i} \tag{3.15}$$

where, $\lfloor \cdot \rfloor$ is floor operator and P_{siso} is BER of SISO obtained from equation (3.9).

3.5.2.4 Equal Gain Combining

The average of M identical PD's responses are combined to obtain a suitable EGC response. The combined response is $Y = \frac{\eta\sqrt{P_t T_b} s I_e}{M} + n$, where $I_e = I_a I_{sum}$ and $I_{sum} = \sum_{i=0}^{M} I_i$. The sum of M independent log-normal random variables having identical mean and variance is also a log-normally distributed random variable [Fenton (1960)]. Hence, $I_{sum} = \exp(2U)$ is log-normal distributed random variable, here U is Gaussian distribute random variable with mean μ_U and variance σ_U^2 [Lee and Chan (2004)]. The density function is given as,

$$f_{I_e}(I_e) = \frac{1}{2I_e\sqrt{2\pi\sigma_U^2}} \exp\left(-\frac{\left(\ln(I_e/I_a) - 2\mu_U\right)^2}{8\sigma_U^2}\right) \tag{3.16}$$

where, the Gaussian mean and variance are $\mu_U = \frac{1}{2}\ln(M\mathbb{E}(I)) - \sigma_U^2$ and $\sigma_U^2 = \frac{1}{4}\ln\left(1 + \frac{\exp(4\sigma_X^2)-1}{M}\right)$ respectively, the detailed derivation is given in Appendix D.

The BER equation of EGC with OOK modulation is obtained in a similar way of equation (3.9) as,

$$P_{egc} \approx \frac{1}{\sqrt{\pi}} \sum_{i=1}^{l} W_i \mathbb{Q}\left(\frac{\zeta I_a}{M} \exp\left(x_i\sqrt{8\sigma_U^2} + 2\mu_U\right)\right) \tag{3.17}$$

3.5.2.5 BCH Code

When decoded code-word is not identical to the transmitted code-word, a decoding error is said to occur. An upper bound on the probability of decoding error P_d associated with a $(n,\ k,\ t)$ binary BCH code over $GF(2^m)$ with t symbol error correcting capability and cross over symbol error probability p is given by [Blahut (2003)],

$$P_d \leq \sum_{i=t+1}^{n} \binom{n}{i} p^i \left(1 - p\right)^{n-i} \tag{3.18}$$

where p represents the binary symmetric channel transition probability. In our analysis, p corresponds to P_{siso} in equation (3.9), P_{sc} in equation (3.14), P_{mlc} in

Table 3.4: System parameters

System parameters	Value
Wavelength (λ)	470 nm
Bandwidth (B)	2 MHz
Noise variance (σ^2)	5.65×10^{-16}
Temperature (T_e)	256 k
Responsivity (η)	0.15 A/W
Background noise power (P_{BG})	0.1 nW
Attenuation coefficient (C)	0.303 m^{-1}

equation (3.15) and P_{EGC} in equation (3.17) for SISO, SC, MLC and EGC schemes with code-rate $r = \frac{k}{n}$ respectively.

3.6 Experimental and Analytical Results

The system parameters are listed in the Table 3.4. In the proposed UWOC system, the information bit stream at the transmitter is processed through the BCH encoder and then OOK modulated using 470 nm blue light LED ($LXML-PB01-0040$). The modulated data is propagated through the turbid water channel which is created using insoluble particles (Kaolin powder). Turbulence in the channel is created using underwater jets and wavemaking paddles. At the receiver side, the optical beam is detected and information stream is retrieved using multiple PD's employed with appropriate combining schemes.

In this section, we present analytical and experimental BER results with respect to transmit power for SISO, 1×3 receiver combining (SC, MLC and EGC) schemes with and without coding for channels having turbidity values of 5 and 10 NTU respectively. The values of attenuation coefficients at $\lambda = 470$ nm wavelength determined using spectrophotometer are $C = 0.303$ m^{-1} for 5 NTU and $C = 0.4505$ m^{-1} for 10 NTU turbidity channel.

Figure 3.9 shows the un-coded experimental and analytical BER results of 5 and 10 NTU turbidity level turbulent underwater channels respectively. Figure 3.9a (5 NTU), shows that a transmit power gain of more than 1 dB can be obtained by using SC, 3 dB using MLC and 5 dB using EGC over SISO at BER of 10^{-5}. From Figure 3.9b, (10 NTU) it can be inferred that a power gain of 0.3 dB can be obtained by using SC, 3.5 dB using MLC and 5 dB using EGC over SISO at a BER of 10^{-5}.

Figure 3.10 illustrates the results obtained by employing a ($n = 31,\ k = 11$) BCH code in the UWOC set up. The experimental and analytical BER results

obtained by passing optically modulated data at 5 NTU and 10 NTU turbidity levels respectively are illustrated in Figure (3.10a). From this plot it can be inferred that BCH coded SC scheme can deliver a transmit power gain of 0.3 dB, BCH coded MLC can deliver a transmit power gain of 2 dB and BCH coded EGC can deliver a transmit power gain of 4.5 dB over BCH coded SISO at BER of 10^{-5}. Similarly, for 10 NTU turbidity channel more-than 3 dB transmit power gain from MLC to SISO and 4 dB transmit power gain from coded EGC to coded SISO can be observed. Thus we can conclude that a transmit power gain of at least 3 dB is available when a $(n = 31,\ k = 11)$ BCH coded diversity reception is employed.

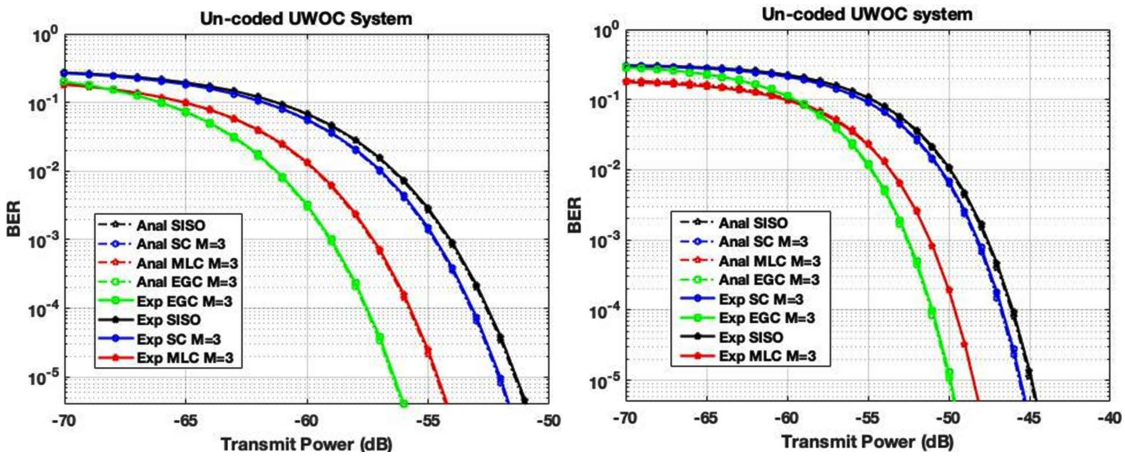

Figure 3.9: BER results of (a)Un-coded for 5 NTU turbid channel, (b) Un-coded for 10 NTU turbid channel.

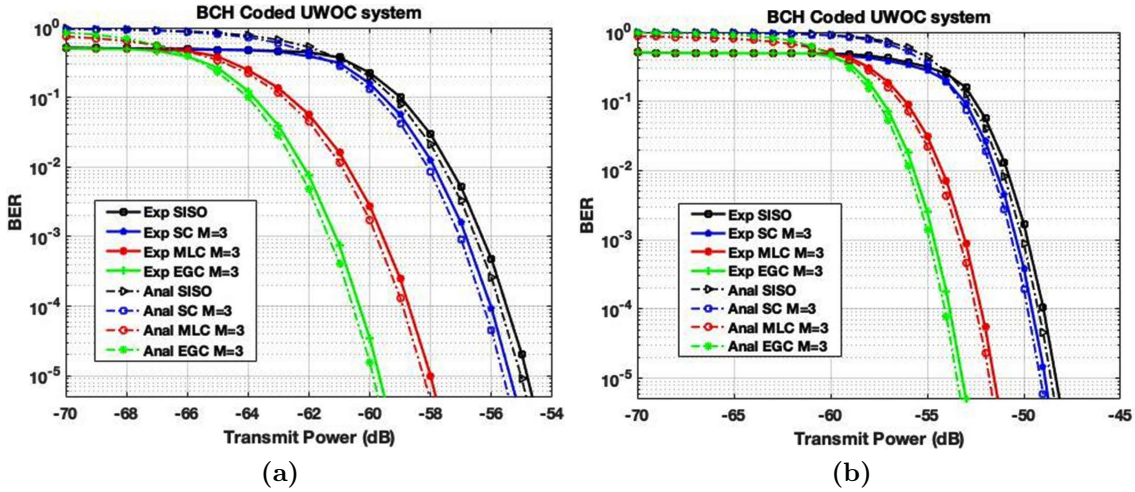

Figure 3.10: BER results of (a) BCH Coded for 5 NTU turbid channel (b) BCH Coded for 10 NTU turbid channel.

3.7 Conclusion

The statistical distribution of received irradiance in an underwater channel filled with seawater in the presence of turbidity and turbulence has been experimentally evaluated. The closed-form expressions for the BER of a UWOC system with OOK modulation in the presence of weak turbulence induced by air bubbles and beam attenuation for a 5 m link evaluated. We have demonstrated the accuracy of these analytic results by cross-checking the BER values obtained from these expressions with experimental data obtained by setting up an OOK modulated UWOC system with a 470 nm LED source working in an environment characterized by turbulence generated by air bubbles for a given channel. In the last part of the chapter, experimental BER results obtained in the presence of turbulence-induced air bubbles at 5 and 10 NTU turbidity levels have been evaluated and plotted. From the plots presented in the chapter, it has been demonstrated that at most 8 dB transmit power improvement can be obtained by the use of BCH coded EGC when compared with un-coded SISO for both turbidity levels.

Chapter 4

High-Speed and Reliable UWOC System using MIMO and Channel Coding Techniques

In this chapter, we investigate the performance of an UWOC system employing on-off keying modulation at a data-rate of 500 Mbps. Transmit/ receive diversity schemes, namely Multiple-Input to Single-Output (MISO), Single-Input to Multiple-Output (SIMO) and Multiple-Input to Multiple-Output (MIMO) techniques with and without RS-coding have been employed to mitigate the effects of weak oceanic turbulence and beam attenuation. Several novel closed-form analytical Bit Error Rate (BER) expressions pertaining to Single-Input to Single-Output (SISO), SIMO, MISO and MIMO links for un-coded and RS-coded cases have been computed using the hyperbolic tangent distribution and validated with Monte-Carlo simulation results. The obtained BER results show that the use of (63, 51) RS-coded 4×5 MIMO UWOC system offers at-least 35 dB of transmit power gain compared with the un-coded SISO UWOC system at a BER of 10^{-5}. At this point in time, it is evident that emerging technologies like the fifth-generation (5G) networks and the Internet of Underwater Things (IoUT) will have a high impact on the design of UWOC systems in future. These systems require a high degree of information integrity, high data rates and energy efficiency when employed for the purpose of data transfer between underwater vehicles and objects. The proposed RS coded MIMO UWOC system offers high reliability along with power efficiency and it has the potential to be gainfully employed in IoUT applications.

4.1 Introduction

In recent years, a number of researchers have turned their attention to the study, analysis and design of UWOC systems. This is because of the advantage of high transmission speeds and reliable communication over short-medium ranges ($\sim$ tens-hundreds of meters) in the ocean/seawater channels. Recently, it has been proposed that underwater sensors can be interconnected with the data aggregating nodes through UWOC links to achieve high data-rate and reliability using IoUT [Domingo (2012), Kao *et al.* (2017)]. The major limiting factors of the UWOC systems are beam absorption, scattering and underwater turbulence. Absorption reduces the intensity level and scattering causes deviation of the beam path away from the line of sight path directed towards the receiver. The combined effect of absorption and scattering will result in optical beam attenuation. The effect of attenuation can be minimized by the use of optical sources operating in the range $400 - 530$ nm wavelength [Kaushal and Kaddoum (2016), Ramavath *et al.* (2018)].

4.1.1 Contributions

The contributions of this chapter are as follows. The BER performance of an On-Off Keying (OOK) modulation based UWOC system in medium experiencing weak turbulence has been studied in this chapter. We have sought to understand and model the behavior of light wave propagation through a medium characterized by weak turbulence and propagation loss. We have taken up SISO, SIMO, MISO and MIMO schemes for study and evaluation. The improvement in performance of the links by employing a (63, 51) RS-code is determined and compared with un-coded system performance. RS-codes are employed in such applications because of their moderate encoding/ decoding complexity and ability to correct burst errors [Simpson *et al.* (2010)]. In our study, the transmission speed is fixed at 500 $Mbps$. This data transfer speed has been employed by many researchers working in this domain [Wang *et al.* (2019)]. The analytical closed-form expressions for the BER have been derived by use of the Hyperbolic Tangent Distribution (HTD) family and validated with Monte-Carlo simulations. Throughout this chapter, the performance improvement is defined in terms of 'transmit power gain', which is the reduction in transmit power observed to obtain a BER of 10^{-5} when the two competing schemes are compared.

The remaining part of the chapter is organized as follows. Section 4.2 describes the system and channel model of UWOC system. RS-code encoding and decoding are presented in Section 4.3. A closed-form expression for the BER pertaining

to the UWOC system employing different diversity and MIMO techniques for uncoded and RS-coded cases are presented in Section 4.4. Monte-Carlo simulation and analytical results specifying the BER as a function of transmit power are provided in Section 4.5. The chapter is concluded in Section 4.6 with a brief discussion of the analytic and simulation results obtained and their significance.

4.2 System and Channel Model

The system and channel models of a UWOC link operating under the influence of weak oceanic turbulence and beam attenuation scenarios are presented in this section.

4.2.1 System Model

Consider an OOK modulated UWOC system with N number of LASER sources ($\lambda = 470\ nm$ wavelength) at the transmitter and M number of photo-detectors (PD) at the receiver. The same data is transmitted from all the sources and the data symbols received by M detectors are combined using EGC. Figure 4.1, depicts the UWOC system schematic diagram. We have considered an UWOC system with a link-range of $L = 300\ m$ between the transmitter-receiver array and a separation of $\Delta l = 0.05\ m$ between the adjacent PDs. The LASER sources (represented with $T_1,\ T_2, \cdots,\ T_N$ in Figure 4.2) are assumed to be in line of sight path with the detectors (represented with $D_1,\ D_2, \cdots,\ D_M$ in Figure 4.2) and the Divergence Angle (DA) of LASER sources are within the Field Of View (FOV) of all available PDs as shown in Figure 4.2 [Dong and Liu (2016), Zhang and Dong (2016)]. This requirement can be realized with the help of collimating lens at the receiver as shown in Figure 4.3. A collimating lens of focal length f_r and diameter d_r is placed at a distance d from the array of PDs (d is chosen such that the transmitter can point to all the PDs at the same time) [Ghazy *et al.*]. Hence, the LASER source is able to convey energy to all M PDs simultaneously. Figures 4.2 and 4.4 illustrate the link geometry and structure of the MIMO UWOC transmitter and receiver array.

A binary '1' is communicated with P_t watts of optical power (amplitude across individual source is $A = \sqrt{P_t T_b / N}$ among N available sources) and a binary '0' is communicated with 0 watts of optical power (amplitude $A = 0$) for a duration of $T_b\ sec$ (Conventional OOK modulated system) through the N sources. The

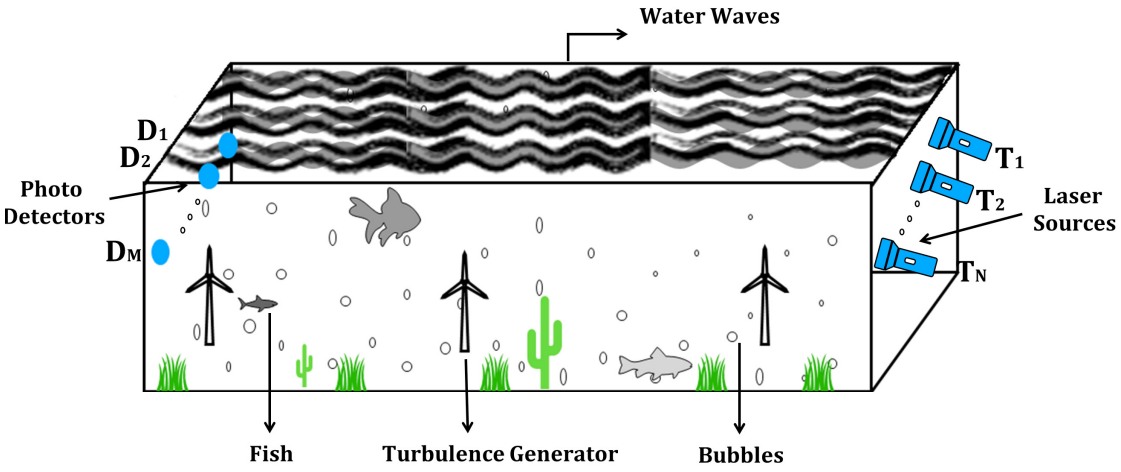

Figure 4.1: Schematic diagram of a UWOC system.

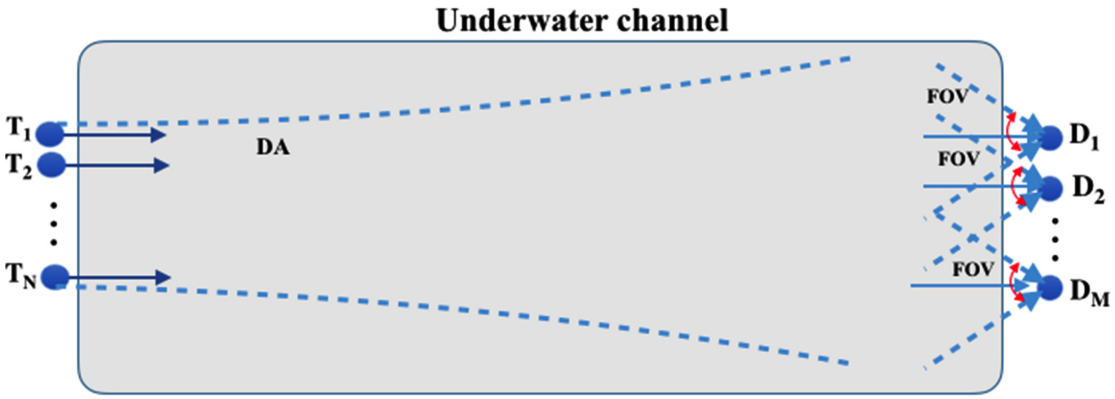

Figure 4.2: Link geometry of MIMO UWOC system.

received symbol at the i^{th} PD can be expressed as [Popoola *et al.* (2008)],

$$Y_i = \eta_i A \left(\sum_{j=1}^{N} I_{ij} \right) s + n_i = \eta_i \sqrt{\frac{P_t T_b}{N}} \left(\sum_{j=1}^{N} I_{ij} \right) s + n_i, \quad 1 \leq i \leq M \tag{4.1}$$

In this expression, Y_i represents the response of i^{th} PD after trans-impedance amplification. This quantity is expressed in terms of volts. P_t represents the transmit power per bit (mW), $s \in (0, 1)$ represents the information bits, η_i represents detector's responsivity (A/W), I_{ij} is irradiance received from j^{th} source to i^{th} detector and channel noise n_i is the additive white Gaussian noise with zero mean and variance σ^2. Here, we have assumed the source of noise variance to be thermal noise only and ignored the noise variance due to background and shot noise (due to these noise variances being significantly smaller in magnitude than the variance of thermal noise source). Thus, noise variance is specified as $\sigma^2 = 4K_b T_e B/R_L$, where $K_b = 1.38 \times 10^{-23}\ J/K$ is the Boltzmann's constant, $T_e = 256\ K$ is the

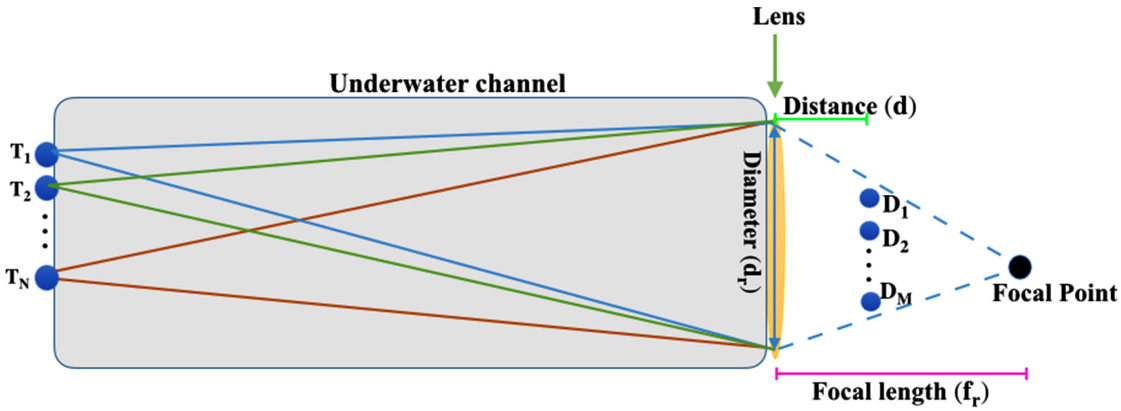

Figure 4.3: Line of sight obtained using collimating lens.

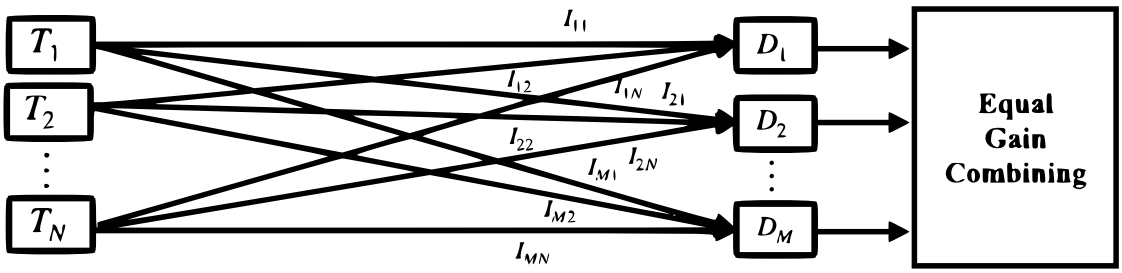

Figure 4.4: Structure of transmit and receive array.

absolute receiver temperature, $B = 2\ GHz$ is electronic bandwidth, $R_L = 100\ \Omega$ is load resistance of the detector, which leads the noise variance $\sigma^2 = 2.82 \times 10^{-13}$ [Jamali and Salehi (2015)].

4.2.2 Channel model

In this section, we present the channel models in the presence of weak turbulence and beam attenuation.

4.2.2.1 Attenuation channel model

UWOC channel exhibits beam attenuation due to absorption and scattering. Beam attenuation in UWOC channel is deterministic in nature and it can be determined by use of Beer-Lambert's law, which is given as [Kaushal and Kaddoum (2016)],

$$I_a = \exp\left(-C(\lambda)L\right) \tag{4.2}$$

In this expression, $C(\lambda) = A(\lambda) + B(\lambda)$ is attenuation coefficient, $A(\lambda)$ and $B(\lambda)$ are absorption and scattering coefficients respectively and these values changes with the different wavelength sources and different types of water.

As is evident from Figure 4.5, the spacing between the neighboring PDs is fixed at $\Delta l = 0.05m$. Assuming that LASER 1 and PD1 are linearly placed (no elevation angle between them), the maximum distance between a given LASER source at transmitter end and the most distant PD (*i.e.*, M^{th} PD) at the receiver is $\sqrt{L^2 + ((M-1)\Delta l)^2} \approx L$ (for $M < 10$). This model can be repeated for each transmitting laser source and each one of the PDs at the receiver. The link-range between the source to all possible detectors is approximately equal to L, so the effect of attenuation will nearly same for all PDs. We have presented an analysis below that confirms that the Beer-Lambert's law is applicable to this arrangement of optical sources and receivers.

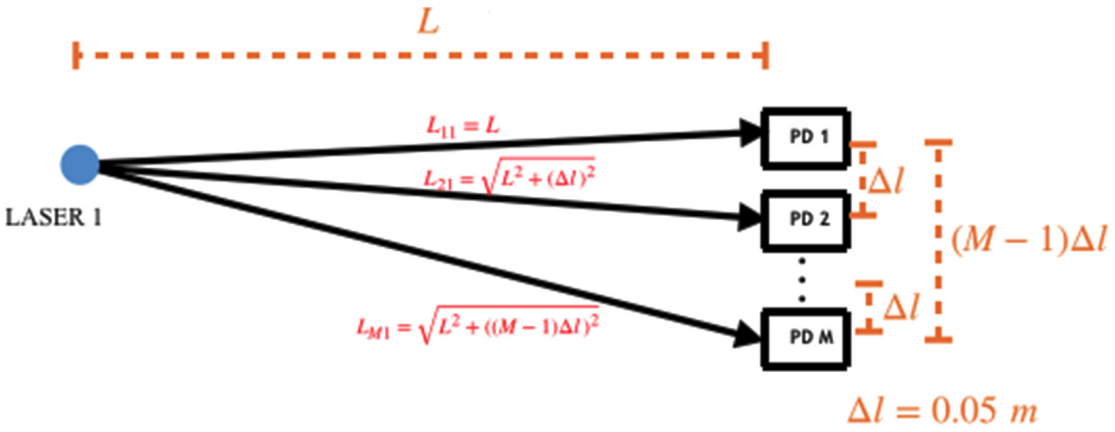

Figure 4.5: Link-range variation between source to M detectors.

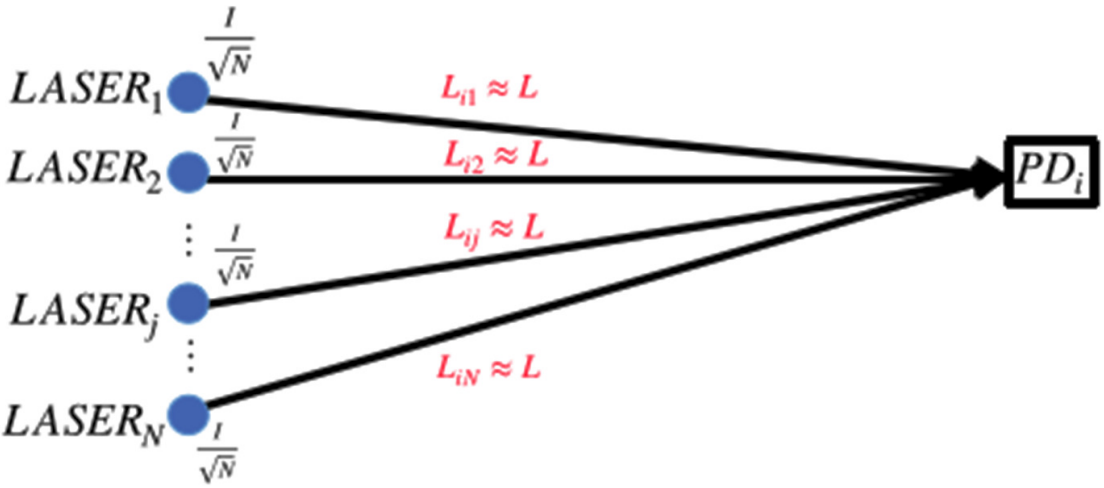

Figure 4.6: Received intensity of multiple source to single detector.

As a MIMO scheme with N transmitting sources is being used, the drive current to each source is scaled by $\frac{1}{\sqrt{N}}$. This is done to arrive at a meaningful comparison

with a SISO and SIMO system operating with the same total power. Figure 4.6 shows the N number of LASER sources where each source produces an intensity equal to $\frac{I}{N}$. This optical power is communicated through the medium in the presence of channel induced attenuation to the PD array. The received intensity at the detector (assuming attenuation as the loss factor) is the sum of intensities delivered by all of the N transmitting sources. The received intensity at the i^{th} PD can be specified as $Y_i = Y_{i1} + Y_{i2} + \cdots + Y_{iN}$; where $1 \leq i \leq M$, $Y_{i1} = \frac{I}{N}e^{-cL_{i1}}$, $Y_{i2} = \frac{I}{N}e^{-cL_{i2}}, \cdots, Y_{ij} = \frac{I}{N}e^{-cL_{ij}}$ and $Y_{iN} = \frac{I}{N}e^{-cL_{iN}}$. Hence, the overall intensity received at the i^{th} PD is,

$$Y_i = Y_{i1} + Y_{i2} + \cdots + Y_{iN} \approx Ie^{-cL} \tag{4.3}$$

From this equation, it is evident that the received intensity in a MIMO UWOC system can be described by the Beer-Lambert law.

4.2.2.2 Turbulence channel model

Turbulence due to movement of water medium can fluctuate the optical signal strength. The irradiance (I_t) fluctuation due to underwater weak turbulence is characterized by log-normal density function [Jamali *et al.* (2018), Tabeshnezhad and Pourmina (2017)]. The Probability Density Function (PDF) of a log-normally distributed random variable I is given by,

$$f_{I_t}(I_t) = \frac{1}{2I_t}\frac{1}{\sqrt{2\pi\sigma_X^2}}exp\left(-\frac{(ln(I_t) - 2\mu_X)^2}{8\sigma_X^2}\right) \tag{4.4}$$

where μ_X and σ_X^2 are mean and variance respectively of the Gaussian distributed random variable $X = \ln(I_t)/2$. Normalized log-normal PDF is obtained by assigning the expectation, $\mathbb{E}(I_t) = 1$, which results in the variance taking on a value $\mu_X = -\sigma_X^2$. In the above expression Gaussian variance $\sigma_X^2 = 0.25\ln\left(\sigma_{I_t}^2 + 1\right)$. $\sigma_{I_t}^2$ denotes the scintillation index (SI). The SI for a plane wave in the presence of underwater turbulence is given as [Ata and Baykal (2014), Korotkova *et al.* (2012)],

$$\sigma_{I_t}^2 = 8\pi^2 k^2 L \int_0^1 \int_0^\infty \mathcal{K}\Phi_n(\mathcal{K})\left(1 - \cos\left(\frac{L\mathscr{L}\mathcal{K}^2}{k}\right)\right) d\mathcal{K}d\mathscr{L} \tag{4.5}$$

where $k = 2\pi/\lambda$ is the wave-number, λ is the wavelength of the LASER source, L is link-range and $\Phi_n(\mathcal{K})$ is power spectrum of oceanic water. This is described by

[Korotkova *et al.* (2012)]],

$$\Phi_n(\mathcal{K}) = \frac{0.388 \times 10^{-8} \epsilon^{-1/3} \mathcal{K}^{-11/3} \chi_T}{\omega^2} \left[1 + 2.35\,(\mathcal{K}\xi)^{2/3}\right] \left(\omega^2 e^{-A_T\delta} + e^{-A_S\delta} - 2\omega e^{-A_{TS}\delta}\right) \tag{4.6}$$

where $\delta = 8.284\,(\mathcal{K}\xi)^{4/3} + 12.978\,(\mathcal{K}\xi)^2$, turbulence kinetic energy dissipation rate is denoted by ϵ, dissipation rate temperature and salinity is represented by χ_t, relative varying temperature-salinity parameter is represented by ω (unit-less quantity) and the Kolmogorov micro-scale length $\xi = 10^{-3}\ m$, $A_T = 1.863 \times 10^{-2}$, $A_S = 1.9 \times 10^{-4}$ and $A_{TS} = 9.41 \times 10^{-3}$ [Korotkova *et al.* (2012)]. The change in SI with respect to system parameters is shown in Figure 4.7. Figure 4.7a, shows the 3D plot of SI variation with respect to χ_t and L at $\epsilon = 10^{-8}\ m^2/s^3$ and $\omega = -2.5$. From this plot it can be inferred that SI increases with increase in link range. The value of SI at $L = 250\ m$ and $\chi_t = 6 \times 10^{-5}\ K^2/s$ is 0.935. Figure 4.7b, shows the SI variation with respect to L and ϵ for a value of $\chi_t = 6 \times 10^{-5}\ K^2/s$ and $\omega = -2.5$. Similarly Figures 4.7b and 4.7c represents SI variation with respect to (ϵ, L) and (ω, L). From this figure 4.7c, it can be inferred that for a fixed link distance, SI increases with decrease in ω.

4.2.2.3 Combined channel model

The channel gain due to the combined effect of underwater turbulence and propagation loss due to attenuation is $I = I_t I_a$ and corresponding PDF is obtained as,

$$f_I(I) = \frac{1}{2I\sqrt{2\pi\sigma_X^2}} \exp\left(-\frac{(\ln(I/I_a) - 2\mu_X)^2}{8\sigma_X^2}\right) \tag{4.7}$$

4.3 Reed-Solomon Encoding and Decoding

In underwater channels, the data transmission can be occasionally blocked for certain durations due to the movement of large water mammals or schools of fish. During this duration, the transmission path could be entirely blocked due to which burst or random error could be induced in the information stream. Channel codes can correct random or burst errors. Turbo codes and low-density parity-check codes (LDPC) are efficient random error-correcting codes, whereas RS-codes possess excellent burst error-correcting capability [Moon (2005), Blahut (2003)]. In UWOC systems, the probability of encountering burst errors is high. Hence, we have proposed the use of RS-codes in UWOC systems to improve the integrity of information transmission. The procedure of RS encoding and decoding is briefly

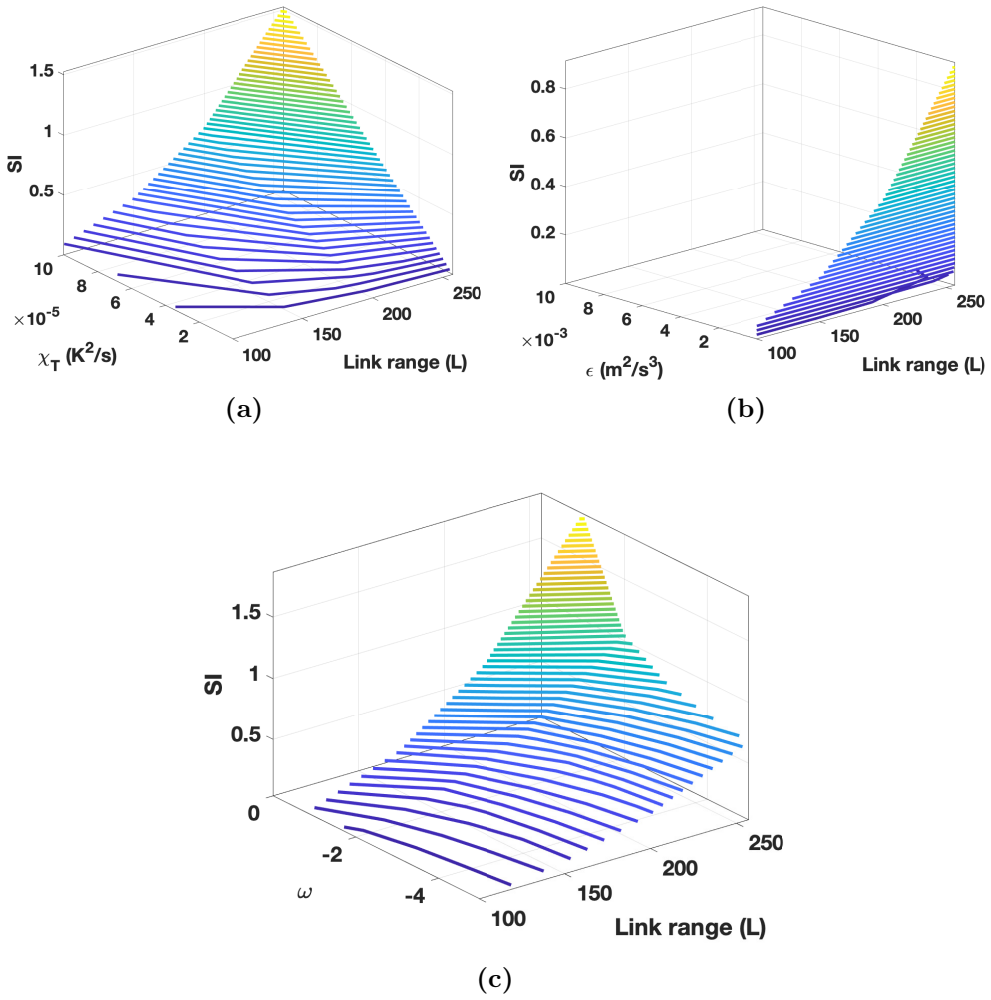

Figure 4.7: SI variation with respect to (a) L and χ_t, (b) L and ϵ, (c) L and ω.

described in the following paragraphs.

4.3.1 Encoding and decoding of $(n,\ k,\ t)$ RS-codes

The generator polynomial of an n-length RS-code over Galois Field $GF(q)$, ($q = p^m$, p is a prime number, m is the order of the field extension and $n|\,(p^m - 1)$) with t symbol error correcting capability is defined by, $g(x) = (x-\alpha^b)(x-\alpha^{b+1})\ldots(x-\alpha^{b+\delta-2})$, where α is a primitive element of the $GF(p^m)$, $b \geq 0$ is any real positive integer and $\delta = 2t+1$. The generator polynomial of $(n,\ k)$ RS-code with $b = 1$ (typical choice) and t symbol error correcting capability can be expressed as [Moon (2005)],

$$g(x) = (x-\alpha)(x-\alpha^2)\ldots(x-\alpha^{2t-1})(x-\alpha^{2t}) \tag{4.8}$$

where all the computations are performed in the field $GF(p^m)$. The code-word polynomial is defined by $c(x) = g(x) \times s(x)$, where $g(x)$ is the generator polynomial and $s(x) = s_0 + s_1x + s_2x^2 + \cdots + s_{k-1}x^{k-1}$ is the message polynomial obtained by representing the k message symbols $s_0, s_1, s_2, \cdots s_{k-1}$ as a polynomial in the indeterminate x. The $n-$ length code-word is represented in ploynomial form as $c(x) = c_0 + c_1x + c_2x^2 + \cdots + c_{n-1}x^{n-1}$ and bears one to one correspondence to the information bearing (message) polynomial $s(x) = s_0 + s_1x + s_2x^2 + \cdots + s_{k-1}x^{k-1}$. In this chapter, a $(n = 63,\ k = 51)$ RS code over the field $GF(2^6)$ has been designed and employed for error detection/ correction. Each symbol from the field $GF(2^6)$ can be expressed as a binary 6-tuple. Each individual symbol of the code-word polynomial is converted into 6-tuple of binary bits and communicated through the UWOC channel via an OOK modulated LASER source. At the receiver, the incoming bits are combined into 6 bit symbols lying in the field $GF(2^6)$. A set of successive 63 6-bit symbols constitutes the received vector $r(x) = r_{(0)} + r_{(1)}x + r_{(2)}x^2 + \cdots + r_{(n-1)}x^{n-1}$, where $r_{(i)}$ represents the extracted i^{th} symbol, $i = 0, 1, \ldots, n-1$, which is then processed to determine the error locations and error magnitudes. Berlekamp-Massey algorithm and Chien search algorithm are employed for determining the locations in which the channel has induced errors and Forney's algorithm is used to determine the error magnitudes. The estimate of transmitted code-word is then determined by $\hat{c}(x) = r(x) - e(x)$, where $e(x) = \sum_{i=0}^{n-1} e_i x^i$, e_i is the i^{th} error magnitude obtained by the use of Forney's algorithm and x^i represents the i^{th} error location obtained by making use of Berlekamp-Massey and Chien search algorithms.

4.4 Analytical BER Evaluation

A closed-form BER expression corresponding to the use of SISO, SIMO, MISO and MIMO schemes for un-coded and RS-coded cases has been evaluated in this section.

4.4.1 Single-Input Single-Output

The received OOK modulated symbol in the presence of combined underwater channel is given as,

$$Y = \eta I \sqrt{P_t T_b} s + n \tag{4.9}$$

The BER of SISO (P_{siso}) with equiprobable input bits (assuming known log-normally distributed channel) is specified by,

$$P_{siso} = \frac{1}{2}\int_0^{\infty}\left(P\left(\frac{\hat{s}=1}{s=0,I}\right)+P\left(\frac{\hat{s}=0}{s=1,I}\right)\right)f_I(I)dI \tag{4.10}$$

where, $P_0 = P\left(\frac{\hat{s}=1}{s=0,I}\right)$ is the probability of estimated data being inferred as '1' when transmitted data is '0', $P_1 = P\left(\frac{\hat{s}=0}{s=1,I}\right)$ is the probability of estimated data being inferred as '0' when transmitted data is '1' and $f_I(I)$ is log-normal density function. The BER of SISO link operating by setting the threshold equal to $\eta I\sqrt{P_tT_b}/2$ between the received levels corresponding the two binary symbols and substituting Equation (4.4) in (4.10) is,

$$P_{siso} = \int_0^{\infty}\mathbb{Q}\left(\eta I\sqrt{\frac{P_tT_b}{4\sigma^2}}\right)\frac{1}{2I}\frac{1}{\sqrt{2\pi\sigma_X^2}}\exp\left(-\frac{\left(ln(I/I_a)-2\mu_X\right)^2}{8\sigma_X^2}\right)dI \tag{4.11}$$

where $\mathbb{Q}(x) \triangleq (1/\sqrt{2\pi})\int_x^{\infty}\exp(-y^2/2)dy$ is Gaussian Q-function. Substituting $I/I_a = t$ in Equation (4.11), the obtained equation is given as,

$$P_{siso} = \int_0^{\infty}\mathbb{Q}\left(\eta I_a t\sqrt{\frac{P_tT_b}{4\sigma^2}}\right)\frac{1}{2t}\frac{1}{\sqrt{2\pi\sigma_X^2}}\exp\left(-\frac{\left(ln(t)-2\mu_X\right)^2}{8\sigma_X^2}\right)dt \tag{4.12}$$

A closed-form solutions can be obtained by use of Gauss-Hermite Quadrature [Popoola *et al.* (2008)] and power series method proposed in [Yang *et al.* (2014).]

In this chapter, to facilitate the determination of closed-form solutions, we have used the Hyperbolic Tangent Distribution (HTD) family to specify the Log-Normal PDF in algebraic form, so that a closed-form solution to Equation (4.12) can be obtained and the BER results obtained by enploying HTD correspond fairly with the simulations obtained by Monte-Carlo method. The Log-Normal PDF representation using the HTD family is given in Appendix E. By substituting Log-Normal PDF generated by HTD in Equation (4.12), the reformulated Equation is given as,

$$P_{siso} \approx \int_0^{\infty}\left(\frac{1}{12}\exp\left(-\frac{\zeta^2t^2}{2}\right)+\frac{1}{4}\exp\left(-\frac{2\zeta^2t^2}{3}\right)\right)\left(\frac{b\exp(2a)t^{b-1}}{\left(1+\exp\left(2a\right)t^b\right)^2}\right)dt \tag{4.13}$$

where $\zeta = \eta I_a\sqrt{\frac{P_tT_b}{4\sigma^2}}$, $\mathbb{Q}(x)$ is approximated using [Chiani *et al.* (2003*b*)] as $\mathbb{Q}(x) \approx 1/12\exp\left(-x^2/2\right)+1/4\exp\left(-2x^2/3\right)$. The closed-form expression is obtained by substitution and then integration of Equation (4.13) using (21) of [Adamchik and

Marichev (1990)] and the obtained expression is given as,

$$P_{siso} \approx 2\exp(2a)\left(\frac{b}{2\pi}\right)^{\frac{b+1}{2}}\left[\frac{\mathscr{C}_1}{12}+\frac{\mathscr{C}_2}{4}\right] \tag{4.14}$$

where $\mathscr{C}_1 = \left(\sqrt{2}/\zeta\right)^b G_{2+b,2}^{2,2+b}\left(\begin{matrix}-\frac{1}{2},0,\frac{i-\frac{b}{2}}{b}\\ 0,\frac{1}{2}\end{matrix}\middle| b^b\mathscr{P}_1^2\right)$, $\mathscr{P}_1 = \exp(2a)\left(\sqrt{2}/\zeta\right)^b$, $\mathscr{C}_2 = \left(\sqrt{1.5}/\zeta\right)^b G_{2+b,2}^{2,2+b}\left(\begin{matrix}-\frac{1}{2},0,\frac{i-\frac{b}{2}}{b}\\ 0,\frac{1}{2}\end{matrix}\middle| b^b\mathscr{P}_2^2\right)$, $i = 1,2,\ldots,b$; $\mathscr{P}_2 = \exp(2a)\left(\sqrt{1.5}/\zeta\right)^b$ and $G[\cdot]$ is Meijer G-function.

4.4.2 Single-Input Multiple-Output

It is assumed that a LASER source transmits data through the UWOC channel and SIMO scheme averages (EGC) the response produced by all individual detectors. The average of the combined response produced by M detectors is $Y = \frac{\eta\sqrt{P_t T_b} s I_m I_a}{M} + n$, where $I_m = \sum_{i=0}^{M} I_i$ and I_i's are independent log-normal random variables with identical mean and variances. The sum of M independent log-normal random variables having identical mean and variance is also a log-normally distributed random variable. Hence, $I_m = \exp(2\mathscr{M})$ is also a log-normally distributed random variable, where $\mathscr{M}$ is normal random variable with mean μ_m and variance σ_m^2 (mean and variance of $\mathscr{M}$ given in Appendix D). The density function of the sum of M Log-Normal random variables is given as,

$$f_{I_m}(I_m) = \frac{1}{2I_m\sqrt{2\pi\sigma_m^2}}\exp\left(-\frac{\left(\ln(I_m)-2\mu_m\right)^2}{8\sigma_m^2}\right) \tag{4.15}$$

where, $\mu_m = \frac{1}{2}\ln(M) - \frac{1}{4}\ln\left(1+\frac{\exp\left(4\sigma_X^2\right)-1}{M}\right)$ and $\sigma_m^2 = \frac{1}{4}\ln\left(1+\frac{\exp\left(4\sigma_X^2\right)-1}{M}\right)$ are mean and variance of normal random variable $\mathscr{M}$. The BER asociated with SIMO system is given as,

$$P_{simo} = \int_0^\infty \mathbb{Q}\left(\zeta\frac{I_m}{M}\right) f_{I_m}(I_m) dI_m \tag{4.16}$$

Equation (4.16) is also computed in a similar manner to (4.13). The analytical BER obtained as,

$$P_{simo} \approx 2\exp(2a)\left(\frac{b}{2\pi}\right)^{\frac{b+1}{2}}\left[\frac{\mathscr{D}_1}{12}+\frac{\mathscr{D}_2}{4}\right] \tag{4.17}$$

where $\mathscr{D}_1 = \left(\sqrt{2M}/\zeta\right)^b G_{2+b,2}^{2,2+b}\left(\begin{matrix}-\frac{1}{2}, 0, \frac{i-\frac{b}{2}}{b} \\ 0, \frac{1}{2}\end{matrix}\middle| b^b \mathscr{R}_1^2\right)$, $i = 1, 2, \ldots, b$;
$\mathscr{R}_1 = \exp(2a)\left(\sqrt{2}M/\zeta\right)^b$, $\mathscr{D}_2 = \left(\sqrt{1.5M}/\zeta\right)^b G_{2+b,2}^{2,2+b}\left(\begin{matrix}-\frac{1}{2}, 0, \frac{i-\frac{b}{2}}{b} \\ 0, \frac{1}{2}\end{matrix}\middle| b^b \mathscr{R}_2^2\right)$, $\mathscr{R}_2 = \exp(2a)\left(\sqrt{1.5}M/\zeta\right)^b$.

4.4.3 Multiple-Input Single-Output

Assume that N transmit sources transmit the same data through the underwater channel and the detector's response is $Y = \eta I_a I_n \sqrt{(P_t T_b/N)} s + n$ where $I_n = I_1 + I_2 + \cdots + I_N$. Since I_i's are log-normal random variables, $I_n = \exp(2\mathscr{N})$ is also a log-normal random variable and $\mathscr{N}$ is normal random variable with mean $\mu_n = \frac{1}{2}\ln(N) - \frac{1}{4}\ln\left(1 + \frac{\exp\left(4\sigma_X^2\right)-1}{N}\right)$ and variance $\sigma_n^2 = \frac{1}{4}\ln\left(1 + \frac{\exp\left(4\sigma_X^2\right)-1}{N}\right)$. The BER of MISO system is given as,

$$P_{miso} = \int_0^\infty \mathbb{Q}\left(\frac{\zeta I_n}{\sqrt{N}}\right) f_{I_n}(I_n) dI \tag{4.18}$$

where $f_{I_n}(I_n)$ is log-normal PDF and it is obtained into algebraic form using HTD. The simplified BER equation can be obtained by solving similar way of BER of SISO and it is given as,

$$P_{miso} \approx 2\exp(2a)\left(\frac{b}{2\pi}\right)^{\frac{b+1}{2}}\left[\frac{\mathscr{C}_1}{12} + \frac{\mathscr{C}_2}{4}\right] \tag{4.19}$$

where $\mathscr{C}_1 = \left(\sqrt{2N}/\zeta\right)^b G_{2+b,2}^{2,2+b}\left(\begin{matrix}-\frac{1}{2}, 0, \frac{i-\frac{b}{2}}{b} \\ 0, \frac{1}{2}\end{matrix}\middle| b^b \mathscr{P}_1^2\right)$, $\mathscr{P}_1$, $\mathscr{P}_2$ are given under Equation (4.14), $\mathscr{C}_2 = \left(\sqrt{1.5N}/\zeta\right)^b G_{2+b,2}^{2,2+b}\left(\begin{matrix}-\frac{1}{2}, 0, \frac{i-\frac{b}{2}}{b} \\ 0, \frac{1}{2}\end{matrix}\middle| b^b \mathscr{P}_2^2\right)$.

4.4.4 Multiple-Input Multiple-Output

Multiple transmit sources T_1, T_2, $\ldots$, T_N are used to transmit same information through the channel and the detector's responses are combined using EGC at the receiver. The combined response is $Y = \sum_{i=1}^{M} \frac{Y_i}{M}$, where $Y_i = \eta I_a \left(\sum_{j=1}^{N} I_{ij}\right)\sqrt{P_t T_b} s + n$, $I_{11}, \ldots, I_{MN}$ are independent log-normal random variables, the resultant summation ($I_{mn} = \exp(\mathscr{O})$) is also a log-normal random variable, where $\mathscr{O}$ is a normally distributed random variable with mean $\mu_{mn} = \frac{1}{2}\ln(MN) - \frac{1}{4}\ln\left(1 + \frac{\exp\left(4\sigma_X^2\right)-1}{MN}\right)$

and variance $\sigma_{mn}^2 = \frac{1}{4}\ln\left(1+\frac{\exp\left(4\sigma_X^2\right)-1}{MN}\right)$. The probability of error associated with this MIMO scheme can be expressed as,

$$P_{mimo} = \int_0^\infty \mathbb{Q}\left(\frac{\zeta I_{mn}}{M\sqrt{N}}\right) f_{I_{mn}}(I_{mn}) dI_{mn} \tag{4.20}$$

where $I_{mn} = I_{11} + I_{12} + \cdots + I_{MN}$ and $f_{I_{mn}}(I_{mn})$ is PDF of log-normal random variable I_{mn}. Similar to Equation (4.17), the closed-form solution is,

$$P_{mimo} \approx 2\exp(2a)\left(\frac{b}{2\pi}\right)^{\frac{b+1}{2}}\left[\frac{\mathscr{D}_1}{12}+\frac{\mathscr{D}_2}{4}\right] \tag{4.21}$$

where $\mathscr{D}_1 = \left(M\sqrt{2N}/\zeta\right)^b G_{2+b,2}^{2,2+b}\left(\begin{matrix}-\frac{1}{2},0,\frac{i-\frac{b}{2}}{b}\\ 0,\frac{1}{2}\end{matrix}\middle| b^b\mathscr{R}_1^2\right)$ and $\mathscr{D}_2 = \left(M\sqrt{1.5N}/\zeta\right)^b \times G_{2+b,2}^{2,2+b}\left(\begin{matrix}-\frac{1}{2},0,\frac{i-\frac{b}{2}}{b}\\ 0,\frac{1}{2}\end{matrix}\middle| b^b\mathscr{R}_2^2\right)$.

4.4.5 Coded BER Evaluation

When the decoded code-word is not identical to the transmitted code-word, a decoding error is said to occur. An upper bound on the BER (P_d) associated with a (n, k, t) non-binary RS-code over $GF(2^m)$ with t symbol error correcting capability and symbol error probability P_s is given by [Cox *et al.* (2008)],

$$P_d \leq \sum_{i=t+1}^{n}\binom{n}{i}P_s^i\left(1-P_s\right)^{n-i} \tag{4.22}$$

where $P_s = 1-(1-p_b)^m$, p_b represents the transition probability of the binary symmetric channel. In the presented analysis, p_b corresponds to P_{siso} in Equation (4.14), P_{simo} in Equation (4.17), P_{miso} in Equation (4.19) and P_{mimo} in Equation (4.21) for SISO, SIMO, MISO and MIMO schemes respectively with code-rate $r = k/n$.

4.5 Results and discussions

In this section, we present the simulation and analytical BER results of the OOK modulated UWOC system as a function of transmit power per bit in dB. Considered systme parameters are tabulated in Table 4.1.

The simulations of the BER of the UWOC system are based on the transmission

Table 4.1: System parameters

System parameters	Value
Link range (L)	300 m
Transmitter-receiver spacing (Δl)	0.05 m
Order of field extension (m)	6

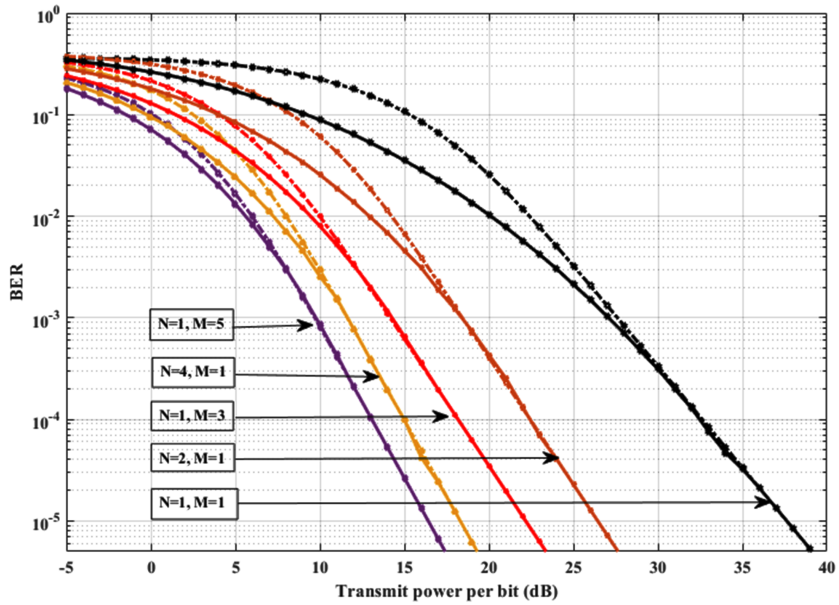

(a)

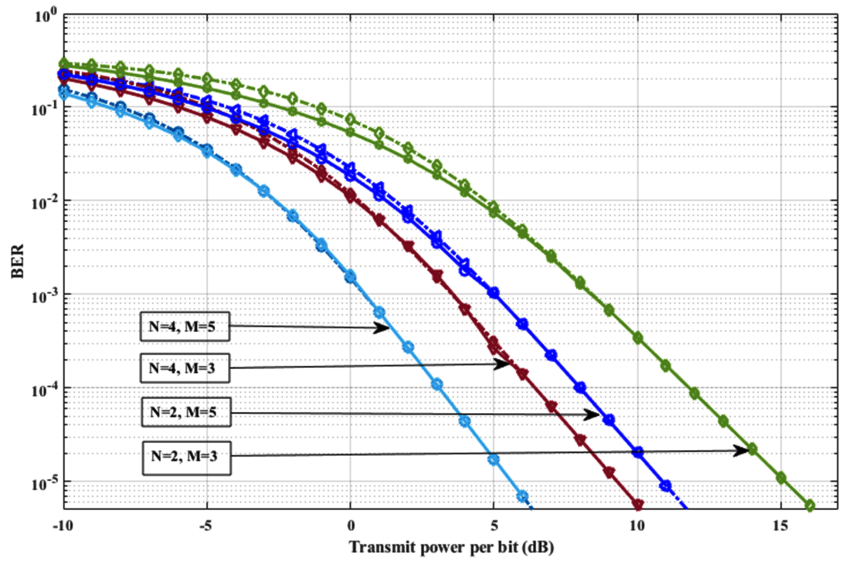

(b)

Figure 4.8: Simulation and analytical BER results of uncoded (a) SISO, SIMO and MISO, (b) MIMO.

of $l = 10^6$ binary data bits (s) generated using a pseudo-random binary generator. Each data sample drives a N number of laser sources in parallel. The irradiance

produced by the laser sources is then communicated through the UWOC channel. The irradiance values received by the M detectors are processed to determine the estimate of the communicated data bit ($\hat{s}$). The BER is computed as $\sum_i^l (s_i \oplus \hat{s}_i)/l$ for varying transmit powers, where $\oplus$ denotes exclusive-or operation. Analytical BER results are determined based on the equations (4.14), (4.17), (4.19) and (4.21) derived in this chapter. All these equations are as a function of transmit powers, so the analytical BER results obtained by varying the transmit powers in the obtained equations.

The system parameters used in simulation and computation are $\eta = 0.8\ A/W$, data-rate $R_b = 500\ Mbps$, bit duration $T_b = 1/R_b = 2\ ns$. The parameters used for calculation of scintillation index for plane wave propagating in water are $\omega = -2.5$, $\chi_t = 5.84 \times 10^{-5}\ K^2/s$ and $\epsilon = 1 \times 10^{-5}\ m^2/s^3$ and remaining parameters are the same values as in [Korotkova *et al.* (2012)]. These values substituted in Equation (4.5) yields $\sigma_I^2 = 0.9328$ and $\sigma_X^2 = 0.1647$. The attenuation coefficient considered for evaluating system behaviour in the presence of beam attenuation is $C(\lambda = 470\ nm) = 0.1514\ m^{-1}$ for clear ocean water.

Figure 4.8 illustrates the variation of the BER simulation values (solid lines) and analytic values (dash and dot line) for an uncoded UWOC system for SISO, SIMO, MISO and MIMO configurations. An examination of Figures 4.8a and 4.8b show that the analytical results are close correspondence with the obtained simulation results and the BER performance improves with increasing M and N. For $N = 2$ and 4 MISO systems, a performance improvement of 11 dB and 19.3 dB respectively from SISO at a BER of 10^{-5} is observed. For SIMO schemes employing $M = 3$ and 5, a performance improvement of 15.5 dB ($M = 3$) and 21.2 dB ($M = 5$) is observed when compared with SISO UWOC system at a BER of 10^{-5}.

From Figure 4.8b, an improvement in performance of nearly $3-4$ dB is observed when we move from $N \times 3$ MIMO to $N \times 5$ MIMO for $N = 2,\ 4$. Further, a performance improvement of nearly $5 - 6$ dB is observed when we move from $2 \times M$ to $4 \times M$ for $M = 3,\ 5$ at BER of 10^{-5}. Figure 4.9a and 4.9b represents the BER plots of simulation and analytical upper bound RS-coded transmit/ receive dievresity (SISO, SIMO and MISO) and MIMO schemes respectively. RS coded SISO can gain 09.70 dB transmit power over uncoded SISO UWOC system and RS coded 4×5 MIMO can gain a transmit powerof 36 dB from un-coded SISO at BER of 10^{-5}, respectively.

From Figure 4.9 represents simulation (solid line) and analytical upper bound (dash-dotted line) BER plots of RS-coded SIMO, MISO and MIMO schemes. The

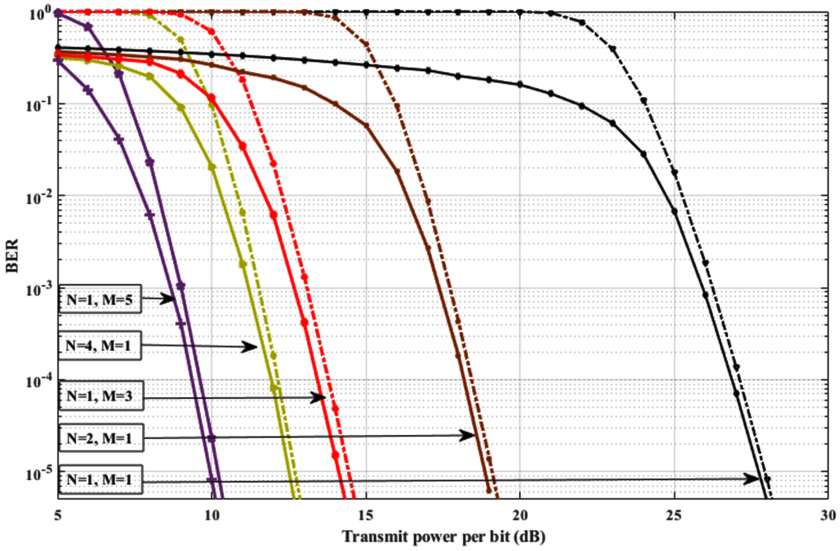

(a)

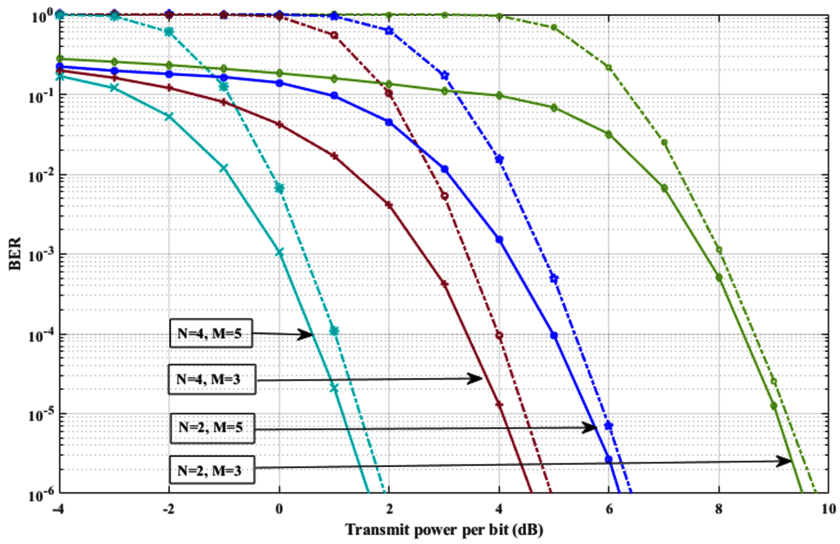

(b)

Figure 4.9: Simulation and analytical BER results of RS coded (a) SISO, SIMO and MISO, and (b) MIMO UWOC system.

close correspondence between the simulation and analytical upper bound BER results obtained for high transmit powers. The BER performance improvement from un-coded SISO to un-coded and RS-coded SIMO, MISO and MIMO schemes are given in Tables 4.2 and 4.3 respectively. The coded BER results presented in Table 4.3 are results obtained by simulation.

Table 4.2: Power gain comparison SIMO, MISO and MIMO schemes with respect to un-coded SISO

Schemes	Transmit power (dB) at BER of 10^{-5}	Power gain (dB) from un-coded SISO
SISO	37.50	-
2×1	26.50	11.00
1×3	22.00	15.50
4×1	18.20	19.30
1×5	16.30	21.20
2×3	15.00	22.50
2×5	11.00	26.50
4×3	09.10	28.40
4×5	05.60	31.90

Table 4.3: Power gain of RS-coded SIMO, MISO and MIMO techniques over un-coded SISO

RS-coded UWOC System	Transmit Power (dB) at BER of 10^{-5}	Power gain (dB) from un-coded SISO (37.50dB)
SISO	27.80	09.70
2×1	18.90	18.60
1×3	19.10	18.40
4×1	12.50	25.00
1×5	09.90	27.60
2×3	09.00	28.50
2×5	05.75	31.75
4×3	04.10	33.40
4×5	01.20	36.30

4.6 Conclusion

In this chapter, we have analyzed the performance of the OOK modulated UWOC system employing SISO, SIMO, MISO and MIMO in the presence and absence of a channel code ((63,51) RS code) over a channel perturbed by weak turbulence. The improvement in performance obtained by the use of MIMO and RS channel code in an UWOC system has been quantified by analysis and simulations. The proposed schemes, namely RS-coded $2 \times 3,\ 2 \times 5,\ 4 \times 3$ and 4×5 MIMO systems are observed to offer nearly 28, 31, 33 and 36 dB of improvement in performance (transmit power gain) respectively when compared with un-coded SISO UWOC system at BER of 10^{-5}. We conclude that the use of MIMO and diversity schemes along with suitable channel codes could be a suitable and efficient technique to realize high-speed and reliable UWOC systems.

Chapter 5

Space-Time Block Codes for MIMO Underwater Communication Links

It is well known that data transmission over an underwater optical communication channel is a very challenging problem due to many impediments such as scattering, absorption and the presence of turbulence. MIMO systems have been integrated with Space-Time (ST) codes to improve further the reliability of information transfer across the wireless channel. STBCs are further divided into two classes, Orthogonal STBCs (OSTBC) and Non-Orthogonal STBCs (NOSTBC). When judiciously combined with ST codes, MIMO systems can significantly improve the integrity of information transfer across wireless channels disturbed by multipath fading. Various MIMO STBC has been proposed to mitigate the effects of multipath fading in wireless systems.

As the UWOC channel perturbed by weak turbulence shares many properties with a wireless channel affected by multipath fading, we have attempted to synthesize a few OSTBCs and NOSTBCs for use over this channel. We have started our study with the most commonly employed OSTBC in wireless systems, namely the Alamouti code. It has become popular due to the simplicity of its encoding and decoding operations. After studying the performance of the Alamouti code in the UWOC environment, we have focused our attention on more powerful NOSTBCs. Use of the ST code yield improved information integrity as well as spectral efficiency. The performance of these codes has been verified by carrying out Monte-Carlo simulations.

Alamouti codes are referred to as rate-1 codes. This is because two symbols are transmitted from two antennas over two-time slots and hence the effective

number of symbols communicated per channel use is one. This chapter has designed OSTBC and NOSTBC schemes, which can be used to improve the performance of an UWOC link. We have synthesized several OSTBCs and NOSTBCs and have suitably conditioned them to operate over an UWOC channel employing intensity modulation and perturbed by weak underwater turbulence channel. Alamouti type STBC coded 2×1 and 2×2 can gain a transmit power of 17 and 28 dB over SISO at the BER of 10^{-5} respectively, whereas higher-order MIMO OSTBC is not much effective than that of 2×1 and 2×2 OSTBC. The performance gain of 4×2 and 4×4 OSTBC over SISO is 23 and 30.5 dB at the BER of 10^{-5}, respectively. NOSTBC performs better for a higher-order MIMO system. NOSTBC comprising of 4×2 and 4×4 MIMO can gain a transmit power of 26.75, 33.20 dB from SISO and 3.5 and 3 dB from 4×2 and 4×4 OSTBC respectively at the BER of 10^{-5}.

5.1 Introduction

The goal of a Space-Time Block Code (STBC) is to work in conjunction with a MIMO wireless system and further improve the integrity of information transfer. Since MIMO systems employ multiple transmit and receive antennas, the ST code must introduce redundancies in both the spatial and the time domains. These codes improve the wireless system's reliability by providing diversity gain and coding gain [Jafarkhani (2005)]. Alamouti type STBC techniques can be employed along with complex modulation schemes (such as phase-shift keying and quadrature amplitude modulation), widely used in the RF environment. The complex signal contains the amplitude and phase information of the transmitted data. However, most optical links employ intensity modulation schemes such as OOK and PPM directly detected at the receiver. Such modulation schemes do not possess a complex signal space representation. The signal waveforms of these modulation schemes are represented by points on the real number line. Simon et al., have proposed a modified Alamouti type STBC for optical links by replacing the conjugate of signal with the complement of the signal. They have shown that with this modification, the Alamouti code can be deployed over free-space optical channels with the same efficacy as over RF channels [Simon and Vilnrotter (2005)]. Optical links using STBCs deployed over free-space environment are presented in [Islam and Majumder (2012)]. Dot product of symbols in different time slots is equal to zero; such constructions referred to as orthogonal else it is non-orthogonal. Assume $\begin{bmatrix} x_1 & -x_2 \\ x_2 & x_1 \end{bmatrix}$ STBC encoded data, the symbols in the first column can be transmitted

at the first time slot and second column in the second time slot. The dot product of transmitted symbols in first and second time slot is $\begin{bmatrix} x_1 & x_2 \end{bmatrix} \cdot \begin{bmatrix} -x_2 \\ x_1 \end{bmatrix} = 0$. Such codes are named as OSTBC. It is well known that OSTBC can not achieve full rate (rate=1) for more than two transmitting sources [Machado and Uchôa-Filho (2006)]. By relaxing the orthogonality constraint of STBC, it is possible to achieve a rate greater than or equal to 1 for any number of transmitting sources. This fact has motivated us to synthesize NOSTBCs and determine their performance over UWOC channels.

5.1.1 Contributions

The contributions of this chapter are as follows. The bit error rate (BER) performance of an On-Off Keying (OOK) modulation based UWOC system in weak turbulence and propagation loss due to beam attenuation regimes are studied for Single-Input to Single-Output (SISO) systems and Multiple-Input to Multiple-Output (MIMO) systems employing orthogonal and non-orthogonal STBC schemes.

The remaining part of the chapter is organized as follows. Section 5.2 describes the system model of orthogonal and non-orthogonal STBCs. This is followed by a description of the steps to be followed to synthesize Orthogonal STBCs (OSTBC) and NOSTBCs and the Maximum Likelihood (ML) decoding approach used to decode the received information-bearing matrices. Monte-Carlo simulation specifying the BER as a function of transmit power is provided in Section 5.4. The chapter is concluded in Section 5.5 with a brief discussion of the simulation results obtained and their significance.

5.2 System model

We consider an $N \times M$ STBC MIMO UWOC system. As depicted in the block diagram, the proposed system consists of N laser sources and M photo-detectors. The laser sources are intensity-modulated using OOK or using a pulse position modulation scheme (PPM). In both the schemes, the input to the optical modulator is a binary bitstream. In this work, we have considered the use of OOK modulation. The input binary data from the source is mapped to an appropriate codeword from the space-time block code. The codeword is a matrix of dimension $N \times T$, here T is symbol duration. Since OOK is employed at the transmitter, the STBCs are constructed over binary field $GF(2)$. Traditionally orthogonal STBCs have been preferred over their non-orthogonal counterparts. The main reason for

this has been that OSTBCs (including Alamouti code) possess simple decoding algorithms. However, many researchers have demonstrated that carefully designed non-orthogonal STBCs can perform equally well under most channel conditions and also provide a higher rate than their orthogonal counterparts [Sripati *et al.* (2004)]. Hence, we have to chosen to study the performance of MIMO UWOC systems employing OSTBCas well as NOSTBC. The block diagram of an UWOC system employing MIMO along with a STBC encoder/ decoder pair is illustrated in Figure 5.1.

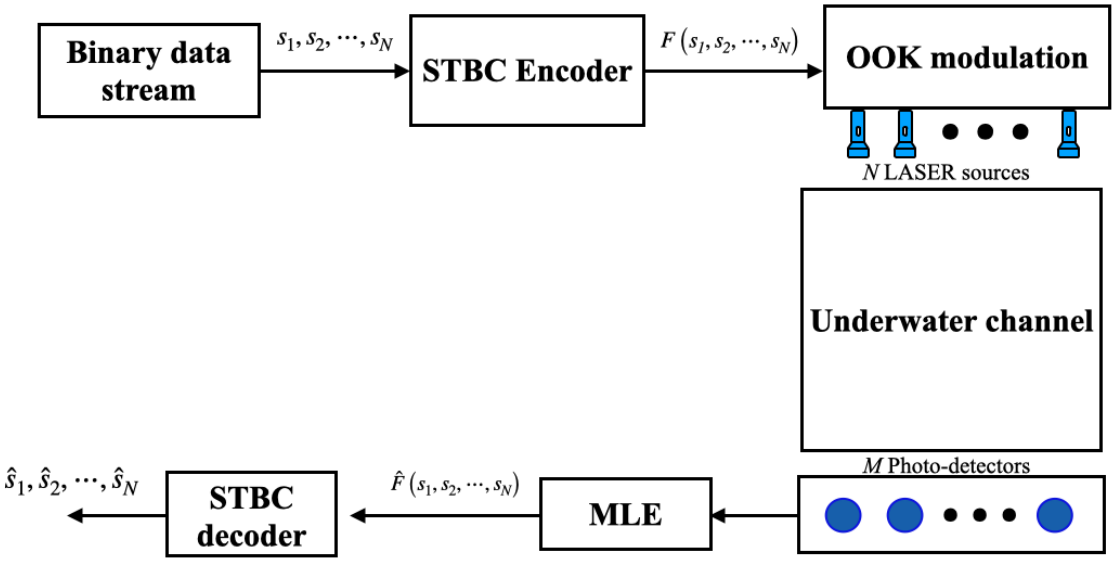

Figure 5.1: Block diagram of UWOC MIMO STBC.

In general, for an $N \times M$ MIMO communication system, the code word matrix at the receiver (assuming T symbol intervals in a code word) is represented by the equation,

$$Y(t) = \eta\sqrt{P_t T_b}\boldsymbol{H}\mathscr{F}(s_1, s_2, \cdots, s_N) + \begin{bmatrix} n_1 & n_{M+1} & \cdots & n_{(T-1)M+1} \\ n_2 & n_{M+2} & \cdots & n_{(T-1)M+2} \\ \vdots & \vdots & \ddots & \vdots \\ n_M & n_{M+M} & \cdots & n_{(T-1)M+M} \end{bmatrix} \tag{5.1}$$

Where $\boldsymbol{H} = \begin{bmatrix} h_{11} & h_{12} & \cdots & h_{1N} \\ h_{21} & h_{22} & \cdots & h_{2N} \\ \vdots & \vdots & \ddots & \vdots \\ h_{M1} & h_{M2} & \cdots & h_{MN} \end{bmatrix}$ represents the $M \times N$ MIMO channel coefficients and $\mathscr{F}(s_1, s_2, \cdots, s_N)$ is a STBC encoded matrix of size $N \times T$, which is

a function of transmitted data symbols *i.e.*, $s_1, s_2, \cdots, s_N$. The relationship between the information block and the encoded STBC code word can be represented as shown in equation below,

$$s_1, s_2, \cdots, s_N \underset{\text{Decoder}}{\overset{\text{Encoder}}{\rightleftharpoons}} \mathscr{F}(s_1, s_2, \cdots, s_N) \tag{5.2}$$

Where $\mathscr{F}(s_1, s_2, \cdots, s_N)$ represents the STBC codeword expressed as a matrix.

Further, Maximum Likelihood Estimation (MLE) decoding can be used to estimate the transmitted code word matrix at the receiver. This process requires knowledge of the channel coefficients. This information is extracted by carrying out channel estimation at the receiver at regular intervals. The process of ML estimation is denoted by the equation presented below.

$$\hat{F}(s_1, s_2, \cdots, s_N) = \underset{\tilde{F} \in \{0,1\}}{argmin} \left|\left| Y(t) - H\tilde{F}(s_1, s_2, \cdots, s_N) \right|\right|^2 \tag{5.3}$$

where $\tilde{F}(s_1, s_2, \cdots, s_N)$ represent the set of all code-words of the ST code. We calculate the Frobenius norm depicted by equation (5.3) for all the code-words of the code and decide in favour of that codeword for which the Frobenius norm evaluates to the minimum value.

The $N \times T$ STBC code word matrix $\mathscr{F}(s_1, s_2, \cdots, s_N)$ can be either orthogonal or non-orthogonal. The rate of the code (STBC) is given as N_d/T, where N_d is the number of data symbols that are transmitted through N transmit antennas in T time slots. In our analysis, we have considered N data symbols have been communicated through the N transmitting antennas *i.e*, $N_d = N$.

5.3 STBC construction

In this section, we have presented the construction of orthogonal and non-orthogonal STBC types.

5.3.1 Orthogonal STBC

Many researchers have proposed using the Rate-1 Alamouti code for deployment as an OSTBC to communicate through 2×1 or 2×2 MIMO schemes over wireless and free-space optical channels [Simon and Vilnrotter (2005)]. Hence, the Alamouti code can be conveniently deployed in a MIMO UWOC system employing two LASER sources at the transmitter and one PD at the receiver (*i.e.*, 2×1 MISO

system). The symbols s_1, s_2 from the data stream are transmitted during the first through the two available LASER sources during the first time interval. The modified symbols $\bar{s_2}$, s_1 are transmitted during the second time interval. Figure 5.2 is the diagrammatic illustrate this process. In the case of the 2×1 STBC, the data received at the PD is expressed as,

$$Y(t) = \begin{bmatrix} y_1 & y_2 \end{bmatrix} = \eta\sqrt{P_t T_b} \begin{bmatrix} h_{11} & h_{12} \end{bmatrix} \mathscr{F}(s_1, s_2) + \begin{bmatrix} n_1 & n_2 \end{bmatrix} \tag{5.4}$$

where η is detector's responsivity, P_t is transmit power, T_b is bit duration, n_1, n_2 are AWGN noise of zero mean σ^2 variance, $\mathscr{F}(s_1, s_2) = \begin{bmatrix} s_1 & \bar{s}_2 \\ s_2 & s_1 \end{bmatrix}$, $\bar{s_i} = A - s_i$, A is a positive constant related to the light intensity

Similar to 2×1 STBC, the data received by 2×2 STBC containing two LASER source and two PDs is given by,

$$Y(t) = \begin{bmatrix} y_1 & y_2 \end{bmatrix} = \eta\sqrt{P_t T_b} \begin{bmatrix} h_{11} & h_{12} \\ h_{21} & h_{22} \end{bmatrix} \mathscr{F}(s_1, s_2) + \begin{bmatrix} n_1 & n_3 \\ n_2 & n_4 \end{bmatrix} \tag{5.5}$$

Since two data symbols are transmitted in two time slots, the code-rate of 2×1 and 2×2 orthogonal STBC scheme is 1. The OSTBC encoded data for $N = 4$ transmitting sources is given as [Jafarkhani (2005)],

$$\mathscr{F}(s_1, s_2, s_3, s_4) = \begin{bmatrix} s_1 & \bar{s}_2 & \bar{s}_3 & s_4 \\ s_2 & s_1 & \bar{s}_4 & \bar{s}_3 \\ s_3 & \bar{s}_4 & s_1 & \bar{s}_2 \\ s_4 & s_3 & s_2 & s_1 \end{bmatrix}$$

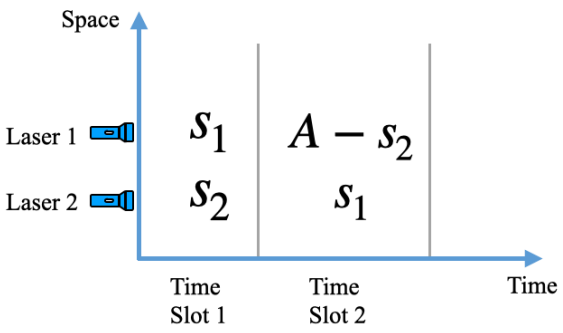

Figure 5.2: Optical OSTBC encoding structure for two sources.

It has been shown that the rate of STBC (defined as the number of data symbols transmitted in T time slots) is equal to one, only in case of Alamouti code (2×1 and 2×2) and is always less than one for higher order orthogonal STBCs (OSTBC).

5.3.2 Non-orthogonal STBC

The literature shows that the rate of higher-order STBCs could be increased to more than or equal to 1 by relaxing the orthogonality constraint, but it increases the complexity of signal processing operations at the receiver. However, these difficulties have been largely resolved with the use of software-defined processing and the availability of high-speed processors capable of performing hundreds of millions of floating-point operations in one second. In [Sripati *et al.* (2004)], it has shown that the use of error control codes as space-time block codes improves the performance of the MIMO system and provides a better rate compared to orthogonal counterparts. In this work, we employ NOSTBC obtained from full rank cyclic codes [Raghavendra and Acharya (2019)]. Since OOK is employed as the modulation scheme in the physical layer, the NOSTBCs are designed over the field $GF(2)$ and the use of rank preserving maps for transforming data from the finite field to the complex number field is not necessary. The cyclic codes are constructed over the Galois field $GF(2^m)$ and viewed as matrix codes over the Galois field $GF(2)$.

The Galois Field Fourier Transform (GFFT) approach can be used to synthesize cyclic codes in which all the non-zero codewords can be viewed as $m \times n$ (where $n = 2^m - 1$ or $n|(2^m - 1)$ is number of symbols in a codeword) matrices over $GF(2)$ possessing full rank property [Sripati *et al.* (2004)]. Let $\mathbf{a} = (a_0, a_1, \cdots, a_{n-1}) \in GF(2^m)$ and $\mathbf{A} = (A_0, A_1, \cdots, A_{n-1}) \in GF(2)$ respectively represent $n-$ length GFFT pairs ($i.e,\ a \overset{\text{GFFT}}{\longleftrightarrow} A$). The j^{th} transform domain component is defined by Sripati (2011)],

$$A_j = \sum_{i=0}^{n-1} \alpha^{ij} a_i, \qquad 0 \leq j \leq n-1. \tag{5.6}$$

where α is a primitive element of $(2^m - 1)^{th}$ root of unity in $GF(2^m)$, $\mathbf{a}$ and $\mathbf{A}$ are refered to as time domain and corresponding Galois field transform domain vectors respectively. The inverse Galois Field Fourier Transform (IGFFT) is defined by,

$$a_i = \frac{1}{n \ modulo \ p} \sum_{j=0}^{n-1} \alpha^{-ij} A_j, \qquad 0 \leq i \leq n-1. \tag{5.7}$$

where p is the characteristic value of the field.In this thesis, since all constructions are over the field $GF(2)$, $p = 2$. Following Theorems 1 and 2 of [Raghavendra and Acharya (2020)], we consider design of full rank $(m, 1)$ cyclic code $\mathscr{C}$ over $GF(2^m)$. The codewords of $\mathscr{C}$ are square matrices with dimension $m \times m$ with elements over $GF(2)$. Let the free transform component be C_1. Since, $C_1 \in GF(2^m)$ there will be 2^m codeword matrices in $\mathscr{C}$. The full rank codewords of $GF\,(2^m)$ for $m = 2, 3, 4$ given in Table 5.1.

Table 5.1: Full rank codes from cyclic of respective field.

Field	**NOSTBC**	**Matrix codewords of Full rank codes** $i.e,\ \mathscr{F}(s_1, s_2, \cdots, s_N)$
$GF(2^2)$	$2 \times M$	$C_1 = \underset{\{0,0\}}{0} \rightarrow \begin{bmatrix} 0 & 0 \\ 0 & 0 \end{bmatrix}$ $C_1 = \underset{\{0,1\}}{1} \rightarrow \begin{bmatrix} 1 & 1 \\ 0 & 1 \end{bmatrix}$, $C_1 = \underset{\{1,0\}}{\alpha} \rightarrow \begin{bmatrix} 0 & 1 \\ 1 & 0 \end{bmatrix}$ $C_1 = \underset{\{1,0\}}{\alpha^2} \rightarrow \begin{bmatrix} 1 & 0 \\ 1 & 1 \end{bmatrix}$
$GF(2^3)$	$3 \times M$	$C_1 = \underset{\{0,0\}}{0} \rightarrow \begin{bmatrix} 0 & 0 & 0 \\ 0 & 0 & 0 \\ 0 & 0 & 0 \end{bmatrix}$ $C_1 = \underset{\{0,0\}}{1} \rightarrow \begin{bmatrix} 1 & 1 & 1 \\ 0 & 0 & 1 \\ 0 & 1 & 1 \end{bmatrix}$ $C_1 = \underset{\{0,0\}}{\alpha} \rightarrow \begin{bmatrix} 0 & 1 & 1 \\ 1 & 0 & 0 \\ 0 & 0 & 1 \end{bmatrix}$ $C_1 = \underset{\{0,0\}}{\alpha^2} \rightarrow \begin{bmatrix} 0 & 0 & 1 \\ 0 & 1 & 0 \\ 1 & 0 & 0 \end{bmatrix}$ $C_1 = \underset{\{0,0\}}{\alpha^3} \rightarrow \begin{bmatrix} 1 & 0 & 0 \\ 1 & 0 & 1 \\ 0 & 1 & 0 \end{bmatrix}$ $C_1 = \underset{\{0,0\}}{\alpha^4} \rightarrow \begin{bmatrix} 0 & 1 & 0 \\ 1 & 1 & 0 \\ 1 & 0 & 1 \end{bmatrix}$ $C_1 = \underset{\{0,0\}}{\alpha^5} \rightarrow \begin{bmatrix} 1 & 0 & 1 \\ 1 & 1 & 1 \\ 1 & 1 & 0 \end{bmatrix}$ $C_1 = \underset{\{0,0\}}{\alpha^6} \rightarrow \begin{bmatrix} 1 & 1 & 0 \\ 0 & 1 & 1 \\ 1 & 1 & 1 \end{bmatrix}$
$GF(2^4)$	$4 \times M$	$C_1 = \underset{\{0,0\}}{0} \rightarrow \begin{bmatrix} 0 & 0 & 0 & 0 \\ 0 & 0 & 0 & 0 \\ 0 & 0 & 0 & 0 \\ 0 & 0 & 0 & 0 \end{bmatrix}$ $C_1 = \underset{\{0,0\}}{1} \rightarrow \begin{bmatrix} 1 & 1 & 1 & 1 \\ 0 & 0 & 0 & 1 \\ 0 & 0 & 1 & 1 \\ 0 & 1 & 1 & 1 \end{bmatrix}$ $C_1 = \underset{\{0,0\}}{\alpha} \rightarrow \begin{bmatrix} 0 & 1 & 1 & 1 \\ 1 & 0 & 0 & 0 \\ 0 & 0 & 0 & 1 \\ 0 & 0 & 1 & 1 \end{bmatrix}$ $C_1 = \underset{\{0,0\}}{\alpha^2} \rightarrow \begin{bmatrix} 0 & 0 & 1 & 1 \\ 0 & 1 & 0 & 0 \\ 1 & 0 & 0 & 0 \\ 0 & 0 & 0 & 1 \end{bmatrix}$ $C_1 = \underset{\{0,0\}}{\alpha^3} \rightarrow \begin{bmatrix} 0 & 0 & 0 & 1 \\ 0 & 0 & 1 & 0 \\ 0 & 1 & 0 & 0 \\ 1 & 0 & 0 & 0 \end{bmatrix}$ $C_1 = \underset{\{0,0\}}{\alpha^4} \rightarrow \begin{bmatrix} 1 & 0 & 0 & 0 \\ 1 & 0 & 0 & 1 \\ 0 & 0 & 1 & 0 \\ 0 & 1 & 0 & 0 \end{bmatrix}$ $C_1 = \underset{\{0,0\}}{\alpha^5} \rightarrow \begin{bmatrix} 0 & 1 & 0 & 0 \\ 1 & 1 & 0 & 0 \\ 1 & 0 & 0 & 1 \\ 0 & 0 & 1 & 0 \end{bmatrix}$ $C_1 = \underset{\{0,0\}}{\alpha^6} \rightarrow \begin{bmatrix} 0 & 0 & 1 & 0 \\ 0 & 1 & 1 & 0 \\ 1 & 1 & 0 & 0 \\ 1 & 0 & 0 & 1 \end{bmatrix}$ $C_1 = \underset{\{0,0\}}{\alpha^7} \rightarrow \begin{bmatrix} 1 & 0 & 0 & 1 \\ 1 & 0 & 1 & 1 \\ 0 & 1 & 1 & 0 \\ 1 & 1 & 0 & 0 \end{bmatrix}$ $C_1 = \underset{\{0,0\}}{\alpha^8} \rightarrow \begin{bmatrix} 1 & 1 & 0 & 0 \\ 0 & 1 & 0 & 1 \\ 1 & 0 & 1 & 1 \\ 0 & 1 & 1 & 0 \end{bmatrix}$ $C_1 = \underset{\{0,0\}}{\alpha^9} \rightarrow \begin{bmatrix} 0 & 1 & 1 & 0 \\ 1 & 0 & 1 & 0 \\ 0 & 1 & 0 & 1 \\ 1 & 0 & 1 & 1 \end{bmatrix}$ $C_1 = \underset{\{0,0\}}{\alpha^{10}} \rightarrow \begin{bmatrix} 1 & 0 & 1 & 1 \\ 1 & 1 & 0 & 1 \\ 1 & 0 & 1 & 0 \\ 0 & 1 & 0 & 1 \end{bmatrix}$ $C_1 = \underset{\{0,0\}}{\alpha^{11}} \rightarrow \begin{bmatrix} 0 & 1 & 0 & 1 \\ 1 & 1 & 1 & 0 \\ 1 & 1 & 0 & 1 \\ 1 & 0 & 1 & 0 \end{bmatrix}$ $C_1 = \underset{\{0,0\}}{\alpha^{12}} \rightarrow \begin{bmatrix} 1 & 0 & 1 & 0 \\ 1 & 1 & 1 & 1 \\ 1 & 1 & 1 & 0 \\ 1 & 1 & 0 & 1 \end{bmatrix}$ $C_1 = \underset{\{0,0\}}{\alpha^{13}} \rightarrow \begin{bmatrix} 1 & 1 & 0 & 1 \\ 0 & 1 & 1 & 1 \\ 1 & 1 & 1 & 1 \\ 1 & 1 & 1 & 0 \end{bmatrix}$ $C_1 = \underset{\{0,0\}}{\alpha^{14}} \rightarrow \begin{bmatrix} 1 & 1 & 1 & 0 \\ 0 & 0 & 1 & 1 \\ 0 & 1 & 1 & 1 \\ 1 & 1 & 1 & 1 \end{bmatrix}$

5.3.2.1 Complexity

Since we are employing OOK the computation of ML metric at the receiver is defined over binary codeword matrices. The ML metric is given by:

$$\left\| Y(t) - \eta\sqrt{P_t T_b} H\tilde{F}\left(s_1, s_2, \cdots, s_N\right) \right\|^2 \tag{5.8}$$

Since, H is $M \times N$ channel matrix and $\tilde{F}\left(s_1, s_2, \cdots, s_N\right)$ is $N \times T$ transmitted codeword matrix. For each computation of $H\tilde{F}\left(s_1, s_2, \cdots, s_N\right)$ there are at most MNT multiplications and $M(N-1)T$ additions. Since $\tilde{F}\left(s_1, s_2, \cdots, s_N\right)$ is defined over binary field, the computation can be thought of addition of real symbols of each row of H corresponding to $1^{'}s$ in each column of $\hat{F}\left(s_1, s_2, \cdots, s_N\right)$ matrix. After obtaining $H\tilde{F}\left(s_1, s_2, \cdots, s_N\right)$, the computation of L2-norm in equation (5.8) requires MN subtractions (additions) and MN multiplications. Figure 5.3, shows the number of multiplications, additions/ subtractions for evaluating ML metric with respect to various MIMO STBC schemes. Since there are 2^m codeword matrices in $\mathscr{C}$, the total computational complexity involved in detecting one transmitted STBC/NOSTBC is given by

$$2^m \left[M(N + (N-1))T + 2MN\right] \tag{5.9}$$

In this work, we have consider the number of transmitters equal to number of rows of NOSTBC i.e., $N = m$. Equation (5.9) can be written as,

$$2^N \left[M(2N-1)T + 2MN\right] \tag{5.10}$$

The computational complexity based the number of multiplications, additions and subtractions are presented in Table 5.2. For evaluating the compuational complexity we have considered the Rate-1 STBC codes i.e., $T = N$. From the Table 5.2 and Figure 5.3, the compuatational complexity (multiplications, additions) is increasing for higher order MIMO STBC schems.

Table 5.2: Computational complexity of various proposed MIMO STBC schemes.

MIMO STBC scheme	2×1	2×2	2×4	4×1	4×2	4×4
Compuatational Complexity	40	80	160	576	1152	2304

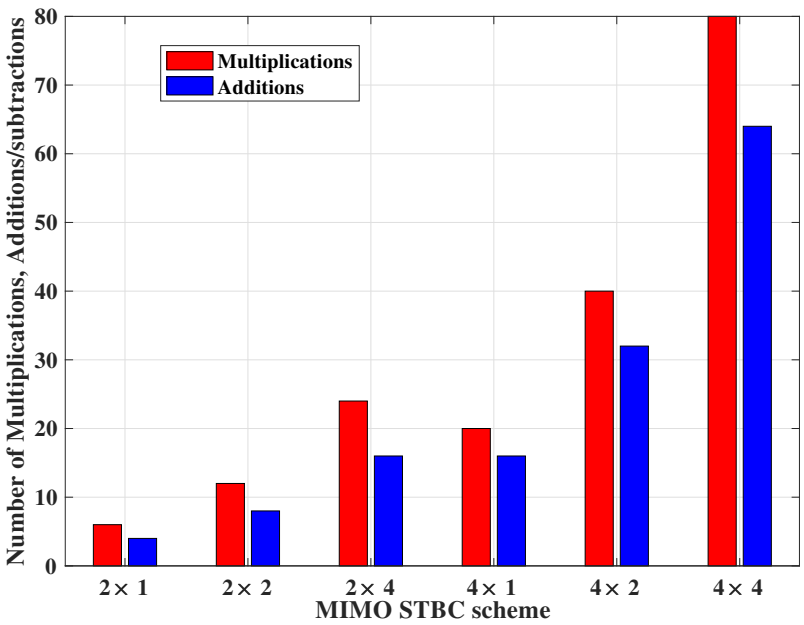

Figure 5.3: Number of Multiplications and additions for various MIMO STBC schemes.

5.4 Results and discussions

In this section, we present the Monte-Carlo BER results of OSTBC and NOSTBC schemes with respect to transmit power (in dB) under the influence of weak turbulence.

Figure 5.4, shows the comparison of BER simulations of the OSTBC scheme with the SISO UWOC system. STBC with the 2×1, 2×2, 2×3, and 2×4 gains a transmit power of 17, 28, 29, and 29.50 dB when compared with the SISO UWOC system at a BER of 10^{-5} respectively. Similarly, the STBC with the 4×1, 4×2, 4×3, and 4×4 gains a transmit power of 7, 23, 30, and 30.50 dB compared with the SISO system at a BER of 10^{-5} respectively. It is also evident that $4 \times M$ STBC performs better than $2 \times M$ STBC schemes. Table 5.3, shows the transmit power required to obtain a BER of 10^{-5} using STBC and SISO systems and transmit power gain comparison of various STBC schemes with the SISO UWOC system.

Figure 5.5 shows the BER comparison of the NOSTBC scheme with the SISO, and it also shows the improvement in the transmit power requirement for an increase in N and M in case of NOSTBC scheme. The gain in transmit power from SISO to 2×1 NOSTBC is 10.90 dB, similarly the improvement in P_t from SISO to 2×2, 3×3, and 4×4 are 19, 28.50 and 33.20 dB respectively at a BER of 10^{-5}

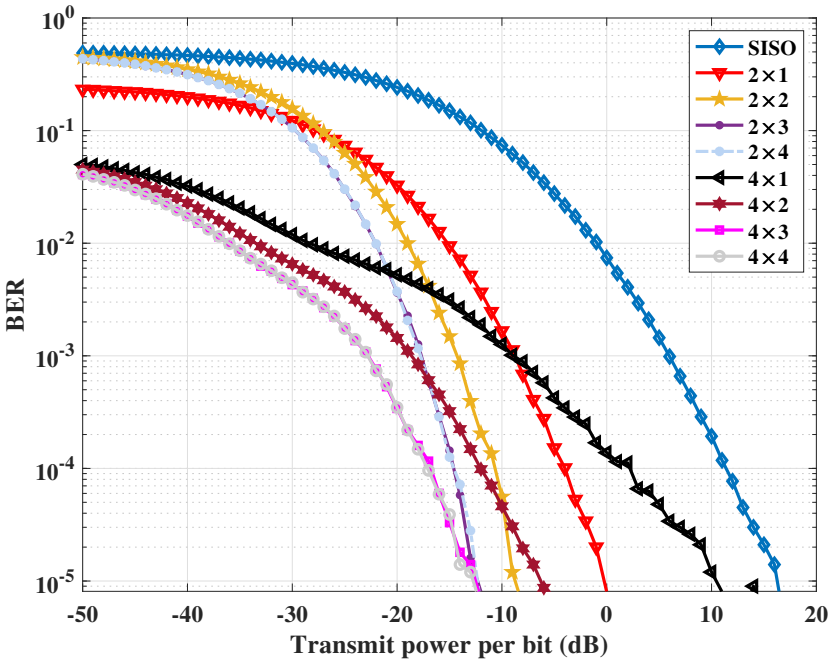

Figure 5.4: BER Simulation results of MIMO UWOC using STBC.

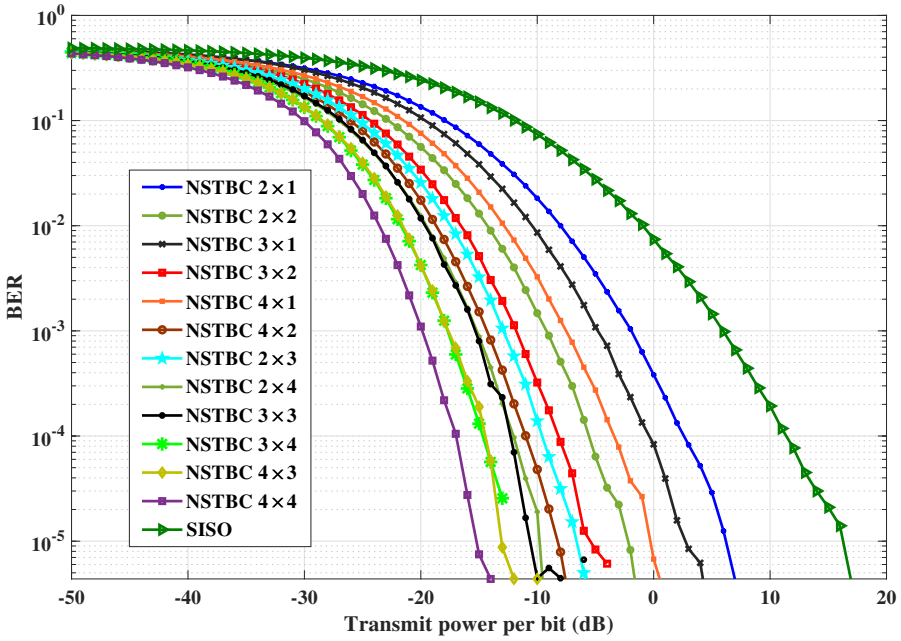

Figure 5.5: BER Simulation results of MIMO UWOC using NOSTBC.

respectively. Table 5.4 shows the transmit power required to obtain a BER of 10^{-5} and transmit power gain comparison of various NOSTBC schemes with the SISO.

From Figures 5.4 and 5.5, it is evident that certain NOSTBC scheme perform

Table 5.3: Power gain comparison of OSTBC with SISO

STBC	**Transmit Power (dB) at BER of 10^{-5}**	**Power gain (dB) from un-coded SISO**
SISO	17.00	-
2×1	00.00	17.00
2×2	-11.00	28.00
2×3	-12.00	29.00
2×4	-12.50	29.50
4×1	10.00	07.00
4×2	-06.00	23.00
4×3	-13.00	30.00
4×4	-13.50	30.50

Table 5.4: Power gain comparison of NOSTBC with SISO

NOSTBC	**Transmit Power (dB) at BER of 10^{-5}**	**Power gain (dB) from un-coded SISO**
SISO	17.00	-
2×1	06.10	10.90
2×2	-02.05	19.05
2×3	-07.50	24.50
2×4	-10.10	27.10
3×1	02.95	14.05
3×2	-06.50	23.50
3×3	-11.50	28.50
3×4	-14.50	31.50
4×1	-00.50	17.50
4×2	-09.75	26.75
4×3	-13.00	30.00
4×4	-16.20	33.20

better than the corresponding OSTBC schemes. This improvement is usually evident for higher order MIMO systems ($4 \times M, M = 1, 2, 3, 4$). In the case of 2×1 and 1×2 schemes, the performance of OSTBC is superior to that of NOSTBC schemes. For higher order MIMO schemes the Euclidean distance between the NOSTNBC code-words is more than that of the code-words generated using OSTBC schems. Hence, NOSTBC superior for higher order MIMO than OSTBC MIMO. The transmit power gain in dB for NOSTBC schemes when compared with OSTBC is tabulated in Table 5.5.

Table 5.5: Power gain comparison of NOSTBC with OSTBC

$N \times M$	**STBC**	**NOSTBC**	**Power gain (dB) of NOSTBC from STBC**
2×1	00.00	06.10	-06.00
2×2	-11.00	-02.50	-08.50
2×3	-12.00	-07.50	-04.50
2×4	-12.50	-10.10	-02.40
4×1	10.00	-00.50	09.50
4×2	-06.00	-09.75	03.75
4×3	-13.00	-13.00	00.00
4×4	-13.50	-16.20	02.70

5.5 Conclusion

In this chapter, we have constructed the binary STBC schemes using orthogonal and non-orthogonal constraints for OOK modulated UWOC system. This system provides higher throughput than the system proposed in Chapter 3 and provides an improvement in the reliability of communication. However, there is a corresponding increase in computational complexity. Hence this system can be employed in scenarios where the higher throughput and reliability are primary requirements, and the increase in complexity can be accommodated.

Chapter 6

Performance Analysis of Co-operative RF-UWOC Link

In this chapter, we have proposed and analyzed the outage probability and average Bit Error Rate (BER) performance of a co-operative Radio Frequency - Underwater Wireless Optical Communication (RF-UWOC) system. In recent years, UWOC has found increasing application in enabling scientific activities carried out under the surface of water such as monitoring climate change, underwater exploration, oceanic studies, surveillance and monitoring. The study of these phenomena is greatly facilitated by the availability of underwater wireless optical sensor networks and Internet of Underwater Things (IoUT). The proposed co-operative RF-UWOC system can be used to establish a reliable and high speed connection between an underwater vehicle inside the ocean to a terrestrial ground station using amplify-forward and decode-forward relay. The RF link between the terrestrial ground station to relay is modeled by the Rayleigh distribution. The UWOC link between the relay and underwater vehicle is modeled by employing the Hyperbolic Tangent Log-Normal (HTLN) distribution. To the best of our knowledge, it is for the first time that the perturbations due to weak oceanic turbulence are being modeled using HTLN distribution. The HTLN distribution is a class of log-normal distribution derived from hyperbolic tangent distribution. Novel closed form expressions have been derived for the outage probability and average BER for various modulation techniques that can be employed in the proposed system. The analytical results are evaluated and validated with Monte-Carlo simulations both in the presence and absence of pointing errors. Our analytic and simulation results show that in the presence of pointing errors, a SNR penalty of approximately 10 dB has to be paid to achieve a BER of 10^{-6} when compared to a system operating without pointing errors.

6.1 Introduction

In a co-operative communication system, the relay nodes are used to establish the communication link between the source and destination [Miridakis *et al.* (2014), Laneman *et al.* (2004), Lee *et al.* (2011)]. This communication system involves multiple distributed links operating over different kinds of fading environments [Bletsas *et al.* (2007)]. In this chapter, we have studied the design and performance analysis of a co-operative (hybrid) communication system which consists of a Radio-Frequency (RF) link and an UWOC link operating together. Figure 6.1 is an illustration of the proposed RF–UWOC system employed for ocean monitoring.

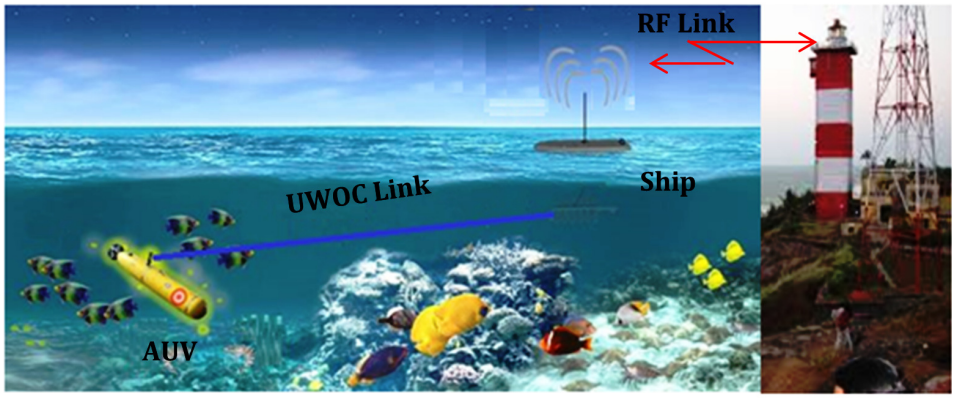

Figure 6.1: Ocean monitoring using RF−UWOC link

6.1.1 Contributions

The contributions made in this chapter are listed below.

- Evaluation of the performance of the RF−UWOC system with and without pointing errors.
- Derivation of expressions to determine the individual outage probabilities of the RF and UWOC subsystems.
- Determining a combined expression for the outage probability of the proposed RF–UWOC composite system (outage probabilities have been separately calculated for the composite link comprising of Amplify-and-Forward (AF) and Decode-and-Forward (DF) relays. A performance comparison between these systems has also been presented).
- Determination of closed-form expressions quantifying the analytical Bit Error Rate (BER) for various modulation techniques.

6.2 System Model

Consider a co-operative communication between the source (S) to destination (D) via a DF or AF relay node (R) as illustrated in Figure 6.2. The RF communication link between $S-R$ is assumed to be Rayleigh distributed. Perturbations induced by weak turbulence over the UWOC link $R-D$ are characterized by the HTLN distribution. Figure 6.2 depicts the system model comprising of a mixed RF−UWOC co-operative communication link, where DF/ AF relay is used to convert the input RF signal into an optical signal by the adoption of sub-carrier intensity modulation [Samimi and Uysal (2013)] and detector is placed on the autonomous underwater vehicle (AUV) represented by D.

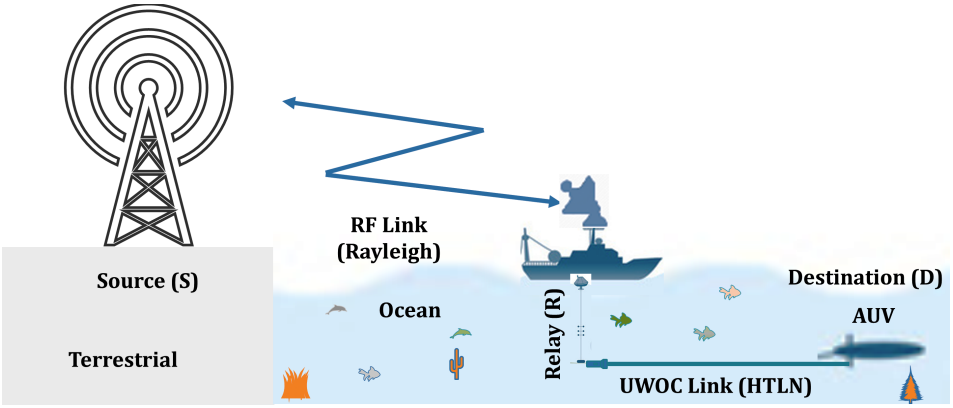

Figure 6.2: RF−UWOC System Model

The data received at node R through the RF link is

$$r = hs + n_1 \tag{6.1}$$

where h denotes the channel gain modeled using the Rayleigh distribution, s represents data present at the source node and n_1 is Additive White Gaussian Noise (AWGN) with zero-mean and variance σ^2_{s-r}. The Signal-to-Noise Ratio (SNR) of the RF link is $\gamma_1 = E_{(s,r)}\left(|h|^2\right)/\sigma^2_{s-r}$, where $E_{(s,r)}$ is energy of data source (s) and the average SNR is specified by $\bar{\gamma_1} = E_{(s,r)}/\sigma^2_{s-r}$. Similarly, the data received at node D through the UWOC link is modeled by,

$$y = \eta I \hat{s} + n_2 \tag{6.2}$$

where η is detector responsivity in terms of Amperes per Watt (A/W), I is received irradiance, $\hat{s}$ is estimate of data transmitted through the RF link, and n_2 is AWGN noise with zero mean and variance σ^2_{r-d}. The SNR of UWOC link

$\gamma_2 = \eta^2 I^2 E_{(r,d)}/\sigma^2_{r-d}$, $E_{(r,d)}$ is energy of $\hat{s}$ and the average SNR is $\bar{\gamma_2} = \eta^2 E_{(r,d)}/\sigma^2_{r-d}$. From [Laneman *et al.* (2004), Miridakis *et al.* (2014)], the overall received SNR of end-to-end RF-UWOC communication link is $\gamma = \min(\gamma_1, \gamma_2)$, which means the resultant SNR is dependent upon the minimum of SNR required to decode the source message at the relay node and the destination nodes respectively.

6.3 Channel Model

The channel models for RF link, UWOC channel (with and without pointing errors) perturbed by weak turbulence have been derived in this section. This is followed by a discussion of the channel model for the composite RF-UWOC link.

6.3.1 RF channel for $S - R$ link

The Rayleigh PDF is frequently used to model RF multipath fading. The PDF of Rayleigh fading channel is given as,

$$f_{\gamma_1}(\gamma_1) = \frac{1}{\bar{\gamma_1}} \exp\left(-\frac{\gamma_1}{\bar{\gamma_1}}\right) \tag{6.3}$$

where γ_1 and $\bar{\gamma_1}$ represent the SNR and average SNR of RF link respectively. The corresponding CDF is given as,

$$F_{\gamma_1}(\gamma_1) = \frac{1}{\bar{\gamma_1}} \left(1 - \exp\left(-\frac{\gamma_1}{\bar{\gamma_1}}\right)\right) \tag{6.4}$$

6.3.2 Turbulent UWOC channel for $R - D$ link

The received irradiance through the underwater channel experiencing weak turbulence can be characterized by Log-Normal (LN) density function [Jamali *et al.* (2018), Ramavath *et al.* (2020)], which is given as,

$$f_{\gamma_a}(\gamma_a) = \frac{1}{2\gamma_a\sqrt{2\pi\sigma_X^2}} \exp\left(-\frac{\left(\ln\left(\frac{\gamma_a}{\bar{\gamma_2}}\right) - 2\mu_X\right)^2}{8\sigma_X^2}\right) \tag{6.5}$$

where γ_a represents the turbulence fading factor, μ_X and σ_X^2 are mean and variance of normal random variable $X = 0.5\ln(\gamma_a/\bar{\gamma_2})$ and $\bar{\gamma_2}$ is the average SNR of UWOC link. Normalizing Equation (6.5) by considering $\mathbb{E}(\gamma_a) = \bar{\gamma_2}$, which yields $\mu_X = -\sigma_X^2$.

During the setting up of a UWOC link, due care is taken to ensure that there is proper alignment between the transmitter and receiver. However, due to motion of the underwater medium, this alignment can be disturbed. This is the reason for origin of pointing errors. Pointing error is modeled as a random variable for the purpose of analysis. The distribution of the PDF of pointing error for this random variable γ_p assuming that the detector has a circular aperture is given by [Sandalidis *et al.* (2008)],

$$f_{\gamma_p}(\gamma_p) = \frac{\zeta^2}{A_0^{\zeta^2}} \gamma_p^{\zeta^2-1}, \quad 0 \leq \gamma_p \leq A_0 \tag{6.6}$$

where ζ is ratio of the beam radius $\left(\omega_{z_{eq}}\right)$ to the standard deviation of pointing error displacement (σ_s) at the receiver, $A_0 = (erf(\vartheta))^2$ is the path loss constant, $\vartheta = \omega_z\sqrt{\pi}/\left(r\sqrt{2}\right)$, ω_z denotes the beam waist and r is the radius of detector.

The channel gain due to the combined effect of underwater turbulence and pointing error is $\gamma_2 = \gamma_p\gamma_a$. The combined PDF of underwater turbulent and pointing error is obtained using Equation (4) of [Yang *et al.* (2014)] as,

$$f_{\gamma_2}(\gamma_2) = \frac{\zeta^2\gamma_2^{\zeta^2-1}}{A_0^{\zeta^2}} \int_{\gamma_2/A_0}^{\infty} \gamma_a^{-\zeta^2} f_{\gamma_a}(\gamma_a) d\gamma_a \tag{6.7}$$

By substituting t with $\gamma_a/\bar{\gamma_2}$ then Equation. (6.7) becomes,

$$f_{\gamma_2}(\gamma_2) = \frac{\zeta^2\gamma_2^{\zeta^2-1}}{(A_0\bar{\gamma_2})^{\zeta^2}} \int_{\frac{\gamma_2}{A_0\bar{\gamma_2}}}^{\infty} t^{-\zeta^2} f(t) dt \tag{6.8}$$

where, $f(t) = \frac{1}{2t\sqrt{2\pi\sigma_X^2}} \exp\left(-\frac{(\ln(t)-2\mu_X)^2}{8\sigma_X^2}\right)$ represents the LN density function. A solution to Equation (6.8) cannot be obtained using the conventional LN description to represent weak turbulence. However, a closed form solution can be obtained if we model $f(t)$ by the HTLN distribution (a detailed derivation is presented in Appendix E) and it is given as,

$$f(t) = \frac{be^{2a}t^{b-1}}{\left(1+e^{2a}t^b\right)^2} \tag{6.9}$$

Substituting Equation (6.9) in (6.8) yields,

$$f_{\gamma_2}(\gamma_2) \approx \frac{be^{2a}\zeta^2}{(A_0\bar{\gamma_2})^{\zeta^2}} \gamma_2^{\zeta^2-1} \int_{\frac{\gamma_2}{A_0\bar{\gamma_2}}}^{\infty} \frac{t^{b-\zeta^2-1}}{\left(1+e^{2a}t^b\right)^2} dt \tag{6.10}$$

Integrating Equation (6.10) using Eqs. (10) and (11) of [Adamchik and Marichev (1990)], and [Wolfram (2001)], we can obtain a closed-form solution for the density function of the LN distributed variable γ_2 as,

$$f_{\gamma_2}(\gamma_2) = \frac{e^{2a}\zeta^2}{(A_0\bar{\gamma_2})^b}\gamma_2^{b-1}G_{1+b,1+b}^{1+b,1}\left(\begin{matrix}-1,\frac{i-b+\zeta^2-1}{b}\\ \frac{i-b+\zeta^2-2}{b},0\end{matrix}\middle| W\gamma_2^b\right) \tag{6.11}$$

where $i = 1, 2, \ldots, b$ and $W = \frac{e^{2a}}{(A_0\bar{\gamma_2})^b}$. The corresponding CDF is,

$$F_{\gamma_2}(\gamma_2) = \mathscr{C}\gamma_2^b G_{1+2b,1+2b}^{1+b,1+b}\left(\begin{matrix}\frac{i-b}{b},-1,\frac{i-b+\zeta^2}{b}\\ \frac{i-b+\zeta^2-1}{b},0,\frac{i-b-1}{b}\end{matrix}\middle| W\gamma_2^b\right) \tag{6.12}$$

where $\mathscr{C} = \frac{e^{2a}\zeta^2}{b(A_0\bar{\gamma_2})^b}$. Equation (6.12) represents the CDF of UWOC channel in the presence of pointing errors. The CDF of UWOC without pointing errors is obtained by substitution and integration of Equation (6.5) with in the limits of 0 to γ_2 and it can be expressed as,

$$F_{\gamma_2}(\gamma_2) = \frac{e^{2a}}{(\bar{\gamma_2})^b}\gamma_2^b G_{1+b,1+b}^{1,1+b}\left(\begin{matrix}\frac{i-b}{b},-1\\ 0,\frac{i-b-1}{b}\end{matrix}\middle| \frac{e^{2a}}{(\bar{\gamma_2})^b}\gamma_2^b\right) \tag{6.13}$$

6.3.3 CDF of DF based co-operative RF–UWOC system

The CDF of a dual hop co-operative wireless communication system (DF based) with SNRs γ_1 and γ_2 for $S-R$ and $R-D$ respectively as [Miridakis *et al.* (2014)],

$$F_\gamma(\gamma) = F_{\gamma_1}(\gamma) + F_{\gamma_2}(\gamma) - F_{\gamma_1}(\gamma)F_{\gamma_2}(\gamma) \tag{6.14}$$

Substituting Equation (6.4) and (6.12) in (6.14), obtained CDF is,

$$\begin{aligned} F_\gamma(\gamma) \;=\; & \frac{1}{\bar{\gamma_1}}\left(1-\exp\left(-\frac{\gamma}{\bar{\gamma_1}}\right)\right) + \left[1-\frac{1}{\bar{\gamma_1}}+\frac{1}{\bar{\gamma_1}}\exp\left(-\frac{\gamma}{\bar{\gamma_1}}\right)\right] \\ & \times\mathscr{C}\gamma^{b+1}G_{1+2b,1+2b}^{1+b,1+b}\left(\begin{matrix}\frac{i-b}{b},-1,\frac{i-b+\zeta^2}{b}\\ \frac{i-b+\zeta^2-1}{b},0,\frac{i-b-1}{b}\end{matrix}\middle| W\gamma^b\right) \end{aligned} \tag{6.15}$$

6.3.4 CDF of AF based co-operative RF–UWOC system

The CDF of a AF based co-operative wireless communication system with SNRs γ_1 and γ_2 for $S-R$ and $R-D$ respectively as,

$$F_\gamma(\gamma) = P\left(\frac{\gamma_1\gamma_2}{1+\gamma_2} < \gamma_{th}\right) = \int_0^\infty F_{\gamma_1}\left(\gamma_{th}\left(1+\gamma_2^{-1}\right)\middle|\gamma_2\right) f_{\gamma_2}(\gamma_2)\, d\gamma_2 \tag{6.16}$$

Substituting Equations. (6.4) and (6.11) in Equation (6.16), the obtained CDF is given as,

$$F_{\gamma}\left(\gamma\right)=\frac{e^{2a}\zeta^{2}}{\left(A_{0}\bar{\gamma}_{2}\right)^{b}}\left(I_{1}-e^{-\frac{\gamma}{\bar{\gamma}_{1}}}\frac{b^{-\left(\frac{2b-1}{2}\right)}}{\left(2\pi\right)^{\frac{b-1}{2}}}\left(\frac{\gamma}{\bar{\gamma}_{1}}\right)^{b}I_{2}(\gamma)\right) \tag{6.17}$$

where $I_{1}=G_{1+b,1+b}^{1+b,1}\left(\begin{matrix}-1,\frac{i-b+\zeta^{2}-1}{b}\\ \frac{i-b+\zeta^{2}-2}{b},0\end{matrix}\middle|W\right)$ and $I_{2}(\gamma)=G_{1+b,1+2b}^{1+2b,1}\left(\begin{matrix}-1,\frac{i-b+\zeta^{2}-1}{b}\\ \frac{i-b+\zeta^{2}-2}{b},0,\frac{i-b-1}{b}\end{matrix}\middle|W\left(\frac{\bar{\gamma}_{1}}{b\gamma}\right)^{b}\right)$

6.4 System Performance

In this section, the outage probability and average BER of the proposed system are derived.

6.4.1 Outage Probability

The end-to-end outage probability for DF and AF based RF-UWOC co-operative communication system is determined in this section.

6.4.1.1 DF based system

The resultant SNR, when the DF relay has been used is $\gamma_{th}>min\{\gamma_{1},\gamma_{2}\}$ and the corresponding outage probability can be obtained as,

$$P_{o}=P\left(\min\{\gamma_{1},\gamma_{2}\}<\gamma_{th}\right)=F_{\gamma}\left(\gamma_{th}\right) \tag{6.18}$$

Substituting Equation (6.16) in (6.18), the obtained outage probability is,

$$\begin{aligned}P_{o}\;=\;&\frac{1}{\bar{\gamma}_{1}}\left(1-\exp\left(-\frac{\gamma_{th}}{\bar{\gamma}_{1}}\right)\right)+\left[\left(1-\frac{1}{\bar{\gamma}_{1}}\right)+\frac{1}{\bar{\gamma}_{1}}\exp\left(-\frac{\gamma_{th}}{\bar{\gamma}_{1}}\right)\right]\\&\times\mathscr{C}\gamma_{th}^{b+1}G_{1+2b,1+2b}^{1+b,1+b}\left(\begin{matrix}\frac{i-b}{b},-1,\frac{i-b+\zeta^{2}}{b}\\ \frac{i-b+\zeta^{2}-1}{b},0,\frac{i-b-1}{b}\end{matrix}\middle|W\gamma_{th}^{b}\right)\end{aligned} \tag{6.19}$$

6.4.1.2 AF based system

The resultant SNR, when the AF relay has been used is given as, $\gamma_{th}>\frac{\gamma_{1}\gamma_{2}}{\gamma_{2}+1}$ and corresponding outage probability is obtained as,

$$P_{o}=\frac{e^{2a}\zeta^{2}}{\left(A_{0}\bar{\gamma}_{2}\right)^{b}}\left(I_{1}-I_{2}\left(\gamma_{th}\right)\right) \tag{6.20}$$

6.4.2 Average Bit Error Rate

The average BER of DF/ AF based RF-UWOC co-operative communication system for various modulation techniques is given as [Zedini *et al.* (2016)],

$$P_e = \frac{\delta}{2\Gamma(p)} \sum_{k=1}^{\mathscr{K}} \left[q_k^p \int_0^\infty e^{-q_k \gamma} \gamma^{p-1} F_\gamma(\gamma) d\gamma \right] \tag{6.21}$$

where δ, p, q_k and $\mathscr{K}$ are parameters that depend on the type of modulation. The values of these parameters for various modulation techniques like OOK, Binary Frequency Shift Keying (BFSK), Binary Phase Shift Keying (BPSK), Differential Binary Phase Shift Keying (DBPSK), M-ary Quadrature Amplitude Modulation (M-QAM) and M-ary Phase Shift Keying modulation (M-PSK) are presented in in Table 6.1 [Ansari *et al.* (2013)]. Substituting Equation (6.16) in (6.21) and then

Table 6.1: BER parameters for different modulation techniques.

Modulation type	p	δ	q_k	$\mathscr{K}$
OOK	0.5	1	0.25	1
BFSK	1	1	0.5	1
BPSK	0.5	1	1	1
DBPSK	1	1	1	1
M-QAM	0.5	$\frac{4}{\log_2 M}\left(1-\frac{1}{\sqrt{M}}\right)$	$\frac{3(2k-1)^2}{2(M-1)}$	$\max\left(\lfloor\frac{\sqrt{M}}{2}\rfloor, 1\right)$
M-PSK	0.5	$\frac{2}{max(\log_2 M,\ 2)}$	$\sin^2\left(\frac{(2k-1)\pi}{M}\right)$	$\max\left(\frac{M}{4},\ 1\right)$

integrating, gives average BER of the DF based RF-UWOC communication system as,

$$P_e = \sum_{k=1}^{n} \left(\sum_{j=1}^{2} \left[\mathscr{D}_{k,j} G_{1+3b,1+2b}^{1+b,1+2b} \left(\begin{matrix} \frac{i-b}{b}, -1, \frac{i-b-p}{b} \frac{i-b+\zeta^2}{b} \\ \frac{i-b+\zeta^2-1}{b}, 0, \frac{i-b-1}{b} \end{matrix} \middle| \mathscr{W}_{k,j} \right) \right] \right) + \sum_{k=1}^{n} \left(\frac{\delta \left[1 - \left(\frac{\bar{\gamma}_1 q_k}{\bar{\gamma}_1 q_k + 1} \right)^p \right]}{2\bar{\gamma}_1} \right) \tag{6.22}$$

where $\mathscr{D}_{k,j} = \frac{\delta \zeta^2 e^{2a} b^{b+p-0.5}}{2\Gamma(p)(\bar{\gamma}_2 A_0)^b q_k^{b+1} (2\pi)^{(b-1)/2}} \mathscr{D}_j$, $\mathscr{D}_1 = \left(1 - \frac{1}{\bar{\gamma}_1}\right)$, $\mathscr{D}_2 = \frac{1}{\bar{\gamma}_1}$, $\mathscr{W}_{k,1} = e^{2a} \left(\frac{b}{A_0 \bar{\gamma}_2 q_k} \right)^b$ and $\mathscr{W}_{k,2} = e^{2a} \left(\frac{b}{A_0 \bar{\gamma}_2 \left(q_k + \frac{1}{\bar{\gamma}_1} \right)} \right)^b$.

Similarly the average BER of AF based RF-UWOC communication system is

obtained as,

$$P_e = \sum_{k=1}^{n} \left(I_1 \Gamma(p) - \frac{q_k^{-b} b^p}{\bar{\gamma_1}^b (2\pi)^{b-1}} G_{1+3b,1+b}^{1,1+3b} \left(\begin{matrix} \frac{2b-i-\zeta^2+2}{b}, 1, \frac{2b-i+1}{b}, \frac{i-b-q}{b} \\ 2, \frac{2b-i-\zeta^2+1}{b} \end{matrix} \middle| \left(\frac{b^2}{q_k \bar{\gamma_1}} \right)^b \frac{1}{W} \right) \right) \times \frac{\delta \zeta^2 e^{2a}}{2\Gamma(p) (A_o \bar{\gamma_2})^b} \tag{6.23}$$

6.5 Results and Discussion

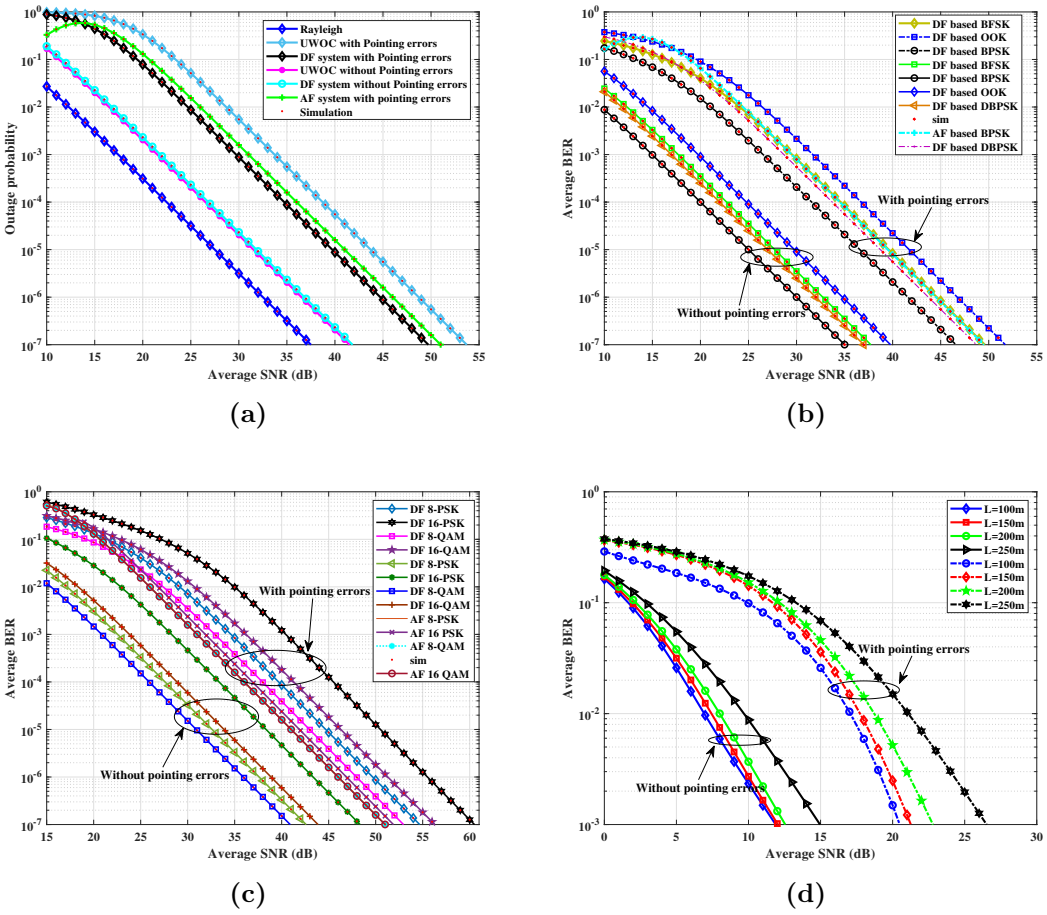

Figure 6.3: (a) Outage probability, (b) Average BER of binary modulated, (c) M-ary modulated RF−UWOC system, and (d) Avergae BER with respect to average SNR for varying link range.

In this section, we have presented plots which specify the outage probability and average BER results of a mixed RF−UWOC communication system as a function of average SNR by employing the closed-form expressions derived in this chapter. It is assumed that average SNR of both links are equal i.e., $\bar{\gamma}_1 = \bar{\gamma}_2$ and outage

probability obtained for individual SNRs (i.e, γ_1, γ_2) less than or equal to 5 dB (i.e, threshold SNR γ_{th}= 5 dB). The parameters considered for evaluating the pointing error on UWOC system are: $A_0 = 0.0764$, $\zeta = 2.3$ (for $\omega_{z_{eq}} = 67.75\ mm$, $r = 13\ mm$, $\vartheta = 0.25$, $\sigma_s^2 = 0.83 \times 10^{-3}$ from [Sandalidis *et al.* (2008)]).

Figure 6.3a shows the outage probability of RF/UWOC system using DF and AF relay with and without pointing errors. It is observed that the performance of mixed RF−UWOC system with pointing errors is inferior to that of the system without pointing errors by 8 and 11 dB (average SNR) respectively at an average BER of 10^{-6}. The difference in performance of BPSK modulated DF relay and AF relay RF–UWOC system is less than 0.5 dB. Figure 6.3b represents, average BER of mixed RF−UWOC system with and without pointing errors for various binary modulation techniques. From Figure 6.3b, it is clear that the performance of the system with pointing errors is inferior to that of the system without pointing errors by at least 10 dB. It is also observed that the RF−UWOC system with BPSK modulation exhibits an average SNR gain of 5 dB when compared with BFSK modulation, 3 dB when compared with OOK modulation and 2 dB when compared with the DPSK modulation systems respectively.

Figure 6.3c shows the average BER of M-ary PSK and QAM modulated mixed RF−UWOC systems for with and without pointing errors. From this figure, it can be observed that the presence of pointing error degrades the system performance by 11 dB when compared to the system without pointing errors. DF relay performs nearly 0.5 dB better than the AF relay.

Figure 6.3d, shows the average BER of BPSK modulated RF–UWOC system with and without pointing errors for varying link-ranges. It is observed that the performance of BPSK modulation is superior to all other digital modulation schemes considered in this chapter. Hence, we have plotted Figure 6.3d for BPSK modulation only. These results have been computed for values of constituent parameters as specified below: $\chi_t = 6 \times 10^{-5}\ K^2/s$, $\epsilon = 10^{-8}\ m^2/s^3$, $\omega = -2.5$ and varying UWOC link-ranges $L = 100,\ 150,\ 200,\ 250m$, which varies SI $\sigma_I^2 = 0.053,\ 0.181,\ 0.431,\ 0.934$ respectively. We observe that the presence of pointing error causes a performance deterioration of $(8-10)$ dB when compared to a system without pointing errors for the various distances considered by us at an ABER of 10^{-3}.

6.5.1 ABER performance comparison

In this subsection, we have compared the average BER of the proposed co-operative RF−UWOC system with the system proposed by Anees *et al.*, in [Anees and Deka (2019)]. The authors in [Anees and Deka (2019)] have modeled the perturbations due to the RF fading channel with the Nakagami-m distribution, and the intensity perturbations due to the UWOC channel with the exponentiated generalized Gamma (EGG) distribution. Figure 6.4, shows the ABER comparison between the proposed system with the system proposed by Anees *et al.*, The obtained ABER values are computed at values of SI $(\sigma_I^2) = 0.148$ (from [Anees and Deka (2019)]). The corresponding values of a and b (HTLN PDF) are 0.1485 and 9 respectively. Both the systems are compared at the SI of 0.148. The proposed system shows the average SNR gain of 10 dB compared with the system proposed by Anees *et al.*, at an average BER of 5×10^{-2}.

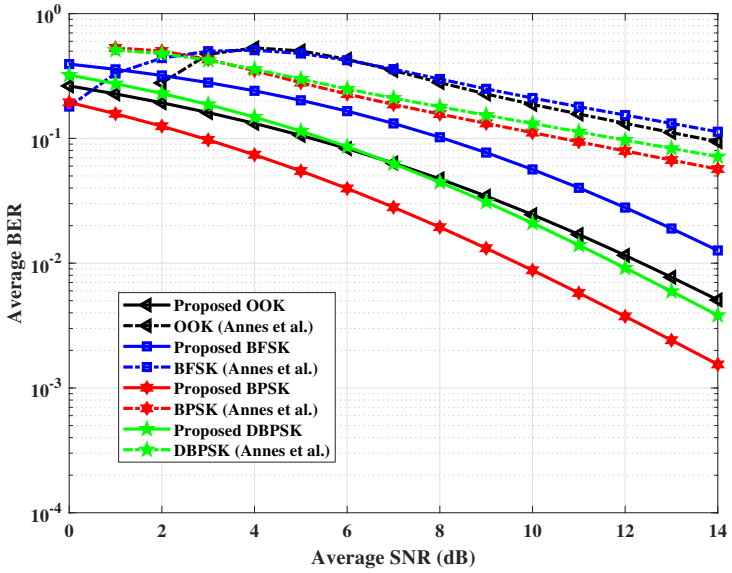

Figure 6.4: ABER performance comparison of proposed system with the system proposed in [Anees and Deka (2019)].

6.6 Conclusion

In this chapter, we have derived novel closed form expressions which determine the outage probability and BER of the proposed mixed RF–UWOC system. The performance of the system with and without pointing errors has been evaluated for various modulation schemes. It is observed that the analytic results are in close

agreement with results obtained by Monte-Carlo simulations. The analytic as well as the simulation curves emphasize the significant effect of pointing errors in RF-UWOC system. The performance of the proposed system is significantly superior to the system proposed by [Anees and Deka (2019)] et.al. Thus we feel that the proposed co-operative RF–UWOC system can be a useful candidate for deployment in ocean monitoring and internet of underwater things (IoUT) applications.

Chapter 7

Underwater Image Transmission through the Oceanic Turbulent Optical Medium

Underwater imaging is a science that is concerned with capturing images from the depths of the ocean and seafloor. Transmitting images from these regions is a challenging task due to the harsh oceanic environment. In this chapter, we have evaluated the performance of a system tasked with the transmission of seafloor images using high-speed optical signaling through the underwater channels by means of Monte-Carlo simulation. The transmitted irradiance is affected by underwater turbulence and beam attenuation. Mean and adaptive median filters are employed to improve the quality of images transmitted over the underwater channel.

In this chapter, we have performed simulation studies to understand the factors affecting the reception of an underwater image transmitted over the weak turbulent oceanic water medium using blue LASER. The received image exhibits distortion due to the presence of underwater turbulence and beam attenuation. The presence of turbulence can fluctuate the optical signal strength from higher intensities into lower intensities, which can induce errors in the received data. In order to mitigate the turbulence-induced errors, we have used a MIMO scheme employing N transmitting LASER sources and M Photo-Detectors (PDs) at the receiver. The responses of all the PD are combined using Equal Gain Combining (EGC). The output of the EGC scheme is used to form the estimate of the transmitted image. The performance improvement is quantified in terms of the gain (reduction in transmit power requirement) from Single-Input to Single-Output (SISO) to the diversity scheme at a Bit Error Rate (BER) of 2×10^{-6}. The Peak Signal to Noise Ratio (PSNR) of the received image is calculated and enhanced using median and

adaptive median filters. An improvement in PSNR is observed for filtered images. The PSNR variation with respect to transmit power of LASER is shown in Section 7.2.2.

The remaining part of this chapter is organized as follows, Section 7.1 introduces the system model. The BER results obtained by Monte-Carlo simulations are discussed in Section 7.2.1. The transmitted and received images in the presence of beam attenuation and turbulence and the corresponding histograms are presented in Section 7.2.2. The chapter is concluded in Section 7.3 with a discussion of the results.

7.1 System model

The pixel values of captured underwater images are converted into binary data. This data is conveyed using On-Off Keying (OOK) modulation by employing a blue LASER source. The light pulses propagate through the turbulent underwater channel. The main impediments to the transmission of the optical beam through the underwater channel are beam attenuation and underwater turbulence. These channel induced distortions can result in the degradation of the quality of the image. Suitable filters can be employed to mitigate the effect of distortion in the wireless optical channel. Fig. 7.1, shows the proposed system model employed in this chapter. The binary converted pixel data (s) is transmitted through the underwater channel with power P_t watts associated with binary '1' and 0 watts associated with binary '0' by employing a LASER source. Each transmitted pulse has a duration of T_b seconds. This irradiance propagates through the underwater channel experiencing turbulence and beam absorbtion. Hence, the intensity of the irradiance received at the PD is given by,

$$Y = \eta\sqrt{P_t T_b} sI + n \tag{7.1}$$

where I is the obtained irradiance at PD under the influence of beam attenuation and turbulence, η is optical-to-electrical conversion coefficient (responsivity) which is measured in terms of A/W, P_t is the transmit power launched to drive the LASER source and n is the additive Gaussian noise (zero mean and variance σ^2).

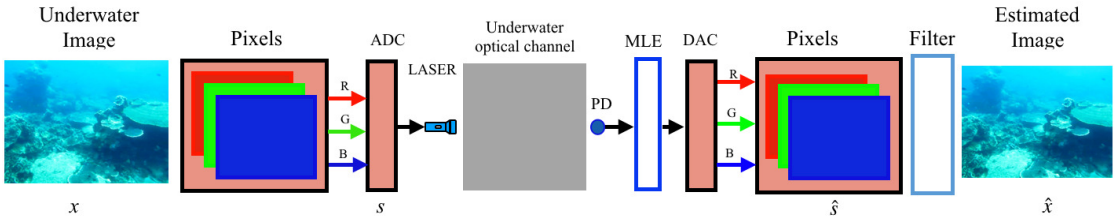

Figure 7.1: Block diagram of proposed image transmission in underwater optical channel

7.2 Results and Discussions

The various parameters associated with image transmission in a UWOC link are studied and quantified in this section. The BER values obtained using Monte-Carlo simulation are presented in subsection 7.2.1, PSNR results are presented in subsection 7.2.2, and the intuitive discussion concerning the results obtained using MIMO, diversity schemes and those obtained using the Adaptive median filter is presented in subsection 7.2.3.

7.2.1 Experiment 1: 1-D BER results

In this section, we have carried out simulations to estimate the BER for an uncoded SISO UWOC system. In order to mitigate the effects of beam attenuation and underwater turbulence, MIMO and diversity schemes are deployed, and their performance is assessed using simulations. The simulation BER plots of SISO and various MIMO schemes are shown in Fig. 7.2. These results show that an increase in N or M (number of transmitting sources and detectors respectively) can bring about an improvement in the system performance. It is shown that a SISO system needs a transmit power of 55 dB to attain a BER of 10^{-5}, whereas, with 1×2 receiver diversity, the same BER can be attained at a transmit power of 52 dB, which means 1×2 provides a transmit power gain of 3 dB over SISO system. Similarly, it is demonstrated that the 2×1 transmit diversity yields a transmit power gain of 7 dB, 2×2 MIMO provides a gain of 13 dB, 4×2 and 2×4 MIMO provides a gain of 17 dB and 4×4 provides a gain of 19 dB over SISO system at a BER of 10^{-5}.

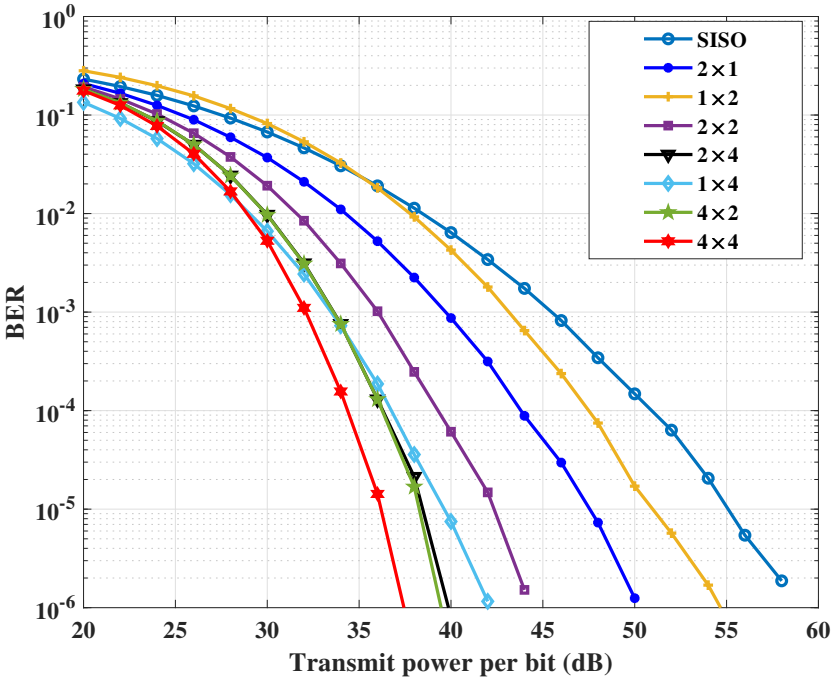

Figure 7.2: BER of MIMO UWOC system.

(a) **(b)**

Figure 7.3: (a) Transmitted image, (b) Received impulsive noise image.

7.2.2 Experiment 2: Result analysis of 2-D underwater images with and without filters

In order to carry out the simulations, an underwater image of size 541 × 2592 converted into binary data, which is then OOK modulated with the help of the LASER source. The light beam propagates through the turbulent underwater channel. At the receiver, the light intensity values are converted into binary and then mapped back into pixels of images. The Transmitted underwater image is shown in Figures 7.3a, and the corresponding received underwater image is shown

in Figure 7.3b. This image is perturbed by impulsive noise, which occurs due to the switching of binary 1 to binary 0 and vice-versa for an adverse communication channel environment. Impulsive noise can be mitigated with the appropriate non-linear filters [Chan *et al.* (2005)]. We have studied the performance of the following non-linear filters, namely, High-density filter, Hybrid filter, PSMF filter, Open-Close Sequence (OCS) filter, Center-Weighted Median (CWM) filter, Median filter, and Adaptive Median filter. We have employed the Peak Signal to Noise Ratio (PSNR) quantity to measure the quality of images. It is well known that Higher PSNR values result in higher image quality. The mathematical expression of PSNR (a measure of image quality) for a grayscale image is given as follows,

$$PSNR(dB) = 10\log_{10}\left(\frac{255^2}{MSE}\right) \tag{7.2}$$

where, $MSE = \frac{1}{m\times n}\sum_{i=0}^{m-1}\sum_{j=0}^{n-1}(y_{ij}-\hat{y}_{ij})^2$ is root mean square error, m and n are pixel size of image, y_{ij} and $\hat{y}_{ij}$ are pixel values of transmitted and received images. The PSNR of the colored RGB image is obtained as follows,

$$PSNR = \frac{PSNR_R + PSNR_G + PSNR_B}{3} \tag{7.3}$$

where, $PSNR_R$, $PSNR_G$, and $PSNR_B$ are PSNR values of red, green, and blue RGB images, respectively. PSNR values obtained for various filters shown in Table 7.1. From this table, it is apparent that the performance of the Adaptive median filter shows is superior to that of other filters listed. Hence, we have employed the Adaptive median filter in all further discussions. The received data has been processed through the Adaptive Median filters (and Median filter also for comparison), and corresponding PSNR values have been tabulated in Table 7.2 for varying transmit powers (P_t = 10, 20, 30 dB). Figure 7.4 shows the responses of various filtered images, and Fig. 7.5 shows the flowchart of the adaptive median filter.

Table 7.1: PSNR values for various filters.

Filter	**PSNR**
High Density Filter (HDF)	29.05
Open-Close Sequence Filter (OCSF)	29.33
Center Weighted Median Filter (CWMF)	15.17
Progressive Switching Median Filter (PSMF)	15.05
Median Filter (MF)	14.98
Adaptive Median Filter (AMF)	40.15

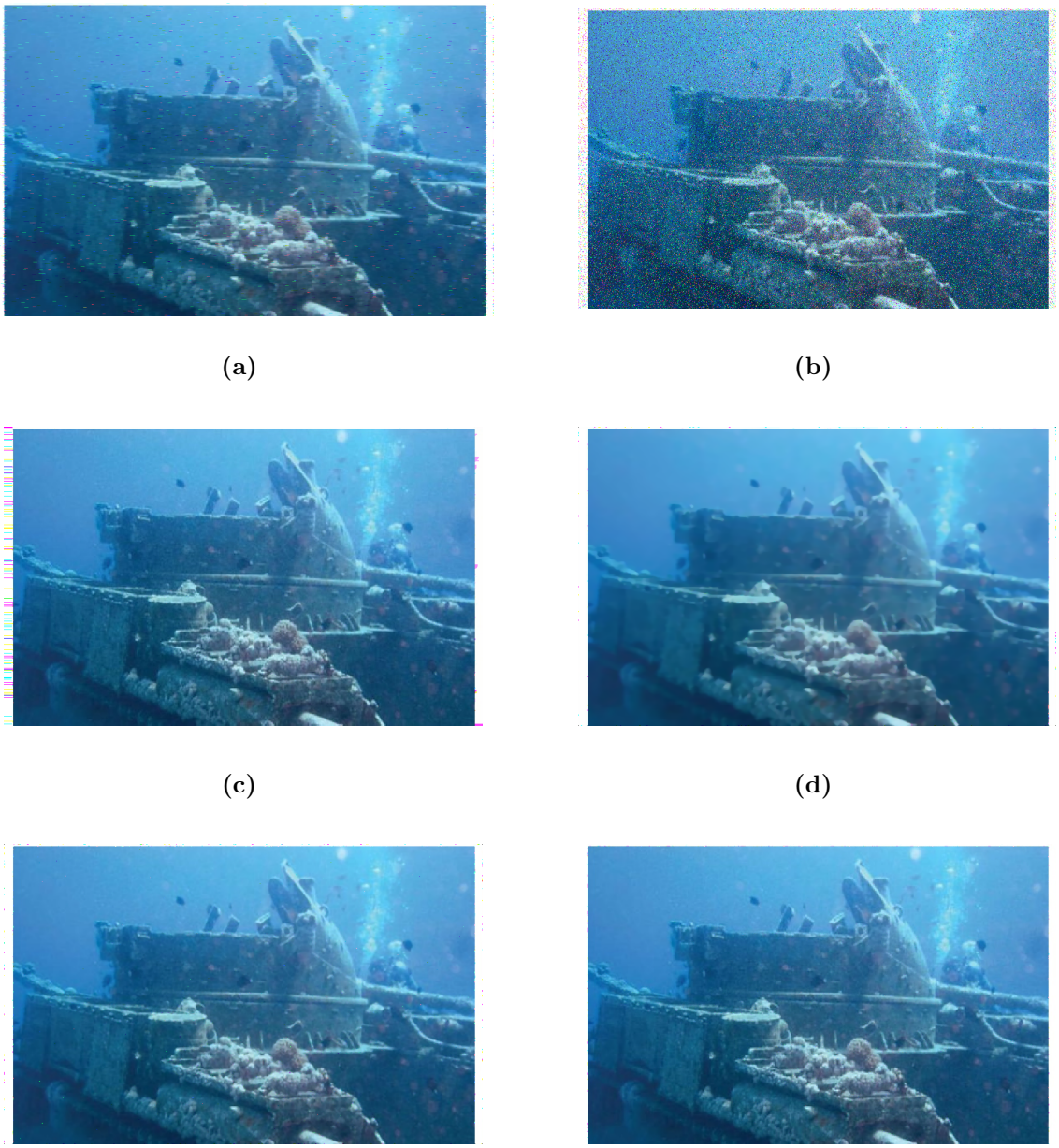

(a) **(b)**

(c) **(d)**

(e) **(f)**

Figure 7.4: Various filtered images (a) OCS (b) CWM (c) High density (d) Hybrid (e) Median (f) Adaptive Median.

PSNR versus transmit power plots for with and without filters augmented with various MIMO schemes have been documented in Fig. 7.6. It is seen that the PSNR performance and received image response of Adaptive Median filter is superior to that of the Median filter. PSNR comparison for various MIMO schemes using with and without filters is shown in Table 7.2.

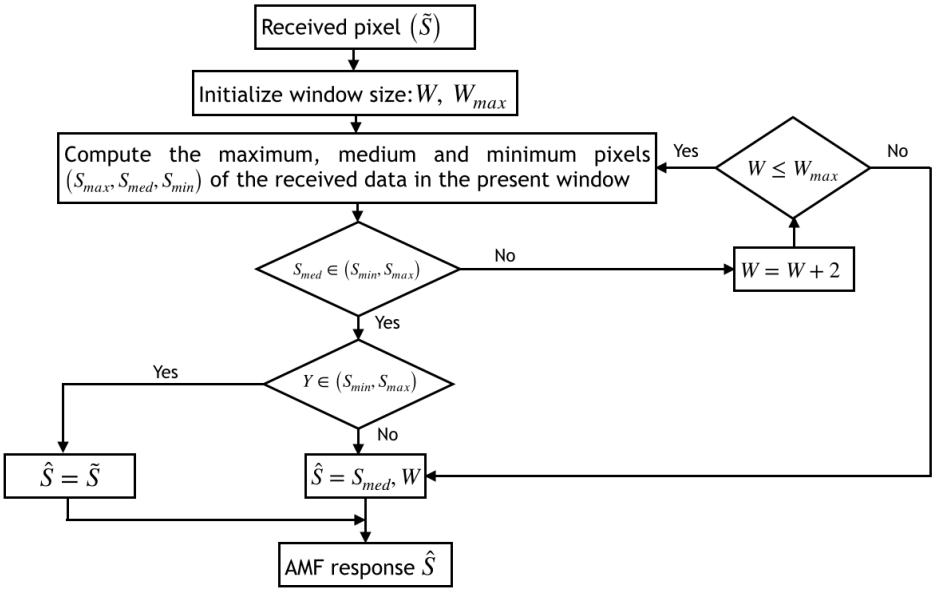

Figure 7.5: Flowchart of adaptive median filter

7.2.2.1 Received images

The images are transmitted and received through the turbulent underwater channel for varying transmit powers (from 10–30 dB) using with and without Median and Adaptiveare filters presented in the Fig. 7.7. The figure also shows the corresponding histograms.

7.2.3 Discussions

The Bit Error Rate (BER) and Mean Square Error (MSE) is the calculations of error rate between the transmitted and received data and image (one dimensional and two-dimensional manner), respectively. The BER and MSE in terms of PSNR are represented by,

$$BER = \frac{1}{L}\sum_{i=0}^{L}(x_i - \hat{x}_i) \tag{7.4}$$

and

$$MSE = \frac{1}{mn}\sum_{i=0}^{m-1}\sum_{j=0}^{n-1}(y_{ij} - \hat{y}_{i,j})^2 = 255^2 10^{-PSNR/10}, \tag{7.5}$$

where $y_{i,j}$ and $\hat{y}_{i,j}$ are analog data of 8-bit binary digits x and $\hat{x}$ respectively $(i.e,\ y = 2^7x_7 + 2^6x_6 + \cdots + 2x_1 + x_0)$. Equation (7.5) implies

$$BER = \sqrt{\frac{MSE}{L}} = \frac{255}{\sqrt{L}}10^{-PSNR/20} \tag{7.6}$$

Table 7.2: PSNR (dB) value under different transmit powers.

Schemes		P_t (dB)	**PSNR (dB)**		
			Received image	**Median filter**	**Adaptive median filter**
SISO		10	06.07	08.03	24.32
		20	08.31	15.97	31.43
		30	13.67	31.87	38.42
MIMO	N=1,M=2	10	05.71	06.94	18.62
		20	07.46	12.80	30.01
		30	12.84	30.57	37.61
	N=1,M=3	10	06.12	08.19	24.74
		20	08.98	18.48	32.51
		30	17.92	36.89	42.44
	N=2, M=1	10	06.11	08.17	24.77
		20	08.76	17.64	32.17
		30	16.30	35.40	41.09
	N=4, M=1	10	06.12	08.19	24.63
		20	09.10	18.93	32.69
		30	19.14	37.74	42.59
	N=2, M=3	10	06.12	08.19	24.74
		20	08.98	18.48	32.51
		30	17.92	36.89	42.44
	N=2, M=5	10	06.12	08.19	24.74
		20	08.98	18.48	32.51
		30	17.92	36.89	42.44
	N=4, M=3	10	06.12	08.19	24.74
		20	08.98	18.48	32.51
		30	17.92	36.89	42.44
	N=4, M=5	10	06.12	08.19	24.74
		20	08.98	18.48	32.51
		30	17.92	36.89	42.44

for $L = 8mn$, $m = 541$ and $n = 2592$. The value of BER obtained using 4×4 MIMO at 30 dB is approximately equal to 5×10^{-3}. The PSNR values of SISO operated MF and AMF at 30 dB are 31.87 and 38.42, respectively and corresponding BER values are 6.5×10^{-3} and 3×10^{-3} respectively. When compared these results with the results obtained using MIMO STBC (shown in Figures 5.4 and 5.5), a transmit power gain of 1 dB can be gained using 4×4 MIMO over Median filter, and 3 dB transmit power gain obtained using Adaptive Median filter over 4×4 MIMO and 5 dB over Median filter at $L = 1.4 \times 10^6$ respectively.

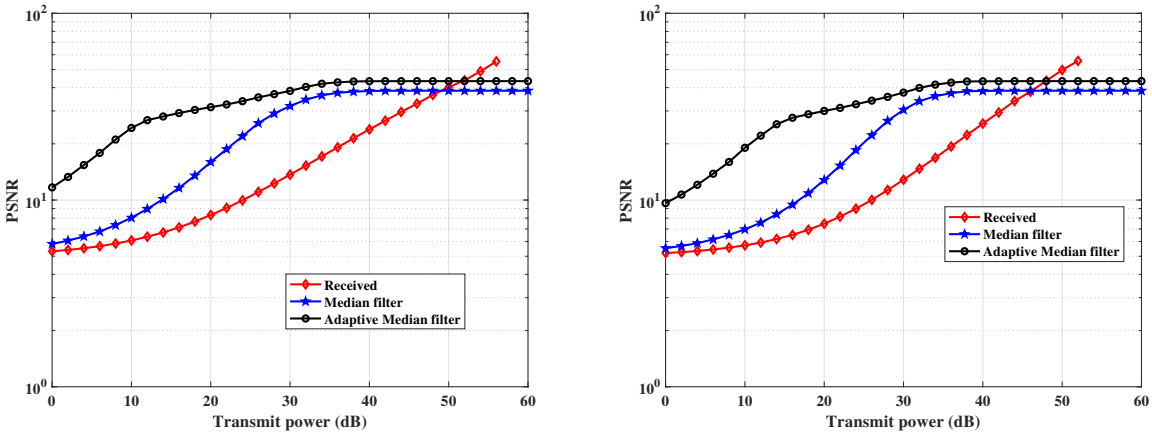

(a) (b)

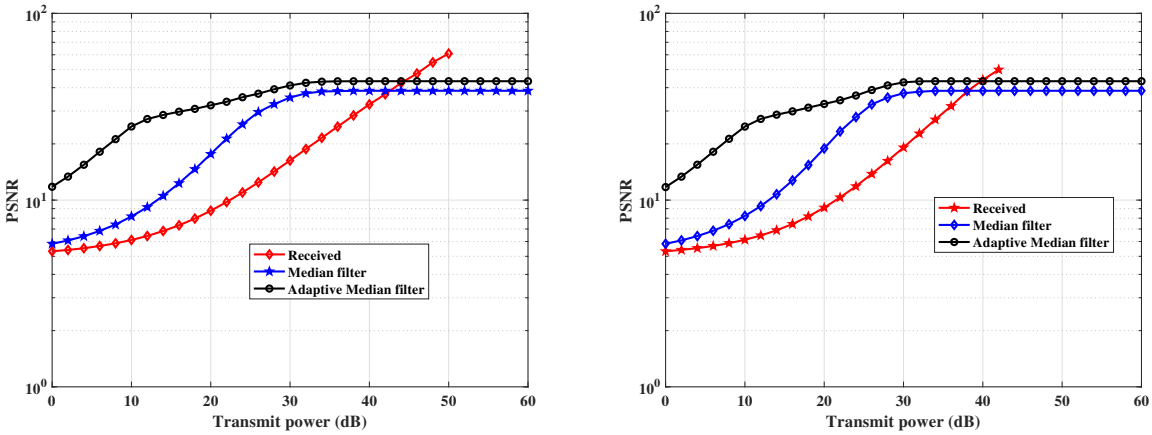

(c) (d)

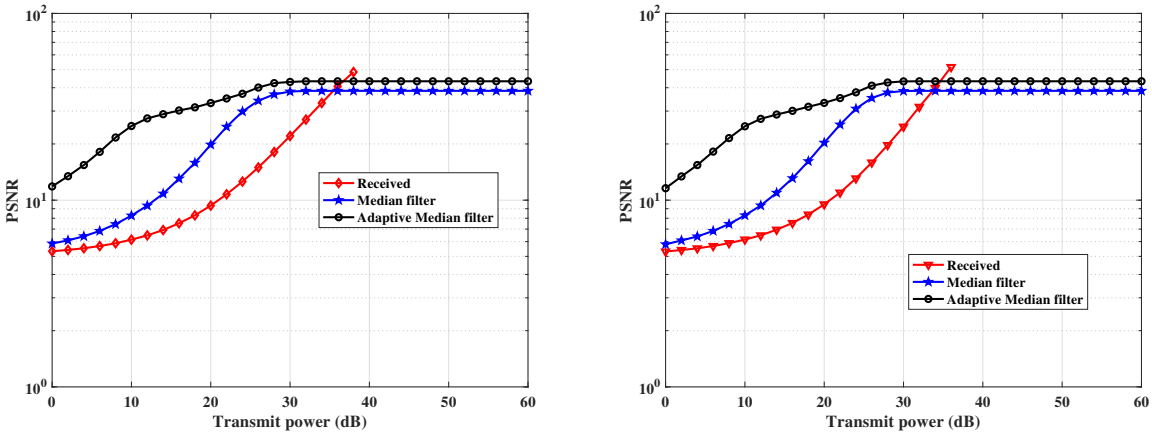

(e) (f)

Figure 7.6: PSNR of (a) SISO, (b) 1×2, (c) 2×1, (d) 2×2, (e) 2×4, (f) 4×4.

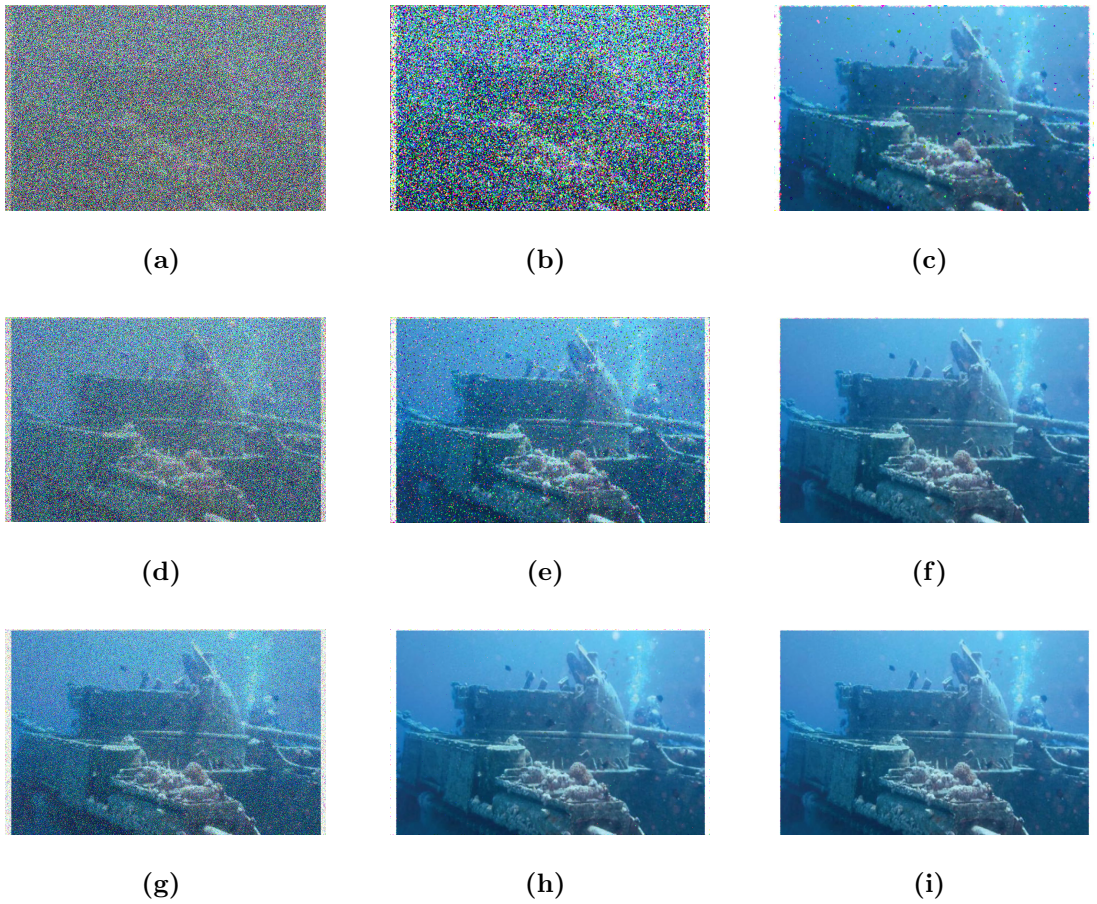

Figure 7.7: Received images using with and without filters; First, second and third rows are at the transmission powers of 10 dB, 20 dB, and 30 dB respectively; First, second and third columns are the received images using without filter, median filter, and adaptive median filters respectively.

7.3 Conclusion

We have studied the problem of underwater image transmission through an underwater medium affected by weak turbulence and beam attenuation. To enhance the data/ image at the receiver, we have employed various MIMO schemes and filters. Using an Adaptive Median filter, a transmit power of 3 dB can be gained over the system operating at a 4×4 MIMO system. Thus a suitable combination of MIMO schemes and filters can be employed to enhance the quality of received images that have propagated through the underwater optical communication link affected by turbulence and beam attenuation.

Chapter 8

Conclusion and Future Scope

8.1 Conclusions

This objective of this research work was to study the various factors that determine the performance of an UWOC system and then proposed constructive techniques to improve and enhance the integrity of the received data at the receiver. The first step in realizing this objective was to determine by experimental means, the optimum wavelength for communication in the underwater medium. This result was cross-checked with results available in scientific literature and was found to be correct. This is followed by a study of various channel models that can be employed to describe the perturbations that are introduced when the light beam propagates through the medium. We then set up an UWOC link in the laboratory and have used it to validate channel models and demonstrate the efficacy of diversity and channel coding schemes for improving the integrity of received information. The BER peroformance of the (31, 11) BCH coded 1×3 EGC scheme gains 8 dB power from uncoded UWOC system at a BER of 10^{-5}. Similarly, (63, 51) RS coded 4×5 MIMO scheme gains a at-least 30 dB from the uncoded UWOC system at a BER of 10^{-5}. This was followed by a determination of a more accurate channel model for describing the perturbations introduced by an UWOC system. We have examined the problems introduced by the misalignment between the transmitter and receiver and have suggested techniques to minimize this error. We have also studied the performance of hybrid (UWOC in water coupled with RF in the atmosphere) links. The ABER performance RF-UWOC system obtained using with and without pointing errors 45 dB and 35 dB respectively. We have proposed various approaches (the combination of MIMO and image processing techniques) that can be used to improve the enhance the quality of received images communicated

over a UWOC system. Median and adaptive median filters can gain a transmit power of -1 dB and 3 dB over the 4×4 MIMO UWOC system respectively. The experimental work and the mathematical/ simulation studies have taken into account the various perturbations that a light beam undergoes as it propagates through an UWOC channel. These limitations are primarily phenomena such as underwater turbulence, beam attenuation, and pointing errors. Transmit/ receive diversity, MIMO and Error Correcting Codes (ECC) are some of the approaches employed by us in this thesis to enhance the reliability of information transfer in an UWOC system. We have demonstrated that a suitable collaboration of MIMO/ transmit/ receive diversity schemes augmented with ECC enhances the reliability of the UWOC link over that which can be achieved using individual MIMO, diversity and ECC systems. The communication schemes proposed by us in this thesis can be gainfully used to enable IoUT applications such as inter submarine communication, submarine to jetty communication, communication between sensors collecting oceanic parameters and aggregating devices, etc. In addition to IoUT, the co-operation of IoT and IoUT is likely to emerge as a solution provider in applications involving monitoring the underwater environment with a view to and predict and mitigate disasters.

After conducting this research work, we have found that a few unsolved problems can be tackled by an interested researcher desiring to work in this field. We have enumerated a few of these in the next section.

8.2 Future Scope

- In Chapter 3, the link range of the UWOC system can be further increased up to 20-30 meters with the same experimental set up using the intermediate light amplifying arrangements. This will require highly directional LASER sources for data transmission. Suitable arrangements for error free data regeneration at the locations of the intermediate amplifiers may be necessary.

- The performance of UWOC links proposed in Chapter 4 can be further enhanced by employing codes with iterative decoding algorithms such as Turbo and Low Density Parity Check (LDPC) codes. However, improved performance will come a the cost of an increase in decoding complexity.

- In Chapter 6, co-operative communication between the RF–UWOC system can be further enhanced using MIMO schemes at the RF stage and UWOC

stage. This will serve to improve the performance of the RF link and further enhance the overall system performance.

- In Chapter 7, the various issues connected with underwater transmission of image data have been explored.Considerable improvement in the quality of image transfer can be obtained with the use of advanced image processing techniques along with use of sophisticated techniques for error detection/ correction. This can constitute a fertile area for further research work.

- In the real underwater scenario, both transmitter and receiver are in relative motion due to the agitation of water, so there is no guarantee that the LOS path once established will always remain intact. An elaborate acquisition and tracking system will have to be designed and installed to ensure that the source and the detector remain optically coupled to each other.

Appendix A

Performance Metrics

A.1 System reliability

Information integrity provided by a system is quantified by the improvement in the BER offered by the system when compared with other competing systems. It is usually quantified in terms of the 'transmit power/ average SNR' gain, which is the reduction in transmit power/ average SNR observed to obtain a particular BER value when the two competing schemes are employed. An example is shown in Figure A.1, where two techniques employed to obtain the system BER and it is observed that the technique two can provide a gain 7 dB in terms of transmit power when compared with technique one at a BER of 10^{-4}.

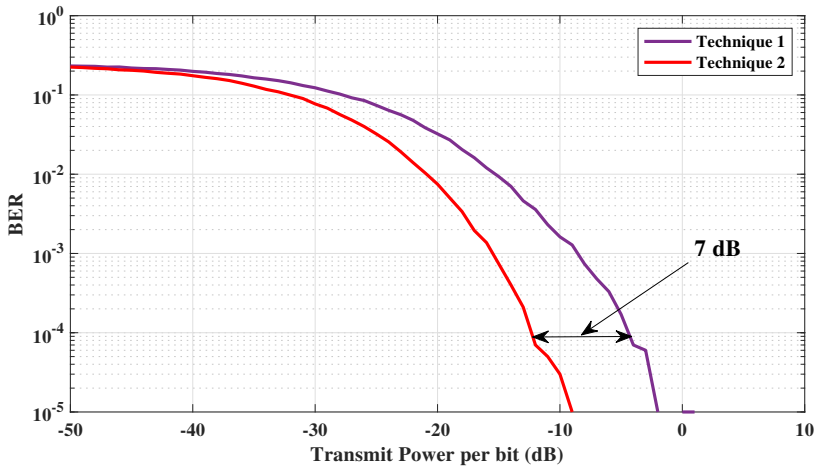

Figure A.1: BER comparison.

(a) **(b)**

(c) **(d)**

Figure A.2: (a) Input image, (b), (c), and (d) are received images.

A.2 PSNR

PSNR measures the quality of the received image, higher the value of PSNR better is the quality of the received image. The PSNR for a grayscale image is quantified as follows,

$$PSNR(dB) = 10\log_{10}\left(\frac{255^2}{MSE}\right) \tag{A.1}$$

where, $MSE = \frac{1}{m\times n}\sum_{i=0}^{m-1}\sum_{j=0}^{n-1}[y_{ij} - \hat{y}_{ij}]^2$ is mean square error, m and n are pixel size of image, y_{ij} and $\hat{y}_{ij}$ are pixel values of transmitted and received images. The PSNR of a colour image is expressed in terms of the PSNR of the R, G and B components that make up the color image. It is described as follows:

$$PSNR = \frac{PSNR_R + PSNR_G + PSNR_B}{3} \tag{A.2}$$

In this equation, $PSNR_R$, $PSNR_G$, and $PSNR_B$ are PSNR values of red, green, and blue pixels of received image, respectively. The PSNR values are of (b), (c), and (d) of Figure A.2 are measured using the (a) of Figure A.2. The obtained

PSNR values are 04.65, 07.24, and 13.34, respectively.

A.3 Complexity analysis comparison with MG PDF

HTLN and MG PDFs have been proposed as more general and complete replacements for the log-normal PDF when deriving channel models for UWOC communication. Here we have compared the proposed HTLN PDF with MG PDF. Proposed HTLN PDF is given as,

$$f_{HTLN}(\gamma) = \frac{b \exp(2a) \gamma^{b-1}}{(1 + \exp(2a) \gamma^{b})^{2}}, \qquad \gamma \geq 0 \tag{A.3}$$

The PDF of MG model is given as [Bhowal and Kshetrimayum (2018)],

$$f_{MG}(\gamma) = \sum_{i=1}^{N} w_i \frac{\beta_i^{\alpha_i} \gamma^{\alpha_i - 1}}{\Gamma(\alpha_i)} e^{-\gamma \alpha_i}, \qquad \gamma \geq 0 \tag{A.4}$$

From Eqs.A.3 and A.4, the number of unknowns in HTLN PDF always 2 (i.e, $a,\ b$), whereas in MG PDF, the number of unknowns are $3N$ (i.e., $\alpha_1, \alpha_2 \cdots, \alpha_N, \beta_1, \beta_2, \cdots \beta_N$, $w_1, w_2, \cdots, w_N$). The complexity of MG distribution depends on the number of

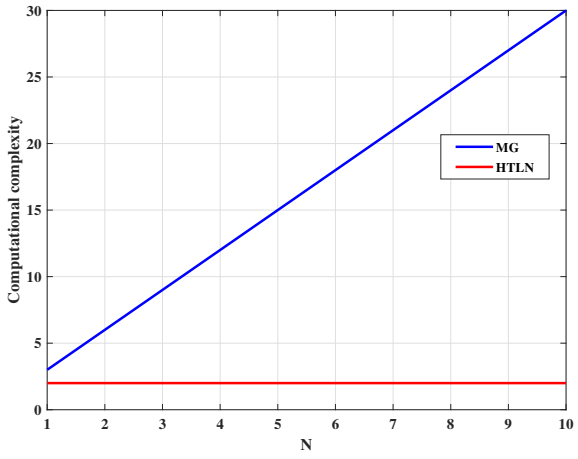

Figure A.3: Complexity comparison of MG and HTLN PDFs.

iterations N. The complexity of finding unknowns of HTLN and MG PDF models is shown in Figure A.3. There is a steep increase in the computational complexity with an increase in the value of N for MG distribution.

Appendix B

Gauss Hermite Quadrature polynomial computation

$$P = \frac{1}{\sqrt{2\pi\sigma_X^2}} \int_0^\infty \exp\left(-\frac{(x-\mu_X)^2}{2\sigma_X^2}\right) \mathbb{Q}\left(\zeta \exp\left(2x\right)\right) dx \tag{B.1}$$

Substituting $\frac{x-\mu_X}{\sqrt{2}\sigma_X} = t$ in equation (B.1), then equation (B.1) becomes,

$$P = \frac{1}{\sqrt{\pi}} \int_0^\infty e^{-t^2} \mathbb{Q}\left(\zeta \exp\left(2\sqrt{2}\sigma_X t + 2\mu_X\right)\right) dt \tag{B.2}$$

Exact solution to equation (B.2) does not exist. To obtain the closed-form solutions, we have considered $f(t) = \mathbb{Q}\left(\zeta \exp\left(2\sqrt{2}\sigma_X t + 2\mu_X\right)\right)$, then equation (B.2) will be in the form of Gauss-Hermite quadrature polynomial. The solution for the Gauss-Hermite quadrature polynomial is given as,

$$\int_{-\infty}^{\infty} e^{-t^2} f\left(t\right) dt \approx \sum_{i=1}^{n} W_i f(t_i) \tag{B.3}$$

where W_i is weight of i^{th} order approximation and is given as $W_i = \frac{2^{n-1} n! \sqrt{\pi}}{n^2 [H_{n-1}(t_i)]^2}$, $H_i(t)$ is Hermite polynomial and it can be obtained recursively using $H_{n+1}(t) = 2tH_n(t) - 2nH_{n-1}(t)$ with initial conditions $H_1(t) = 2t$ and $H_0(t) = 1$. For $n = 10$, Hermite polynomial is given as,

$$H_9\left(t\right) = 512t^9 - 9216t^7 + 48384t^5 - 80640t^3 + 30240t \tag{B.4}$$

Using equation (B.3), (B.2) can be written as,

$$P \approx \frac{1}{\sqrt{\pi}} \sum_{i=1}^{n} W_i \mathbb{Q}\left(\zeta \exp\left(2\sqrt{2}\sigma_X t_i + 2\mu_X\right)\right) \tag{B.5}$$

Table B.1, shows the Gauss-Hermite polynomials weight and $f(t_i)$ computation for $n = 10$.

Table B.1: Gauss-Hermite Quadrature polynomial computation for $n = 10$.

i	t_i	$H_{n-1}(t_i)$	W_i	$f(t_i)$
1	-2.25497400209	2534835.18529564	5.12517237473360e-06	2.53605304749074e-06
2	-1.73853771212	662457.136702375	7.50399202665477e-05	7.47292464334315e-17
3	-1.2340762154	137165.275771642	0.00175032851581273	1.75652117266315e-49
4	-0.737473728545	10047.5119591326	0.326205190105919	3.03267084591841e-150
5	-0.245340708301	-6232.05571106138	0.847901251222623	0
6	0.245340708301	6232.05571106138	0.847901251222623	0
7	0.737473728545	-10047.5119591326	0.326205190105919	0
8	1.23407621540	-137165.275771642	0.00175032851581273	0
9	1.73853771212	-662457.136702375	7.50399202665477e-05	0
10	2.25497400209	-2534835.18529564	5.12517237473360e-06	0

Appendix C

PDF of $I_m = \max\left(I_1,\ I_2, \ldots,\ I_M\right)$

The Cumulative Distribution Function (CDF) $F_{I_m}(I_m)$ for independent and identically distributed *i.i.d* channel (from Eq. (6.7) of [Stüber and Stèuber (1996)]), is

$$\begin{aligned} F_{I_m}(I_m) &= P(I_1 \leq I_m, I_2 \leq I_m, \ldots, I_M \leq I_m) \\ &= F_{I_1}(I_m) F_{I_2}(I_m) \ldots F_{I_M}(I_m) \\ &= (F_I(I_m))^M \end{aligned} \tag{C.1}$$

The PDF takes on the form (Eq. (25) of [Tsiftsis *et al.* (2009)]),

$$\begin{aligned} f_{I_m}(I_m) &= \frac{d}{dI_m}(F_I(I_m))^M \\ &= M(F_I(I_m))^{M-1} f_I(I_m) \end{aligned} \tag{C.2}$$

The log-normal CDF is $F_I(I_m) = \frac{1}{2} + \frac{1}{2} erf\left(\frac{\ln(I_m) - 2\mu_X}{\sqrt{8\sigma_X^2}}\right)$ and PDF $f_I(I_m)$ is described in Eq. (4.4). Hence, the PDF of maximum of M received irradiance takes on the form

$$f_{I_m}(I_m) = \frac{M}{2I_m\sqrt{2\pi\sigma_X^2}} exp\left(-\frac{(\ln(I_m) - 2\mu_X)^2}{8\sigma_X^2}\right)\left(\frac{1}{2} + \frac{1}{2} erf\left(\frac{\ln(I_m) - 2\mu_X}{\sqrt{8\sigma_X^2}}\right)\right)^{M-1} \tag{C.3}$$

Appendix D

Mean and variance of sum of identical, independent Log-Normal random variables

Let I_{sum} is sum of M independent identical log-normal random variables $(I_1,\ I_2, \ldots,\ I_M)$, i.e, $I_{sum} = I_1 + I_2 + \cdots + I_M = MI$, where $I = \exp(2X)$ log-normal random variable, X is normal random variable with mean μ_X and variance σ_X^2. From [Mitchell (1968)], I_{sum} is log-normal random variable with mean $\mathbb{E}\left(I_{sum}\right) = M\mathbb{E}(I)$ and variance $\sigma_{I_{sum}}^2 = M^2\sigma_I^2$, where $\sigma_I^2 = \exp(4\sigma_X^2 - 1) \times \exp(4\sigma_X^2 + 4\mu_X)$. I_{sum} can be represented in exponential form as, $I_{sum} = \exp(2U)$ then $\mathbb{E}\left(I_{sum}\right) = \exp\left(2\mu_U + 2\sigma_U^2\right)$ and $\sigma_{I_{sum}}^2 = \exp\left(4\sigma_U^2 + 4\mu_U\right)\left(\exp\left(4\sigma_U^2\right) - 1\right)$. Equating these equations, yields $\sigma_U^2 = \frac{1}{4}\ln\left(\frac{\exp\left(4\sigma_X^2\right)-1}{M} + 1\right)$ and $\mu_U = \frac{1}{2}\ln(M\mathbb{E}(I)) - \sigma_U^2$.

Appendix E

HTLN distribution function

HTLN distribution is a class of LN distribution derived using Hyperbolic Tangent Distribution (HTD). The CDF of normal random variable x with mean μ_X and variance σ_X^2 is given as,

$$\Phi(x) = \frac{1}{2} erfc\left(\frac{\mu_X - x}{\sqrt{2\sigma_X^2}}\right) \tag{E.1}$$

where $erfc$ is complementary error function. This equation can be represented using HTD as [Robin (1997)],

$$\Phi(x) = \frac{1}{2} + \frac{1}{2}\tanh(bx + a) \tag{E.2}$$

where a and b values are obtained by equating the equations (E.1) and (E.2) for two different values of x. LN distribution is obtained by substituting x with $\ln(t)/2$ in Equations (E.1) and (E.2) i.e., $F(t) = \Phi\left(\frac{\ln(t)}{2}\right)$ is LN distribution. Expanding '$tanh$' into algebraic form, which yields $F(t) = \frac{\exp(2a)t^b}{1+\exp(2a)t^b}$ and corresponding PDF is $f(t) = \frac{b\exp(2a)t^{b-1}}{\left(1+\exp(2a)t^b\right)^2}$. Fig. E.1 depicts the comparisons between the PDF/CDF generated using μ_X, σ_X^2 and HTD.

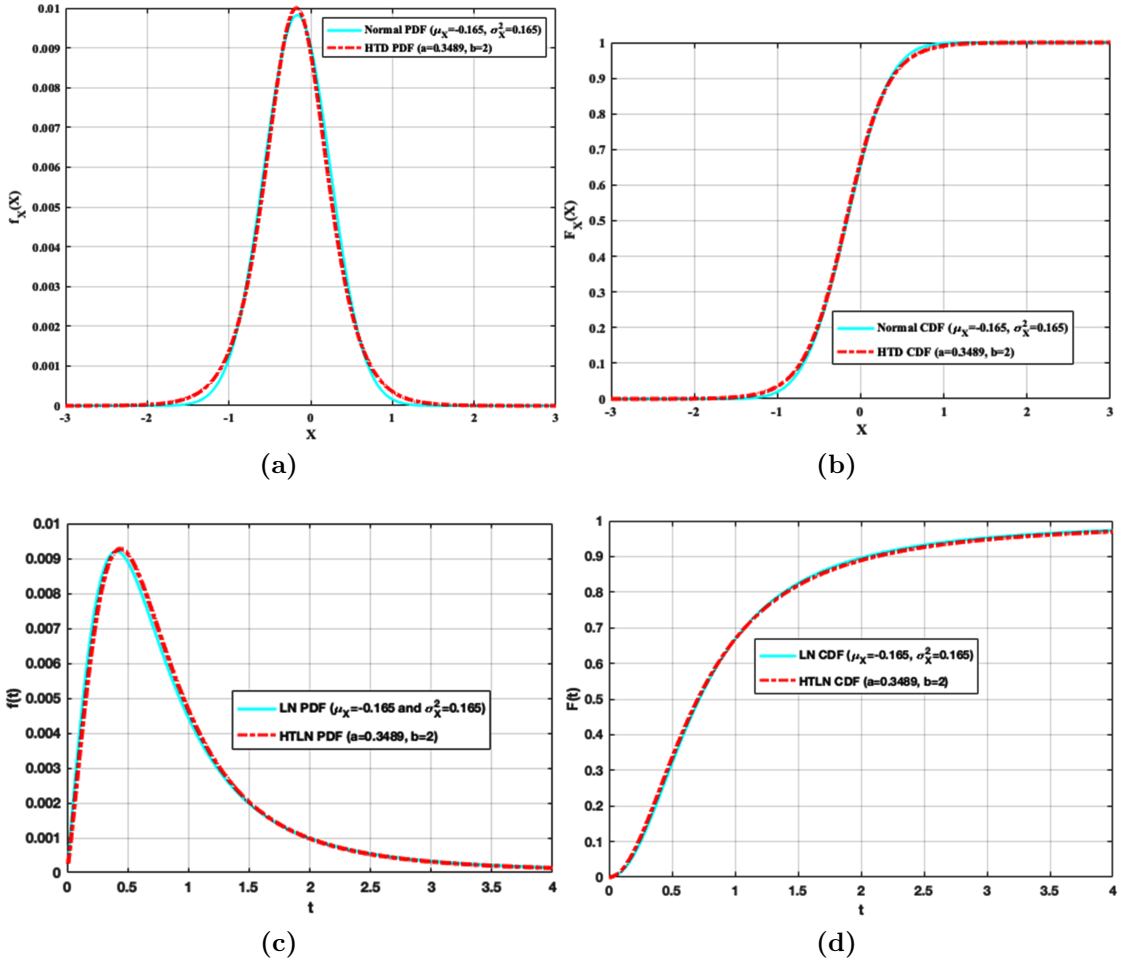

Figure E.1: PDF/CDF generated using μ_X, σ_X^2 and HTD (a) Normal PDF, (b) Normal CDF, (c) LN PDF and (d) LN CDF

Bibliography

Adamchik, V. and **O. Marichev**, The algorithm for calculating integrals of hypergeometric type functions and its realization in reduce system. *In Proceedings of the international symposium on Symbolic and algebraic computation*. ACM, 1990.

Anees, S. and **R. Deka** (2019). On the performance of DF based dual-hop mixed RF/UWOC system. *2019 IEEE 89th Vehicular Technology Conference (VTC2019-Spring)*, 1–5.

Ansari, I. S., **F. Yilmaz**, and **M.-S. Alouini** (2013). Impact of pointing errors on the performance of mixed RF/FSO dual-hop transmission systems. *IEEE Wireless Communications Letters*, **2**(3), 351–354.

Ata, Y. and **Y. Baykal** (2014). Scintillations of optical plane and spherical waves in underwater turbulence. *JOSA A*, **31**(7), 1552–1556.

Baggeroer, A. B., **D. E. Koelsch**, **K. von der Heydt**, and **J. Catipovic**, Dats-a digital acoustic telemetry system for underwater communications. *In OCEANS 81*. IEEE, 1981.

Bayaki, E., **R. Schober**, and **R. K. Mallik** (2009). Performance analysis of mimo free-space optical systems in gamma-gamma fading. *IEEE Transactions on Communications*, **57**(11), 3415–3424.

Bhowal, A. and **R. S. Kshetrimayum** (2018). Performance analysis of one-and two-way relays for underwater optical wireless communications. *OSA Continuum*, **1**(4), 1400–1413.

Blahut, R. E., *Algebraic codes for data transmission*. Cambridge university press, 2003.

Bletsas, A., **H. Shin**, and **M. Win** (2007). Outage analysis for co-operative communication with multiple amplify-and-forward relays. *Electronics Letters*, **43**(6), 51–52.

Boucouvalas, A. C., **K. P. Peppas**, **K. Yiannopoulos**, and **Z. Ghassemlooy** (2016). Underwater optical wireless communications with optical amplification and spatial diversity. *IEEE Photonics technology letters*, **28**(22), 2613–2616.

Chan, R. H., **C.-W. Ho**, and **M. Nikolova** (2005). Salt-and-pepper noise removal by median-type noise detectors and detail-preserving regularization. *IEEE Transactions on image processing*, **14**(10), 1479–1485.

Chiani, M., **D. Dardari**, and **M. K. Simon** (2003*a*). New exponential bounds and approximations for the computation of error probability in fading channels. *IEEE Transactions on Wireless Communications*, **2**(4), 840–845.

Chiani, M., **D. Dardari**, and **M. K. Simon** (2003*b*). New exponential bounds and approximations for the computation of error probability in fading channels. *IEEE Transactions on Wireless Communications*, **2**(4), 840–845.

Cox, W. C., **J. A. Simpson**, **C. P. Domizioli**, **J. F. Muth**, and **B. L. Hughes**, An underwater optical communication system implementing reed-solomon channel coding. *In OCEANS 2008*. IEEE, 2008.

Davies-Colley, R. and **D. Smith** (2001). Turbidity suspeni) ed sediment, and water clarity: a review 1. *JAWRA Journal of the American Water Resources Association*, **37**(5), 1085–1101.

Domingo, M. C. (2012). An overview of the internet of underwater things. *Journal of Network and Computer Applications*, **35**(6), 1879–1890.

Dong, Y. and **J. Liu**, On ber performance of underwater wireless optical miso links under weak turbulence. *In OCEANS 2016-Shanghai*. IEEE, 2016.

Doniec, M., **C. Detweiler**, **I. Vasilescu**, **M. Chitre**, **M. Hoffmann-Kuhnt**, and **D. Rus** (2010). Aquaoptical: A lightweight device for high-rate long-range underwater point-to-point communication. *Marine Technology Society Journal*, **44**(4), 55–65.

Essebbar, A., **G. Loubet**, and **F. Vial**, Underwater acoustic channel simulations for communication. *In OCEANS'94.'Oceans Engineering for Today's Technology and Tomorrow's Preservation.'Proceedings*, volume 3. IEEE, 1994.

Farid, A. A. and **S. Hranilovic** (2007). Outage capacity optimization for free-space optical links with pointing errors. *Journal of Lightwave technology*, **25**(7), 1702–1710.

Farr, N., **A. Bowen**, **J. Ware**, **C. Pontbriand**, and **M. Tivey**, An integrated, underwater optical/acoustic communications system. *In OCEANS 2010 IEEE-Sydney*. IEEE, 2010.

Fenton, L. (1960). The sum of log-normal probability distributions in scatter transmission systems. *IRE Transactions on Communications Systems*, **8**(1), 57–67.

Ghazy, A. S., **S. Hranilovic**, and **M.-A. Khalighi** (). Angular MIMO for underwater wireless optical communications: Channel modelling and capacity.

Islam, M. S. and **S. Majumder**, Performance analysis of a free space optical link using alamouti type space time block code with weak turbulent condition. *In 2012 7th International Conference on Electrical and Computer Engineering*. IEEE, 2012.

Jackson, D. and **I. Kliman** (1992). Underwater communication system. URL https://www.google.com/patents/US5124955. US Patent 5,124,955.

Jafarkhani, H., *Space-time coding: theory and practice*. Cambridge university press, 2005.

Jamali, M. V., **A. Mirani**, **A. Parsay**, **B. Abolhassani**, **P. Nabavi**, **A. Chizari**, **P. Khorramshahi**, **S. Abdollahramezani**, and **J. A. Salehi** (2018). Statistical studies of fading in underwater wireless optical channels in the presence of air bubble, temperature, and salinity random variations. *IEEE Transactions on Communications*, **66**(10), 4706–4723.

Jamali, M. V. and **J. A. Salehi**, On the BER of multiple-input multiple-output underwater wireless optical communication systems. *In 2015 4th International Workshop on Optical Wireless Communications (IWOW)*. IEEE, 2015.

Jamali, M. V., **J. A. Salehi**, and **F. Akhoundi** (2016). Performance studies of underwater wireless optical communication systems with spatial diversity: Mimo scheme. *IEEE Transactions on Communications*, **65**(3), 1176–1192.

Jaruwatanadilok, S. (2008). Underwater wireless optical communication channel modeling and performance evaluation using vector radiative transfer theory. *IEEE Journal on selected areas in communications*, **26**(9), 1620–1627.

Kao, C.-C., **Y.-S. Lin**, **G.-D. Wu**, and **C.-J. Huang** (2017). A comprehensive study on the internet of underwater things: applications, challenges, and channel models. *Sensors*, **17**(7), 1477.

Kaushal, H. and **G. Kaddoum** (2016). Underwater optical wireless communication. *IEEE Access*, **4**, 1518–1547.

Korotkova, O., **N. Farwell**, and **E. Shchepakina** (2012). Light scintillation in oceanic turbulence. *Waves in Random and Complex Media*, **22**(2), 260–266.

Krishnan, P. and **D. S. Kumar** (2014). Bit error rate analysis of free-space optical system with spatial diversity over strong atmospheric turbulence channel with pointing errors. *Optical Engineering*, **53**(12), 126108.

Laneman, J. N., **D. N. Tse**, and **G. W. Wornell** (2004). Cooperative diversity in wireless networks: Efficient protocols and outage behavior. *IEEE Transactions on Information theory*, **50**(12), 3062–3080.

Lee, E., **J. Park**, **D. Han**, and **G. Yoon** (2011). Performance analysis of the asymmetric dual-hop relay transmission with mixed RF/FSO links. *IEEE Photonics Technology Letters*, **23**(21), 1642–1644.

Lee, E. J. and **V. W. Chan** (2004). Part 1: Optical communication over the clear turbulent atmospheric channel using diversity. *IEEE journal on selected areas in communications*, **22**(9), 1896–1906.

Lin, S. and **D. J. Costello**, *Error control coding*. Pearson Education India, 2001.

Liu, W., **Z. Xu**, and **L. Yang** (2015*a*). SIMO detection schemes for underwater optical wireless communication under turbulence. *Photonics Research*, **3**(3), 48–53.

Liu, W., **Z. Xu**, and **L. Yang** (2015*b*). SIMO detection schemes for underwater optical wireless communication under turbulence. *Photonics Research*, **3**(3), 48–53.

LumiLED's (2017). LXML-PB01-0040 blue led. *https://www.lumileds.com/uploads/265/DS68-pdf*.

Machado, R. and **B. F. Uchôa-Filho** (2006). Extended techniques for transmit antenna selection with stbcs. *Journal of Communication and Information Systems*, **21**(3).

MacWilliams, F. J. and **N. J. A. Sloane**, *The theory of error-correcting codes*, volume 16. Elsevier, 1977.

Mattoussi, F., **M. A. Khalighi**, and **S. Bourennane** (2018). Improving the performance of underwater wireless optical communication links by channel coding. *Applied optics*, **57**(9), 2115–2120.

Miller, N. (1959). An underwater communication system. *IRE Transactions on Communications Systems*, **7**(4), 249–251.

Miridakis, N. I., **M. Matthaiou**, and **G. K. Karagiannidis** (2014). Multiuser relaying over mixed RF/FSO links. *IEEE Transactions on Communications*, **62**(5), 1634–1645.

Mitchell, R. L. (1968). Permanence of the log-normal distribution. *JOSA*, **58**(9), 1267–1272.

Moon, T. K., *Error correction coding: mathematical methods and algorithms*. John Wiley & Sons, 2005.

Morel, A. (1974). Optical properties of pure water and pure sea water. *Optical aspects of oceanography*, **1**, 22.

Oubei, H. M., **R. T. ElAfandy**, **K.-H. Park**, **T. K. Ng**, **M.-S. Alouini**, and **B. S. Ooi** (2017). Performance evaluation of underwater wireless optical communications links in the presence of different air bubble populations. *IEEE Photonics Journal*, **9**(2), 1–9.

Peppas, K. P., **A. C. Boucouvalas**, and **Z. Ghassemloy** (2017). Performance of underwater optical wireless communication with multi-pulse pulse-position modulation receivers and spatial diversity. *IET Optoelectronics*, **11**(5), 180–185.

Popoola, W. O., **Z. Ghassemlooy**, **J. Allen**, **E. Leitgeb**, and **S. Gao** (2008). Free-space optical communication employing subcarrier modulation and spatial diversity in atmospheric turbulence channel. *IET optoelectronics*, **2**(1), 16–23.

Quazi, A. and **W. Konrad** (1982). Underwater acoustic communications. *IEEE Communications Magazine*, **20**(2), 24–30.

Raghavendra, M. and **U. S. Acharya** (2019). Non-orthogonal space–frequency block codes from cyclic codes for wireless systems employing mimo-ofdm with index modulation. *Physical Communication*, **34**, 174–187.

Raghavendra, M. and **U. S. Acharya** (2020). Index modulation aided multi carrier power line communication employing rank codes from cyclic codes. *Physical Communication*, **39**, 100975.

Ramavath, P. N., **A. Kumar**, **S. S. Godkhindi**, and **U. S. Acharya** (2018). Experimental studies on the performance of underwater optical communication link with channel coding and interleaving. *CSI Transactions on ICT*, **6**(1), 65–70.

Ramavath, P. N., **S. A. Udupi**, and **P. Krishnan** (2020). Experimental demonstration and analysis of underwater wireless optical communication link: Design, BCH coded receiver diversity over the turbid and turbulent seawater channels. *Microwave and Optical Technology Letters*.

Robin, A. C. (1997). A quick approximation to the normal integral. *The Mathematical Gazette*, **81**(490), 95–96.

Samimi, H. and **M. Uysal** (2013). End-to-end performance of mixed RF/FSO transmission systems. *IEEE/OSA Journal of Optical Communications and Networking*, **5**(11), 1139–1144.

Sandalidis, H. G., **T. A. Tsiftsis**, **G. K. Karagiannidis**, and **M. Uysal** (2008). BER performance of FSO links over strong atmospheric turbulence channels with pointing errors. *IEEE Communications Letters*, **12**(1), 44–46.

Schill, F., **U. R. Zimmer**, and **J. Trumpf**, Visible spectrum optical communication and distance sensing for underwater applications. *In Proceedings of ACRA*. 2004.

Siegel, M. and **R. King** (1973). Electromagnetic propagation between antennas submerged in the ocean. *IEEE Transactions on Antennas and Propagation*, **21**(4), 507–513.

Simon, M. K. and **V. A. Vilnrotter** (2005). Alamouti-type space-time coding for free-space optical communication with direct detection. *IEEE Transactions on Wireless Communications*, **4**(1), 35–39.

Simpson, J. A., **W. C. Cox**, **J. R. Krier**, **B. Cochenour**, **B. L. Hughes**, and **J. F. Muth**, 5 mbps optical wireless communication with error correction coding for underwater sensor nodes. *In OCEANS 2010*. IEEE, 2010.

Sripati, U. (2011). *Space-Time-Block Codes For MIMO Fading Channels From Codes Over Finite Fields*. Ph.D. thesis.

Sripati, U., **B. S. Rajan**, and **V. Shashidhar**, Full-diversity STBCs for block-fading channels from cyclic codes. *In IEEE Global Telecommunications Conference, 2004. GLOBECOM'04.*, volume 1. IEEE, 2004.

Stüber, G. L. and **G. L. Stèuber**, *Principles of mobile communication*, volume 2. Springer, 1996.

Sun, X., **C. H. Kang**, **M. Kong**, **O. Alkhazragi**, **Y. Guo**, **M. Ouhssain**, **Y. Weng**, **B. H. Jones**, **T. K. Ng**, and **B. S. Ooi** (2020). A review on practical considerations and solutions in underwater wireless optical communication. *Journal of Lightwave Technology*, **38**(2), 421–431.

Tabeshnezhad, A. and **M. A. Pourmina** (2017). Outage analysis of relay-assisted underwater wireless optical communication systems. *Optics Communications*, **405**, 297–305.

ThorLab's (2017). Fds 100. *https://www.thorlabs.com/thorproduct.cfm?partnumber=FDS100*.

Tsiftsis, T. A., **H. G. Sandalidis**, **G. K. Karagiannidis**, and **M. Uysal** (2009). Optical wireless links with spatial diversity over strong atmospheric turbulence channels. *IEEE Transactions on Wireless Communications*, **8**(2), 951–957.

Wang, J., **C. Lu**, **S. Li**, and **Z. Xu** (2019). 100 m/500 mbps underwater optical wireless communication using an nrz-ook modulated 520 nm laser diode. *Optics express*, **27**(9), 12171–12181.

Weng, Y., **Y. Guo**, **O. Alkhazragi**, **T. K. Ng**, **J.-H. Guo**, and **B. S. Ooi** (2019). Impact of turbulent-flow-induced scintillation on deep-ocean wireless optical communication. *Journal of Lightwave Technology*, **37**(19), 5083–5090.

Wolfram (2001). The wolfram functions site. URL http://functions.wolfram.com/HypergeometricFunctions/MeijerG/21/02/07/0002/.

Yang, F., **J. Cheng**, and **T. A. Tsiftsis** (2014). Free-space optical communication with nonzero boresight pointing errors. *IEEE Transactions on Communications*, **62**(2), 713–725.

Zedini, E., **H. Soury**, and **M.-S. Alouini** (2016). Dual-hop FSO transmission systems over Gamma–Gamma turbulence with pointing errors. *IEEE Transactions on Wireless Communications*, **16**(2), 784–796.

Zhang, H. and **Y. Dong** (2016). Impulse response modeling for general underwater wireless optical MIMO links. *IEEE Communications Magazine*, **54**(2), 56–61.

Zhao, Y., **A. Wang**, **L. Zhu**, **W. Lv**, **J. Xu**, **S. Li**, and **J. Wang** (2017). Performance evaluation of underwater optical communications using spatial modes subjected to bubbles and obstructions. *Optics letters*, **42**(22), 4699–4702.

Zielinski, A. and **L. Barbour**, Swept carrier acoustic underwater communications. *In OCEANS'78*. IEEE, 1978.

Publications Based on the Thesis

Journals :

1. **Prasad Naik Ramavath**, Shripathi Acharya Udupi and Prabu Krishnan (2020). "Co-operative RF–UWOC Link Performance over Hyperbolic Tangent Log-Normal Distribution Channel with Pointing Errors." Optics Communication. DOI: 10.1016/j.optcom.2020.125774.

2. **Prasad Naik Ramavath**, Shripathi Acharya Udupi and Prabu Krishnan (2020). "Experimental demonstration and analysis of underwater wireless optical communication link: Design, BCH coded receiver diversity over the turbid and turbulent seawater channels." Microwave and Optical Technology Letters.
   DOI: 10.1002/mop.32311.

3. **Prasad Naik Ramavath**, Shripathi Acharya Udupi and Prabu Krishnan (2020). "High-speed and reliable Underwater Wireless Optical Communication system using Multiple-Input Multiple-Output and channel coding techniques for IoUT applications." Optics Communication.
   DOI: 10.1016/j.optcom.2019.125229.

4. **Prasad Naik Ramavath**, Amardeep Kumar, Shrutkirthi Shashikant Godkhindi and U. Shripathi Acharya (2018). "Experimental studies on the performance of underwater optical communication link with channel coding and interleaving." CSI Transactions on ICT.
   DOI: 10.1007/s40012-017-0179-3.

Conferences :

1. **R Prasad Naik**, Shripathi Acharya Udupi and Nitin Kumar Suyan, "Experimental evaluation of Reliable Underwater optical communication in the presence of turbulence and blockage", International Conference on Optical and Wireless Technologies (OWT-2019) organized by MNIT Jaipur in March 16-17, 2019.

2. **R Prasad Naik**, Amardeep Kumar and Shripathi Acharya Udupi "Experimental studies on seawater links applying Channel coding, interleaved codes and diversity techniques", International Conference on Sonar Systems and Sensors (ICONS-2018) organized by NPOL Cochin (DRDO) in February 23-25, 2018.

Bio-data

NAME : Prasad Naik Ramavath

CONTACT DETAILS

Address : S/o R Swamy Naik, D.No: 16/275-120,
Anjaneyamanyam, Nandalpadu,
Tadipathri, Anantapur Dist., Andhra Pradesh–515411

☎ : 8960833802

✉ : prasadnaikr@gmail.com

EDUCATIONAL QUALIFICATIONS

Doctor of Philosophy (Ph.D.)

National Institute of Technology Karnataka, Surathkal 2015–Till date

Master of Technology (M.Tech)

Motilal Nehru National Institute of Technology, Allahabad. 2013–2015

Branch : Communication Systems

Bachelor of Technology (B.Tech)

Annamacharya Institute of Technology and Sciences, Rajampet 2008–2012

Branch : Electronics and Communication Engineering